universität wien

DISSERTATION

Titel der Dissertation

“Structure-Activity Studies on the Opening- and Closure-Mechanism of L-Type Calcium-Channels”

Verfasserin

Mag. pharm. Katrin Depil

angestrebter akademischer Grad

Doktorin der Naturwissenschaften (Dr.rer.nat)

Wien, im Juli 2012

Studienkennzahl lt. Studienblatt:	A 791 449
Dissertationsgebiet lt. Studienblatt:	Pharmazie
Betreuer:	Univ.-Prof. Dr. Steffen Hering

Abstract

The objective of the present study was to identify gating sensitive positions in the segments of the cardiac L-type $Ca_V1.2$ channel. This was supported by homology models that suggested structural details of certain amino acid regions. The main part of this thesis focuses on the highly conserved "G/A/G/A" motif of the bundle crossing region in the S6 segments. A well known autosomal dominant point mutation which causes a channelopathy called Timothy Syndrome is located inside this motif. This inherited disease leads to arrhythmias, autism and neurological defects. The source of this channelopathy is mutation G423S which dramatically reduces inactivation. The prolonged opening of the channel causes increased calcium influx.

This work shows that mutations in all analogous positions in domains II, III and IV accelerate activation. Inactivation in Domains II-IV is not affected. Since inactivation is Domain I specific, a decoupling of the inactivation and the deactivation process can be shown.

Homology modelling demonstrates that all amino acids of the "G/A/G/A" motif form a tightly packed ring in the closed conformation of the channel. We hypothesize that mutating this ring prevents complete channel closure. To investigate influence of voltage sensors on the identified "G/A/G/A" motif, all charged positions in each of the S_4 segments were neutralized.

Neutralization of the S_4 segments in domains I, III and IV lead to a non-functional channel. Interestingly the activation shift of the neutralized segment in domain II ($IIS4_N$) could not be distinguished from the wild-type channel. Combination of $IIS4_N$ with all "G/A/G/A" mutants caused a rescue behaviour with wild-type like activation. In contrast $IIS4_N$ in conjunction with amino acid mutations next to the "G/A/G/A" motif showed no rescue behaviour. This indicates the important function of the "G/A/G/A" motif.

Thermodynamic analysis showed that the voltage sensor IIS_4 is energetically coupled to the "G/A/G/A" ring. This coupling leads to conformational changes of domains II, II and IV.

Zusammenfassung

In der vorliegenden Arbeit wurden *gating*-sensitive Aminosäuren und Sequenzabschnitte in den S6-Segmenten des kardialen L-Typ Kanals $Ca_V1.2$ identifiziert und mit Hilfe von Homologiemodellen Hypothesen zu deren Funktion formuliert. Der Großteil dieser Arbeit befasst sich mit der Struktur-Funktionsanalyse des stark konservierten „G/A/G/A“ Motivs in der „*bundle crossing region*“ der S6-Segmente.

In den Bereich dieses Motivs fällt eine bekannte, autosomal dominante, Punktmutation, die zu einer Kanalerkrankung, dem Timothy Syndrom, führt. Tritt diese Mutation G432S auf, so sind u.a. Arrhythmien, Autismus und neurologische Defekte die Folge. Dabei wird die Inaktivierung aufgehoben und durch die so verlängerte Kanalöffnungszeit strömt vermehrt Kalzium ein. Die Arbeit zeigt, dass Mutationen in allen analogen Positionen der Domänen II, III und IV starke Verschiebungen der Aktivierung auslösen. Eine Entkopplung des Aktivierungsprozesses vom Inaktivierungsprozess für Mutationen in Position 432 konnte nachgewiesen werden.

Darüber hinaus wurde mittels Homologiemodell festgestellt, dass die Aminosäuren des „G/A/G/A“-Motivs wahrscheinlich einen räumlich dicht gepackten Ring in der geschlossenen Konformation des Kanals bilden. Es wird angenommen, dass dieser bei jeglicher Form der Mutation nicht mehr vollständig schließen kann. Um den Einfluss von Spannungssensoren auf das entdeckte „G/A/G/A“ Motiv – und damit das *Gating*-Verhalten – zu untersuchen, wurde jedes $S4$ Segment der vier Domänen neutralisiert.

Durch die Neutralisierung der $S4$ Segmente in den Domänen I, III und IV wurde der Kanal funktionsunfähig. Interessanterweise konnte die Aktivierung des neutralisierten Segments in Domäne II ($IIS4_N$) nicht von jener des Wildtypkanals unterschieden werden. Die Kombination von ($IIS4_N$) mit allen „G/A/G/A“ Mutanten verursachte ein *Rescue*-Verhalten, die Wildtyp-Aktivierung wurde also wiederhergestellt. Die Kombination von $IIS4_N$ mit den „G/A/G/A“ umliegenden Positionen verursachte kein *Rescue*-Verhalten, was auf eine Schlüsselrolle von „G/A/G/A“ für die Kanalöffnung schließen lässt.

Thermodynamische Untersuchungen zeigten, dass der Spannungssensor $IIS4$ energetisch an den „G/A/G/A“ Ring gekoppelt ist und diese Kopplung zu Konformationsänderungen der Domänen II, III und IV führt.

List of Publications

Following are the publications relevant for this cumulative thesis ("*Kumulative Dissertation*").

Accepted Publications

- **Depil K**[1], Beyl S[1], Stary-Weinzinger A[1], Hohaus A, Timin E, Hering S :
  "Timothy mutation disrupts the link between activation and inactivation in $Ca_V1.2$ protein"
  J Biol Chem. 2011 Sep 9;286(36):31557-64. Epub 2011 Jun 17.
- Beyl S[1], **Depil K**[1], Hohaus A, Stary-Weinzinger A, Timin E, Shabbir W, Kudrnac M, Hering S :
  "Physicochemical properties of pore residues predict activation gating of $Ca_V1.2$: a correlation mutation analysis"
  Pflugers Arch. 2011 Jan;461(1):53-63. Epub 2010 Oct 7.

Submitted Publications

- Beyl S, **Depil K**, Hohaus A, Stary-Weinzinger A, Linder T, Timin E, Hering S :
  "Neutralization of a single voltage sensor (IIS4) affects gating determinants in all four pore forming S6 segments of $Ca_V1.2$"
  Submitted to Journal of General Physiology in June 2012

[1] **authors contributed equally to this work**

Contents

1 Introduction **1**

1.1 Overview . . . 2
1.1.1 Timothy-Syndrome Mutations Provide New Insights into Structure and Function of L-Type Calcium Channels . . . 2
1.1.2 Destabilization of the Closed Pore . . . 2
1.1.3 Physicochemical Properties of Pore Residues Predict Activation Gating of $Ca_V1.2$ . . . 3
1.1.4 Charge Neutralization in Segment IIS_4 Rescues Gating Disturbances in the G/A/G/A-Ring in Segments IS6-IVS6 . . . 4
1.2 Methods . . . 5
1.2.1 Patch-Clamp Technique . . . 5
1.2.2 Ionic Current Recordings and Data Acquisition . . . 5
1.2.3 Cell Culture and Transient Transfection . . . 6
1.2.4 Mutagenesis . . . 6
1.2.5 Calculation of Amino Acid Descriptors . . . 7
1.2.6 Correlating Amino Acid Properties with ΔV_{act} . . . 7
1.2.7 Correlating Amino Acid Properties with ΔG . . . 8
1.2.8 Conservation Analysis . . . 8
1.2.9 Homology Modeling . . . 8
1.2.10 Accessibility Calculations . . . 9
1.2.11 Confocal Imaging . . . 9
1.3 Structure . . . 10
1.3.1 Topology of Voltage Gated Calcium Channels . . . 10
1.3.2 Crystal Structures of Voltage Gated Potassium and Sodium Channels and Topology of Voltage Gated Potassium and Sodium Channels . . . 12
1.3.3 Selectivity Filter of Potassium Channels . . . 12
1.3.4 Selectivity Filter of Na_V and Ca_V . . . 12
1.3.5 Pore Gating . . . 17
1.3.6 Voltage Sensors . . . 17
1.4 Nomenclature of Voltage-Gated Calcium Channels . . . 19
1.5 Classification based on Gating and Conduction . . . 22
1.5.1 $Ca_V1.2$ and its Role in Excitation-Contraction Coupling . . . 22

1.6 Subunits . . . 26
1.6.1 The $\alpha_2\delta$-Subunits . . . 26
1.6.2 The β-Subunits . . . 27
1.6.3 The γ-Subunits . . . 28
1.7 Inactivation . . . 31
1.7.1 Voltage Dependent Inactivation . . . 31
1.7.2 Calcium/Calmodulin Dependent Inactivation CDI . . . 32
1.8 L-Type Calcium Channel Dysfunction Channelopathies . . . 34
1.8.1 Hypokalemic Periodic Paralysis Type 1 (HypoPP1) . . . 34
1.8.2 Malignant Hyperthermia Susceptibility Type 5 (MHS5) . . . 34
1.8.3 Incomplete Congenital Stationary Night Blindness Type 2 . . . 34
1.8.4 Brugada Syndrome (BrS3) . . . 35
1.8.5 Sinoatrial Node Dysfunction and Deafness (SANDD) . . . 36
1.8.6 Timothy Syndrome . . . 36
1.9 References . . . 37

2 Timothy Mutation Disrupts the Link between Activation and Inactivation in $Ca_V1.2$ 52
2.1 Introduction . . . 53
2.2 Experimental Procedures . . . 55
2.2.1 Conservation Analysis . . . 55
2.2.2 Homology Modeling . . . 55
2.2.3 Accessibility Calculations . . . 55
2.2.4 Mutagenesis . . . 55
2.2.5 Cell Culture and Transient Transfection . . . 56
2.2.6 Ionic Current Recordings and Data Acquisition . . . 56
2.2.7 Calculation of Amino Acid Descriptors . . . 57
2.3 Results . . . 58
2.3.1 The "Timothy Gly-432" Is Part of a Motif of Small Residues at the Inner Channel Mouth . . . 58
2.3.2 Mutations of Gly-432 Shift the Activation Curve . . . 59
2.3.3 Substitutions of Gly-432 Remove Channel Inactivation . . . 59
2.3.4 Mutations of Ala-780, Gly-1193, and Ala-1503 (Homologous to Gly-432) Affect Channel Activation but Preserve Inactivation . . . 63
2.3.5 Structural Analysis of the G/A/G/A Motif . . . 63
2.4 Discussion . . . 68
2.4.1 Mutations of G/A/G/A Residues Affect Activation Gating . . . 68
2.4.2 Structural Model of the G/A/G/A Region . . . 69
2.4.3 Exclusive Role of Gly-432 in Channel Inactivation . . . 69
2.4.4 Conclusions and Outlook . . . 70
2.5 Supplemental Data . . . 72
2.6 References . . . 76

3 Physicochemical Properties of Pore Residues Predict Activation Gating of $Ca_V1.2$ 79
3.1 Introduction . . . 80
3.2 Materials and Methods . . . 82
3.2.1 Mutagenesis . . . 82
3.2.2 Cell Culture and Transient Transfection . . . 82
3.2.3 Ionic Current Recordings and Data Acquisition . . . 82
3.2.4 Calculation of Amino Acid Descriptors . . . 84
3.2.5 Correlating Amino Acid Properties with ΔV_{act} . . . 84
3.2.6 Correlating Amino Acid Properties with ΔG . . . 85
3.3 Results . . . 87
3.3.1 G1193 is a Gating-Sensitive Residue in IIIS6 . . . 87
3.3.2 Mutating G1193 to Residues with Different Properties . . . 87
3.3.3 Mutation Correlation Analysis in Position G1193 . . . 89
3.3.4 Correlation Analysis in Gating-Sensitive Position L434 (IS6) . . . 94
3.3.5 Modulation of Hydrophobic Interactions in I781 (IIS6) by other Amino Acid Properties . . . 95
3.4 Discussion . . . 96
3.4.1 G1193 is a Gating-Related Residue in Segment IIIS6 . . . 96
3.4.2 Changes in the accessible surface area of all polar atoms in position G1193 (IIIS6) predict the shifts of the activation curve 96
3.4.3 Number of Rotatable Bonds and a Side-Chain Amino Acid Flexibility Index Predict the Shift of the Activation Curve by Mutations in Position L434 (IS6) . . . 97
3.4.4 Co-Correlations Provide Additional Insight into Modulatory Properties of Amino Acid Residues . . . 98
3.4.5 Link between ΔV_{act} and Changes in Free Energy (ΔG) . . . 98
3.5 Conclusions and Outlook . . . 101
3.6 Supplemental Data . . . 102
3.7 References . . . 106

4 Neutralization of a Single Voltage Sensor Affects Gating Determinants in $Ca_V1.2$ 109
4.1 Introduction . . . 110
4.2 Methods . . . 112
4.2.1 Mutagenesis . . . 112
4.2.2 Cell Culture and Transient Transfection . . . 112
4.2.3 Ionic Current Recordings and Data Acquisition . . . 112
4.2.4 Confocal Imaging . . . 113
4.2.5 Modeling . . . 113
4.2.6 Online Supplemental Material . . . 114
4.3 Results . . . 115
4.3.1 Charge Neutralization in IIS4 Induces Only Small Gating Disturbances in $Ca_V1.2$ . . . 115

4.3.2 Charge Neutralization in Segment IIS4 Rescues Gating Disturbances in the GAGA Ring in Segments IS6-IVS6 115
4.3.3 Charge Neutralization in IIS4 does not Affect Gating Disturbances in Positions Neighbouring to GAGA 117
4.3.4 Charge Neutralization in Segment IIS4 Modulates Kinetics of IIS6 Pore Mutants 117
4.3.5 Mutant Cycle Analysis Reveals Energetic Coupling Between IIS4 and Residues of the GAGA Ring 121
4.4 Discussion 123
4.4.1 IIS4 Interactions with Segments IS6-IVS6 123
4.4.2 Dual Role of A780? 124
4.5 Conclusions and Outlook 125
4.6 Tables 128
4.7 Supplemental Materials 130
4.7.1 Charge neutralization in IIS4 has small effect on channel gating 130
4.7.2 Figure S1 131
4.7.3 Fingerprints of the IIS4 – IIS6 interaction 132
4.7.4 Figure S2 133
4.7.5 Figure S3 134
4.8 References 135

Curriculum Vitæ **141**

List of Figures

1.1 Whole-cell patch-clamp configurations. 5
1.2 Schematic structure of voltage gated calcium channels. 10
1.3 Schematic diagram of the α_1-subunit and ancillary subunits of a voltage gated calcium channel. 11
1.4 The location of the voltage sensing module S1-S4 in two domains. . . 11
1.5 Potassium channel and sodium channel topology 13
1.6 Side view of the open $K_V1.2$ conformation crystal structure. 14
1.7 Top view of the open $K_V1.2$ conformation crystal structure 14
1.8 The K_V selectivity filter. 15
1.9 The top view of NavAb. 16
1.10 The Na_V selectivity filter 16
1.11 Multiple sequence alignment of S6 helices of Ca_V channels with selected K^+ channels. 17
1.12 Different models of voltage sensing. 19
1.13 Phylogenetic tree 21
1.14 Dendrogram illustrating the genetic similarity 21
1.15 Time scale of calcium signalling effects 24
1.16 Illustration of the cardiomyocyte and intracellular organelles. 25
1.17 The Cavb-AID complex structure. 28
1.18 Current traces with 300 ms pulses to +30 mV showing voltage-gated inactivation kinetics. 32
1.19 Model of CDI induction by CaM in $Ca_V1.2$ Ca^{2+} channels. 32

2.1 Multiple sequence alignment of S6 helices of Ca_V channels with selected K^+ channels. 58
2.2 Gating changes induced by mutations of G432 in segment IS6 of $Ca_V1.2$. 60
2.3 Inactivation changes induced by mutations of G432 in segment IS6 of $Ca_V1.2$. 62
2.4 Mutations in the pore segments IIS6, IIIS6 and IVS6 in positions homologous to G432 in IS6 induce significant shifts of activation and inactivation curves. 64
2.5 Correlation between shifts of the midpoint of the inactivation and activation curves for G/A/G/A mutations in segments IIS6-IVS6. 65

2.6 Hypothetical role of small amino acids in helix-helix packing of voltage gated ion channels 66
2.7 Alignment of S6 helices from all ten human Ca_V channels 72
2.8 Role of residue size in channel activation in S6 segments of $Ca_V1.2$. . . 73
2.9 Schematic illustration of packing distortions due to insertion of bulky hydrophobic residues in position G432. 74
2.10 Mutation S435G partially rescue channel inactivation. 75

3.1 Gating changes induced by threonine mutations in segment IIIS6 of $Ca_V1.2$. 88
3.2 Gating changes induced by mutations of G1193 in segment IIIS6 of $Ca_V1.2$. 89
3.3 The accessible surface area of all polar atoms in position G1193 (IIIS6) predicts the shift of the activation curve. 91
3.4 Gating changes induced by mutations of L434 in segment IS6 of $Ca_V1.2$. 94
3.5 Side-chain flexibility in position L434 (IS6) predicts the shifts of the activation curve. 95
3.6 Hydrophobicity in position I781 (IIS6) predicts the shifts of the activation curve. 99
3.7 Correlation between ΔV_{act} and changes in free energy (ΔG). 102

4.1 Charge neutralization in segment IIS4 of $Ca_V1.2$ has minor effects on activation gating. 116
4.2 Charge neutralization in IIS4 rescues a gating disturbances induced by G432W in segment IS6. 118
4.3 Charge neutralization in domain II (IIS4) rescues gating disturbances in GAGA positions of domains I, III and IV. 119
4.4 Interaction of IIS4 with IIS6. 120
4.5 $Ca_V1.2$ homology model based on NavAb crystal structure illustrates the location of the G/A/G/A ring with respect to S4. 126
4.6 Effects of mutations in IIS4 on $Ca_V1.2$ gating. 131
4.7 Localization of wild-type and mutant $Ca_V1.2$ α_1-subunits within tsA-201cells. 133
4.8 Charge neutralization in domain II (IIS4) rescues gating disturbances in position G432 of domains I. 134

List of Tables

1.1 Proposed nomenclature for cloned voltage-gated calcium channel α_1-subunits. 20
1.2 Classification of high and low activated calcium channels 23
1.3 Effects and tissue distribution of $\alpha_2\delta$ subunits. 27
1.4 Effects and tissue distribution of β-subunits. 29
1.5 Effects and tissue distribution of γ-subunits. 30

2.1 Pore mutations affect voltage-dependent gating of $Ca_V1.2$ 61
2.2 Potential interactions of G/A/G/A residues in the closed channel state (see model in Fig. 2.6). 65
2.3 Accessibility of residues at the contact interface between S6 (M2) helices. 67

3.1 Pore mutations affect voltage-dependent gating of $Ca_V1.2$ 86
3.2 Identification of leading descriptors predicting ΔV_{act}. 92
3.3 Combined descriptor analysis. 93
3.4 Amino acid descriptors. 103
3.5 Calculated amino acid descriptors. 104

4.1 Midpoints and slope factors (k) of the activation curves and free energy changes during channel opening. 128

List of Abbreviations

aa	amino acids
ABP	alpha binding pocket
AID	alpha interaction domain
AMPAR	α-amino-3-hydroxy-5-methyl-4-isoxazolepropionic acid receptor
BID	beta interaction domain
Ca_V	voltage-gated calcium channel
CDI	calcium-dependent inactivation
DHP	dihydropyridine
DHPR	dihydropyridine receptor
EDTA	Ethylendiamintetraessigsäure
EGTA	Ethylenglycol-bis(aminoethylether)-N,N,N′,N′-tetraessigsäure
ER	endoplasmatic reticulum
G_{max}	maximum Gibbs free energy
G/A/G/A	G432/A780/G1193/A1503 motif
GFP	green fluorescent protein
GK	guanylate kinase
HEK	human embryonic kidney
HEPES	2-(4-(2-Hydroxyethyl)- 1-piperazinyl)-ethansulfonsäure
HVA	high-voltage activated
I_{Ba}	current of Barium-ions
I_{max}	maximum current
I-V	current-voltage relationship
K_V	voltage-gated potassium channel
LVA	low-voltage activated

MAGUK	membrane associated guanylate kinase
MOE	molecular operating environment
Na_V	voltage-gated sodium channel
NK	nucleotide kinase
PDB	protein database
PMCA	plasma membrane Ca^{2+} ATPase
S.E.	standard error
$S4_N$	neutralized S4-Segment
SEM	standard error of the mean (value)
SERCA	sarcoplasmic/endoplasmic reticulum calcium ATPase
TARP	transmembrane AMPAR regulatory protein
TM	trans-membrane (segment)
TS	Timothy Syndrome
$V_{0.5,act}$	voltage of half-maximal current-activation
$V_{0.5,inact}$	voltage of half-maximal current-inactivation
V_{rev}	voltage of reversal potential
VDCC	voltage-dependent calcium channel
VDI	voltage-dependent inactivation
WT	wild type
ΔG	changes in Gibbs free energy
τ_{act}	time constant of current-activation
τ_{inact}	time constant of current-inactivation

1 Introduction

1.1 Overview

1.1.1 Timothy-Syndrome Mutations Provide New Insights into Structure and Function of L-Type Calcium Channels

Ion channels are large membrane proteins that conduct potassium, sodium or calcium ions. The human genome encodes 243 voltage-gated ion channels. They regulate electrical signals in the nervous system, control the release of neurotransmitters and are responsible for the regulation of the heart rhythm and muscle contractions. Voltage-gated ion channels open and close in response to changes in membrane potential. The molecular mechanisms underlying this gating process are still unexplored. Voltage-gated calcium channels are expressed in many tissues. These channels control a large variety of cellular functions such as muscle contraction, generation of electrical activity in the sinus node, hearing, vision, release of neurotransmitters and cell differentiation (Catterall, 2005).

Mutations in calcium channels can cause severe inherited diseases such as migraine, night blindness, autism spectrum disorders and Timothy syndrome. The Timothy syndrome is caused by a mutation in $Ca_V1.2$ that leads to severe cardiovascular disorders and prolongs the QT-interval due to enhanced calcium entry and a longer depolarization. The Timothy syndrome was first described in the 90s (Marks et al., 1995, Reichenbach et al., 1992). It often leads to sudden cardiac death in early childhood. In 2004 it was shown that two mutations (G402S and G406R) in calcium channel $Ca_V1.2$, cause symptoms (neurological disorders, autism, severe arrhythmias and webbing of fingers and toes) that are associated with the Timothy syndrome (Splawski et al., 2004, Splawski et al., 2005). Timothy mutations result in enhanced calcium entry caused by defects in channel during an action potential, a process called "inactivation". This in turn induces a calcium overflow causing arrhythmias and multiple disease patterns (Splawski et al., 2004, Splawski et al., 2005).

1.1.2 Destabilization of the Closed Pore

We have recently shown, that Timothy-mutation G402 is part of a highly conserved structure motif, which consists of small amino acids – glycines (G) and alanines (A), which we named the G/A/G/A-motif (Depil et al., 2011). The strongest effect on channel opening occurs when residues from this motif are replaced by larger hydrophobic amino acids. We assume that the Timothy G402 and the whole G/A/G/A-motif are essential for sealing of the closed channel pore. In a homology model these residues interact with bulky phenylalanines from neighbouring S6

helices. Mutations to larger amino acids in the G/A/G/A position might prevent optimal channel closure (Depil et al., 2011).

Our data suggest that the G/A/G/A-residues form an important part of the channel gate. We found a disturbed coupling between the activation and inactivation processes when G402 was mutated to amino acids with different physicochemical properties. We assume that flexibility of Timothy glycine 402 is necessary for helix movement during the inactivation process.

1.1.3 Physicochemical Properties of Pore Residues Predict Activation Gating of $Ca_V1.2$

Guided by systematic mutation of specific pore segments and correlation analysis in $Ca_V1.2$, we identified key amino acid side chain properties, playing a key role in the molecular mechanism of channel opening and closure. Physicochemical properties of amino acids in gating-sensitive positions of S6 segments correlate with the energetics of pore opening (Beyl et al., 2011, Depil et al., 2011). Hydrophobic interactions and side chain size in these S6 positions govern pore stability in $Ca_V1.2$.

The physicochemical properties of amino acid residues in gating-sensitive positions of S6 segments determine the threshold of channel activation of $Ca_V1.2$. Leucine in segment IS6 (L434) and a newly identified activation determinant in segment IIIS6 (G1193) were mutated to a variety of amino acids. The induced leftward shifts of the activation curves and decelerated activation and deactivation currents suggest a destabilization of the closed and a stabilisation of the open channel state for most mutations.

A selection of 17 physicochemical parameters (descriptors) was calculated for these residues and examined for correlation with the shifts of the midpoints of the activation curve (ΔV_{act}). ΔV_{act} correlated with local side-chain flexibility in position L434 (IS6), with the polar accessible surface area of the side chain in position G1193 (IIIS6) and with hydrophobicity in position I781 (IIS6). Combined descriptor analysis for positions I781 and G1193 revealed that additional amino acid properties may contribute to conformational changes during the gating process. The identified physicochemical properties in the analysed gating-sensitive positions (accessible surface area, side-chain flexibility and hydrophobicity) predict the shifts of the activation curves of $Ca_V1.2$ (Beyl et al., 2011).

1.1.4 Charge Neutralization in Segment IIS4 Rescues Gating Disturbances in the G/A/G/A-Ring in Segments IS6-IVS6

To gain insights into the coupling of the voltage sensing machinery to pore residues, we neutralized the charges in each domain of the S_4 segments. Voltage sensors trigger the closed-open transitions in the pore of voltage-gated ion channels. To probe the transmission of voltage sensor signalling to the channel pore of $Ca_V1.2$, we investigated how elimination of positive charges in the S_4 segments (charged residues were replaced by neutral glutamine) modulates gating perturbations induced by mutations in pore-lining S6 segments. Neutralization of all positively charged residues in IIS_4 produced a functional channel (IIS_{4N}) while replacement of the charged residues in other S_4 segments resulted in non-functional channels. The IIS_{4N} channel displayed activation kinetics similar to wild type.

When IIS_{4N} was combined with G/A/G/A mutations, the activation curves were shifted back towards wild type. Current kinetics in segments IS6-IVS6 by IIS_{4N} are highly position-specific. Thermodynamic cycle analysis supports the hypothesis that IIS_4 is energetically coupled with the distantly located G/A/G/A residues. We hypothesize that conformational changes caused by neutralization of IIS_4 are not restricted to domain II (IIS6) but are transmitted to gating structures in domains I, III and IV via the G/A/G/A ring (Beyl et al., 2012).

1.2 Methods

1.2.1 Patch-Clamp Technique

In 1976, Neher and Sakmann (Neher and Sakmann, 1976) developed the patch-clamp-technique that allowed recording of single channel conductance. Critical for the success of this method was the formation of a so called high (Gigaohm) resistance "Giga-Seal" (Hamill et al., 1981) between the tip of the pipette ("patch pipette") and the surface of a cell membrane. This dramatically reduced thermal background noise during ionic current measurements. Several configurations of patch-clamp techniques are known. The most common techniques are single-channel recordings (which allow measuring inside-out patches by ripping the membrane through pulling the pipette) and whole-cell recordings (that enables the measurement of ionic currents through the entire membrane of the cell). Both methods are illustrated in Fig. 1.1. For our electrophysiological recordings we used whole cell configuration patch clamp technique to record many thousands of channels simultaneously.

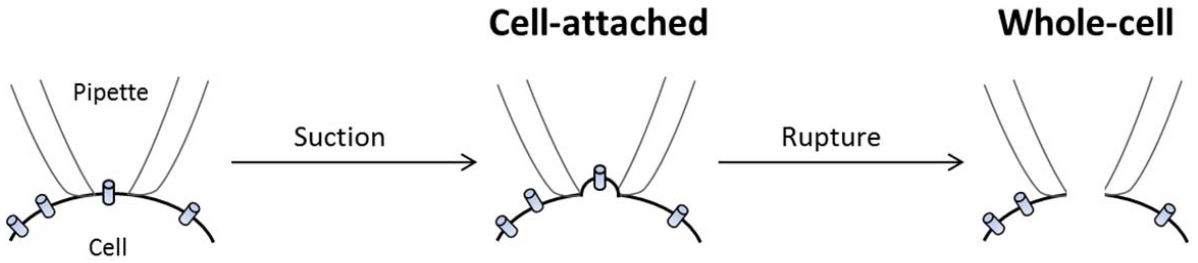

Figure 1.1: These patch-clamp configurations outline the procedures to get a cell-attached formation for single channel recordings and a whole-cell configuration by rupturing the patch of the membrane (Werry, 2009)

1.2.2 Ionic Current Recordings and Data Acquisition

Barium currents (I_{Ba}) through voltage-gated Ca^{2+} channels were recorded at $22 - 25$ °C by patch-clamping (Hamill et al., 1981) using an Axopatch 200A patch-clamp amplifier (Axon Instruments, Foster City) $36 - 48$ h after transfection. The extracellular bath solution (5 mM $BaCl_2$, 1 mM $MgCl_2$, 10 mM HEPES, 140 mM choline chloride) was titrated to pH 7.4 with methanesulfonic acid. Patch pipettes with resistances of $1 - 4$ MΩ were made from borosilicate glass (Clark Electromedical Instruments) and filled with pipette solution (145 mM CsCl, 3 mM $MgCl_2$, 10 mM HEPES, 10 mM EGTA 10), titrated to pH 7.25 with CsOH. All data were digitized

using a DIGIDATA 1200 interface (Axon Instruments), smoothed by means of a four-pole Bessel filter, and saved to disk. 100 ms current traces were sampled at 100 kHz and filtered at 5 kHz; tail currents were sampled at 50 kHz and filtered at 10 kHz. Leak currents were subtracted digitally using average values of scaled leakage currents elicited by a 10 mV hyperpolarizing pulse or electronically by means of an Axopatch 200 amplifier (Axon Instruments). Series resistance and offset voltage were routinely compensated for. The pClamp software package (Version 7.0 Axon Instruments) was used for data acquisition and preliminary analysis. Microcal Origin 7.0 was used for analysis and curve-fitting.

The voltage dependence of activation was determined from I-V curves and fitted to

$$m_\infty = \frac{1}{1 + \exp \frac{V_{0.5,act} - V}{k_{act}}} \tag{1.1}$$

The time course of current activation was fitted to a mono-exponential function,

$$I(t) = A \cdot \exp\left(\frac{t}{\tau}\right) + C \tag{1.2}$$

where $I\,(t)$ is current at time t, A is the amplitude coefficient, τ is the time constant, and C is the steady-state current. Data are given as the mean $\pm S.E.$.

1.2.3 Cell Culture and Transient Transfection

Human embryonic kidney tsA-201 cells were grown at 5 % CO_2 and 37 °C to 80 % confluence in Dulbecco's modified Eagle's/F-12 medium supplemented with 10 % (v/v) fetal calf serum and 100 units/ml penicillin/streptomycin. Cells were split with trypsin/EDTA and plated on 35 mm Petri dishes (Falcon) at $30 - 50$ % confluence 16 h before transfection. Subsequently tsA-201 cells were co-transfected with cDNAs encoding wild-type or mutant $Ca_V1.2$ α_1 subunits with auxiliary β_{2a} and β_{2c} (Perez-Reyes et al., 1992) as well as α_2-δ_1 (Ellis et al., 1988) subunits. The transfection of tsA-201 cells was performed using the FuGENE 6 transfection reagent (Roche Applied Science) following standard protocols. tsA-201 cells were used until passage number 15. No variation in channel gating related to different cell passage numbers was observed.

1.2.4 Mutagenesis

The $Ca_V1.2$ α_1-subunit coding sequence (GenBank™ X15539) in-frame 3′ to the coding region of a modified green fluorescent protein was kindly donated by Dr. M.

Grabner (Grabner et al., 1998). Substitutions in segment IS6, IIS6, IIIS6 and IVS6 of the $Ca_V1.2$ α_1-subunit were introduced using the QuikChange® Lightning site-directed mutagenesis kit (Stratagene) with mutagenic primers according to the manufacturer's instructions. All constructs were checked by restriction site mapping and sequencing.

1.2.5 Calculation of Amino Acid Descriptors

Physicochemical descriptors were calculated for amino acids using the Molecular Operating Environment (MOE; Version 2008.10, Chemical Computing Group, Inc., Montreal, QC, Canada). This software package calculates more than 300 descriptors. Examples include polarity measures, size and shape indices, flexibility, accessible surface area and others. Seventeen out of 327 possible descriptors were selected to analyse their potential role in channel gating.

A turn propensity scale describing the relative turn preferences of the different amino acids in formation of transmembrane helical hairpins was taken from Monné et al. (Monné et al., 1999). The hydrophobicity scales were taken from Kyte and Doolittle (Kyte and Doolittle, 1982), Hessa et al.(Hessa et al., 2005), White and Wimley (White and Wimley, 1999), Guy (Guy, 1985), Eisenberg et al. (Eisenberg et al., 1984) and Hopp and Woods (Hopp and Woods, 1981). Rigidity and flexibility indices accounting for a series of descriptors, i.e. number of bonds, number of rings, number of rings per atoms in molecule, number of rotatable bonds, number of rotatable bonds per atoms in molecule, number of rigid bonds (i.e. aromatic or double bonds), number of rigid bonds per atoms in molecule, longest flexible chain, ditto per atoms in molecule, number of rigid fragments, ditto per atoms in molecule, number of partial flexible chains and ditto per atoms in molecule, were taken from Gottfries and Eriksson (Gottfries and Eriksson, 2010).

1.2.6 Correlating Amino Acid Properties with ΔV_{act}

The capability of a given descriptor to predict the shift of the activation curve was established by ranking the correlation coefficients and its significance (t test). This approach enabled the identification of a "leading descriptor", i.e. the one with the largest correlation coefficient (r) and the highest significance. Linear regressions were calculated using the ORIGIN subroutine which also yielded correlation coefficients and their statistical significance.

Subsequently, we correlated weighted linear combinations of all 17 descriptors with ΔV_{act}. Combined descriptors were calculated as $\Delta D = a\Delta D_1 + b\Delta D_2$ where ΔD_i

represent the difference between descriptor values for mutant and wild-type $Ca_V1.2$. Weighting factors (a and b) were used to estimate the contribution of each descriptor to correlation.

1.2.7 Correlating Amino Acid Properties with ΔG

ΔG in the mutant channels relative to WT channel was calculated according to the equation:

$$\Delta G = RT \left(\frac{V_{0.5,mut}}{k_{mut}} - \frac{V_{0.5,WT}}{k_{WT}} \right) \tag{1.3}$$

with $V_{0.5}$ representing the voltage of half activation and k the slope of the curve at $V_{0.5}$. The shifts of the steady-state activation curves (ΔV_{act}) of the $Ca_V1.2$ mutants compared to wild-type channels and the calculated changes in free energy ΔG were plotted against the descriptor values and analyzed as described above for ΔV_{act}.

1.2.8 Conservation Analysis

Sequences of voltage-gated calcium channels were downloaded from the International Union of Basic and Clinical Pharmacology data base (Harmar et al., 2009). Sequences of all channels from *Homo sapiens* were used to search NCBI BLAST (blastp, Altschul et al., 1990). Initial sequence alignment was performed using ClustalW (Chenna et al., 2003). Sequences of selected potassium channel crystal structures (KcsA, MthK, K_VAP, $K_V1.2$, and MlotiK, NavAb) were aligned manually with Ca_V channels using GENEDOC (Nicholas, K.B., Nicholas H.B. Jr., and Deerfield, D.W. II., 1997).

1.2.9 Homology Modeling

The homology models of the open $Ca_V1.2$ channels are based on different crystal structures of potassium and sodium channels (for details see each manuscript). The models of the closed conformation using the same alignment as for the open conformation were generated using Modeller9v7 (Eswar et al., 2007).

1.2.10 Accessibility Calculations

Amino acid accessibilities were calculated using the WHAT IF webserver (Vriend, 1990). The accessible surface area in this program is defined as the area at the Van der Waals surface that is accessible by a water molecule (1.4 Å). The unit of accessible surface is $Å^2$. Re-entrant surfaces are not considered by WHAT IF.

1.2.11 Confocal Imaging

Images were obtained 30 h after transfection. The images were acquired with a Zeiss Axiovert 200 M microscope equipped with an LSM 510 laser scanning module, using a 63× (1.4 NA) oil immersion objective. Fluorescence from GFP-tagged $Ca_V1.2$ α_1-subunits was excited at 488 nm using an argon laser, and emitted light was recorded with a $505 - 530$ nm bandpass filter. The plasma membrane was stained with 2 µm FM4-64 (an amphiphilic styryl dye, Molecular Probes). The dye was detected with a helium-neon laser (excitation, 543 nm) in combination with a 650 nm long pass filter. The instrument was operated in the multitracking mode to minimize channel cross-talk. Pinholes were adjusted to obtain optical slices of 1 µm thickness for each channel.

1.3 Structure

1.3.1 Topology of Voltage Gated Calcium Channels

Voltage gated calcium channels are integral multi-subunit membrane-protein complexes, which comprise five distinct polypeptides designated the α_1 conduction pore and the auxiliary subunits $\alpha_2\delta$ (two subunits that derive from a single gene product, which are proteolytically cleaved and then disulfide-bonded to each other in the native state), β and γ (found in skeletal muscles, Striessnig, 1999, Snutch, 2009). Expression and kinetics of α_1-subunits are modulated by auxiliary $\alpha_2\delta$, β and γ-subunits (Gurnett et al., 1996). A scheme for calcium channels is shown in Fig. 1.2.

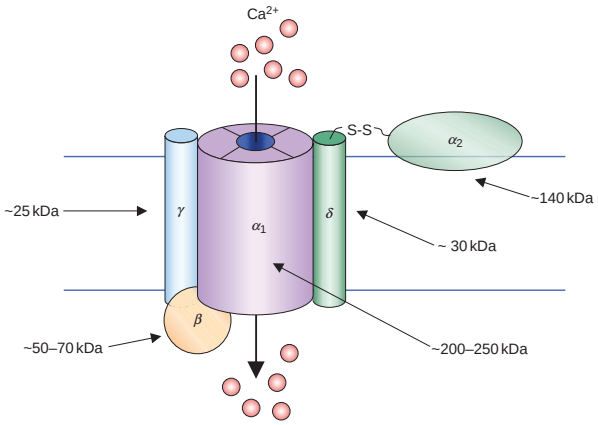

Figure 1.2: In T-tubule membranes of skeletal muscle the voltage gated calcium channel is composed of four subunits α_1, β, $\alpha_2\delta$ and γ. The main subunit that conducts calcium ions has a molecular weight of $200 - 250$ kDa (Snutch, 2009).

Ten genetically different pore-forming α_1-subunits ($200 - 250$ kDa, Ertel et al., 2000b) contain four homologous domains with heterologous sequences each possessing six α-helical transmembrane segments (S1-S6) that are linked together on a single polypeptide (Hofmann et al., 1999, Catterall et al., 2005).

The pore-forming α_1-subunits (Fig. 1.3) of voltage gated calcium channels (Ca_V) carry voltage-sensing S_4 segments which contain positively charged lysine or arginine residues at every third or fourth position (Catterall, 2000). Voltage-gated calcium channels are evolutionary related to voltage-gated sodium and voltage-gated potassium channels. It is assumed that they too consist of four domains which form one channel proper (Catterall et al., 2005). Since no crystal structure of voltage gated calcium channels is available, homology models that are based on crystal structures of related ion channels are used as tool for structure-activity studies.

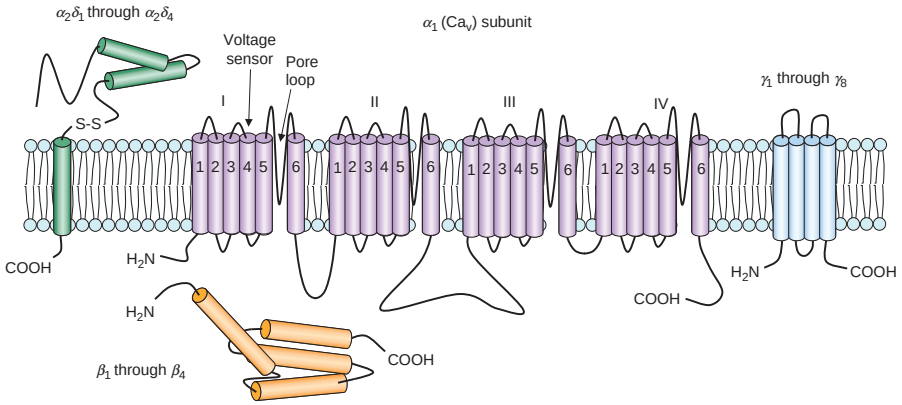

Figure 1.3: Schematic diagram of the α_1-subunit and ancillary subunits of a voltage gated calcium channel (Snutch, 2009). The conducting α_1-subunit is encoded by a single gene which consists of four domains each possessing six α-helical transmembrane helices (S1-S6). At every third and fourth position the S4 segments contain positively charged arginine and lysine residues that are necessary for voltage sensing. The intracellular β-subunit, the transmembrane $\alpha_2\delta$ subunit and the γ-subunit are auxiliary subunits.

In analogy to the crystal structures of voltage gated sodium and potassium channels (Doyle et al., 1998, Long et al., 2007, Payandeh et al., 2011), it is assumed that helices S5 and S6 of the four domains, the P-helix and the loop that connects the helices, form a central pore domain, which contains the Ca^{2+}-selective pathway for ions and the gates of the channel. It is assumed that the pore-lining S6 helices in $Ca_V1.2$ form a bundle-crossing region near the inner channel mouth (Fig. 1.4, Beyl et al., 2009).

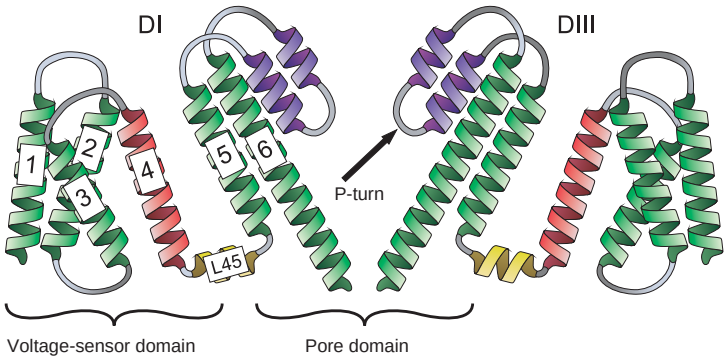

Figure 1.4: The location of the voltage sensing module S1-S4 in two domains is shown. P-helices lie between segments S5 and S6 and form the selectivity filter. The linker connects the voltage sensing segment S4 and the pore forming segment S5 (Senatore et al., 2012).

1.3.2 Crystal Structures of Voltage Gated Potassium and Sodium Channels and Topology of Voltage Gated Potassium and Sodium Channels

Many structures for different conformational states of sodium and potassium channels have been crystallized.

KcsA, NaK, MlotiK, NavAb, $K_{ir}2.2$, $K_{ir}3.1$ chimera, $K_{ir}3.2$, KirBac1.1 and NavAb have been crystalized with a closed activation gate. Open state crystal structures are available for MthK, K_VAP, $K_V1.2$, NaK, K_{ir}Bac3.1 and KcsA (open-inactivated).

Voltage gated potassium channels consist of four identical subunits with six transmembrane spanning segments S1 – S6 (Fig. 1.5). The voltage sensing domains arrange segments S1 – S4, S5 and S6 comprise the pore domain. The re-entrant loop between P-helix and S6 segment serves as selectivity filter. It is located between segments S5 and S6 (see Fig. 1.6 and Fig. 1.7).

1.3.3 Selectivity Filter of Potassium Channels

In 1998 the first potassium channel KcsA from *Streptomyces lividans* was crystallized (Doyle et al., 1998). This bacterial channel without voltage sensing domains and the two transmembrane pore modules provided first insights into selectivity of a potassium channel.

All crystallized selectivity filters of potassium channels show that the carbonyl-backbone oxygen atoms line the narrowest part of the selectivity filter (Fig. 1.8). Each potassium ion has to be dehydrated when entering the selectivity filter. Inside the filter, each ion is then separated by a water molecule. The common pore facing motif in potassium channels in the selectivity filter is T/S-X-G-Y/F-G (X is any hydrophobic residue).

1.3.4 Selectivity Filter of Na_V and Ca_V

Voltage gated sodium channels consist of a single polypeptide and four homologous domains while voltage gated calcium channels contain four heterologous domains with 6 transmembrane segments S1 – S6. They fold into the same general architecture as potassium channels.

The first crystal structure of a voltage gated sodium channel (Fig. 1.9, Payandeh et al., 2011) provides the foundation for understanding the mechanism of selectivity of Na_V and Ca_V channels. The selectivity filter in NavAb is very electronegative,

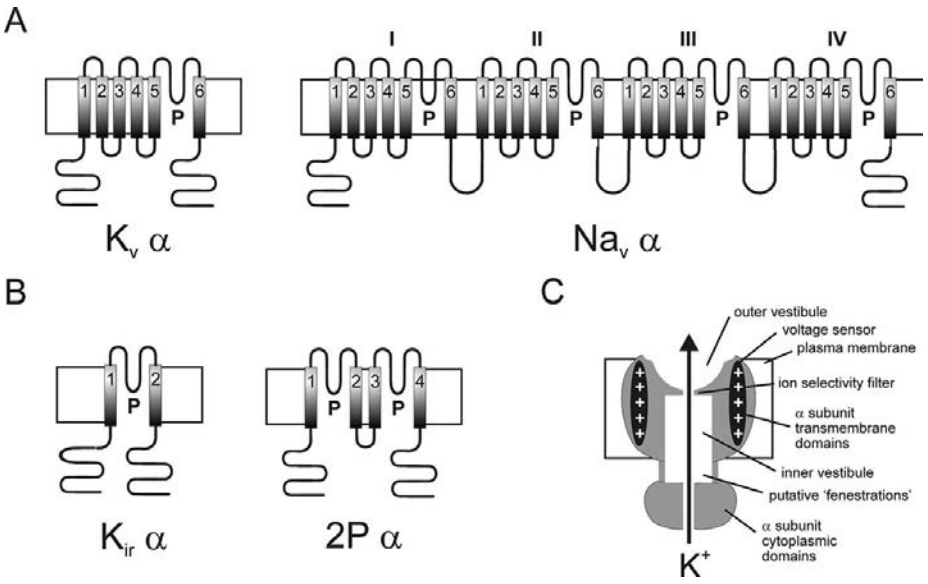

Figure 1.5: Potassium and sodium channel topologies (McCrossan and Abbott, 2004)
A, Schematic representation of a voltage gated sodium (Na_V) and potassium channel (K_V) α-subunits. Each subunit consists of six transmembrane spanning segments. Na_V channels have four identical domains that are linked together on a single polypeptide that comprises the pore while K_V channels contain four non linked homologous domains.
B, Schematic representation of an α-subunit of an inward rectifier (K_{ir}) and a two pore domain (2P) potassium channel. K_{ir} channels consist of two transmembrane segments and one pore region and 2P channels are composed of four transmembrane spanning domains and two pore regions. Four domains arrange the potassium conduction pore.
C, The cross section of one potassium channel shows the pathway of potassium ions through the channel.

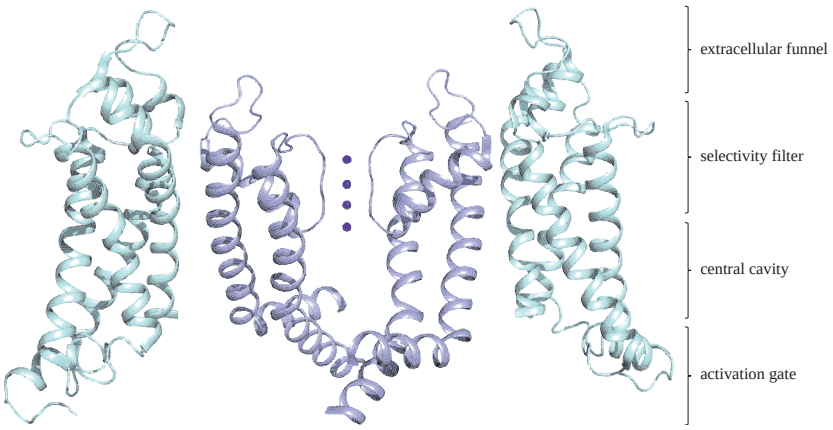

Figure 1.6: Side view of the open $K_V1.2$ conformation crystal structure found with the pdb identifier accession number 2r9r (Long et al., 2007). Here the voltage sensing domains are not in the same domain as the S5 and S6 segments.

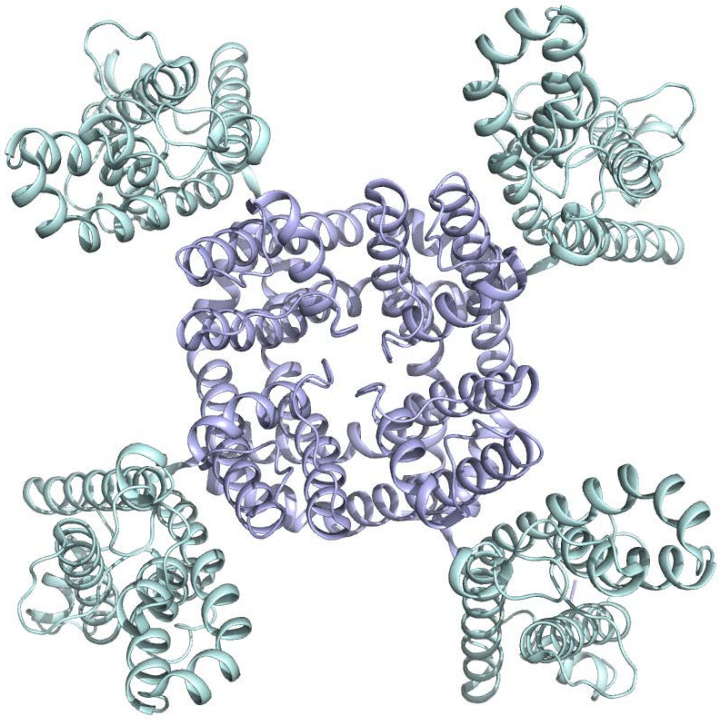

Figure 1.7: Top view of the open $K_V1.2$ conformation crystal structure (Long et al., 2007).

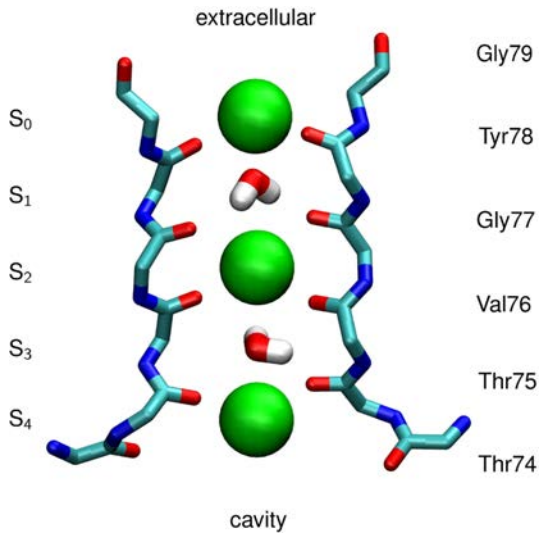

Figure 1.8: The K_V selectivity filter. The green spheres indicate potassium ions. They are separated by water molecules. This illustration was created with PyMol (pdb identifier accession number 1k4c).

four glutamate side chains line the cavity. In HVA (high-voltage activated) calcium channels also four glutamine residues (E413, E731, E1140, E1141 in $Ca_V1.2$ (Biel et al., 1990)) are responsible for ion selectivity. The filter in NavAb is much wider than that of known potassium channels. This filter contains only two rings of carbonyl oxygen atoms at the intracellular side, which are formed by threonine and leucine residues. In the upper part of the filter region four glutamate and four serine side chains are orientated towards the lumen. Since sodium ions were not co-crystallized, the exact mechanism of sodium interaction with the filter is currently unknown. Several investigations are ongoing. It was found, that permeating sodium ions are only partially dehydrated when entering the filter. Three putative binding sides have been identified in the crystal structure which are denoted as S_{HFS}, S_{CEN} and S_{IN} (Fig. 1.10).

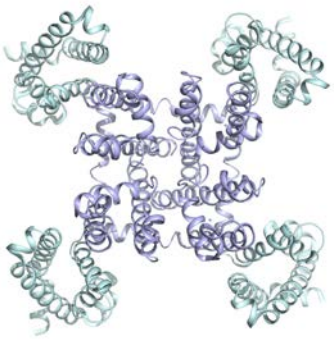

Figure 1.9: The top view of NavAb (Payandeh et al., 2011). Side view of NavAb closed conformation pdb identifier.

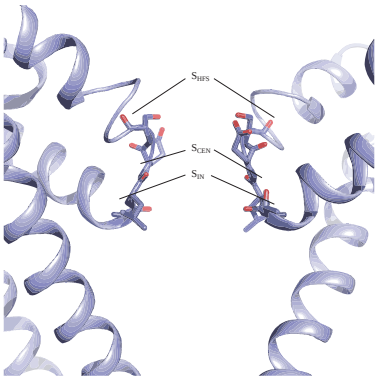

Figure 1.10: The Na_V selectivity filter: The carboxyl-oxygen atoms from residues Thr175 (S_{IN}), Leu176 (S_{CEN}) and Glu177 (S_{HFS}) are interacting with water molecules from the hydration shell of sodium ions (Furini and Domene, 2012).

1.3.5 Pore Gating

No transmembrane spanning segments of voltage gated calcium channels have been crystallized so far. A comparison of the different gating conformational changes of K_V channels provides insights into the conformation of the activation gate changes during gating. In contrast to closed structures the inner helices of the open structures splay open at a highly flexible conserved glycine residue (Fig. 1.11). Thus, several groups proposed that this glycine functions as a hinge for pore opening (Armstrong, 2003, Webster et al., 2004, Zhao et al., 2004, Jiang et al., 2002). However, mutational studies in different ion channels showed that replacement of this glycine by alanine does not always disturb gating (Hardman et al., 2007, Raybaud et al., 2006, Hohaus et al., 2005, Hering et al., 2008). In $Ca_V1.2$ IS6 a proline mutation in position G422 produced non-functional currents (Kudrnac et al., 2009).

```
Cav1.2 I      ELPWVYFVSLVIFGSFFVLNLVLGVISGEFS
Cav2.1 I      TWNWLYFIPLIIIGSFFMLNLVLGVLSGEFA
Cav3.1 I      FYNFIYFILLIIVGSFFMINLCLVVIATQFS
Cav1.2 II     MLVCIYFIILFICGNYILLNVFLAIAVDNLA
Cav2.1 II     MVFSIYFIVLTLFGNYTLLNVFLAIAVDNLA
Cav3.1 II     SWAALYFIALMTFGNYVLFNLLVAILVEGFQ
KcsA          LWGRLVAVVVMVAGITSFG-LVTAALATWFV
MlotiK        FAGRVLAGAVMMSGIGIFG-LWAGILATGFY
Kv1.2         IGGKIVGSLCAIAGVLTIA-LPVPVIVSNFN
KvAP          PIGKVIGIAVMLTGISALT-LLIGTVSNMFQ
```

Figure 1.11: Multiple sequence alignment of S6 helices of Ca_V channels with selected K^+ channels. The glycine residues that were thought to act as glycine hinges are shaded red.

Since no crystal structures of the transmembrane regions of Ca_V channels are available, homology models have been constructed in our lab over the last years (Stary et al., 2008, Kudrnac et al., 2009, Depil et al., 2011, Beyl in revision). All these models were based on potassium channel structures and NachBac models (Shafrir et al., 2008a). The most recent models are based on the NavAb channel (which is evolutionary closer to the Ca_V than K_V, Payandeh et al., 2011).

1.3.6 Voltage Sensors

The S4 helix of voltage gated ion channels is the main voltage sensing segment containing positively charged arginines or lysines at every third position (Aggarwal and MacKinnon, 1996, Seoh et al., 1996). Neutralization of these charges by side directed

mutagenesis provided definitive evidence that these positive charges are the primary charges that are translocated across the electric field of the membrane during gating (Logothtis et al., 1992, Stühmer et al., 1989). Further mutational studies suggested an important role of negatively charged residues in helix S2 (Aggarwal and MacKinnon, 1996). How gating charges move through the lipid bilayer is still an open question.

Several mechanisms have been suggested over the last years: The sliding helix model (Fig. 1.12 A, Catterall, 1986, Catterall, 2010), the helical screw model (Guy and Seetharamulu, 1986) and the paddle model (Fig. 1.12 B, Jiang et al., 2003).

The former two models suggest that the S4 segment is stabilized by forming sequential ion pairs with negatively charged amino acids from helices S1 – S3 (Papazian et al., 1995, DeCaen et al., 2008, 2009). The paddle model is based on a misfolded crystal structure of the voltage gated potassium channel KvAP (Jiang, 2003). The S4 and C terminal half of S3 were suggested to form a paddle like structure that moves more than 20 Å through the lipid bilayer. In this structure the voltage sensing segments were lying nearly parallel to the membrane and the channel was in a non-native state (MacKinnon, 2005). Besides, the paddle model was at odds with a large body of experimental labelling and toxin studies (Larsson et al., 1996, Ahern and Horn, 2004). However, when the $K_V1.2$ channel with a voltage sensor was crystallized, the S4-Segment was in a transmembrane position. A separation of voltage sensing and pore-forming modules was found. All voltage sensors apparently interact with pore-forming segments (Long et al., 2005).

In recent years the helical screw model was updated based on newly available crystal structures (Long et al., 2005, Clayton et al. 2008) of the voltage sensor showing that part of S4 can form a 3_{10} helix. Bob Guy revisited the 3_{10} hypothesis of Noda et al (Noda et al., 1984). His group thus suggested that elastic properties might allow a stretching transition of the alpha helix to 3_{10} or a spring back transition from 3_{10} to α-helix in response to voltage changes (Shafrir et al., 2008b). A recently published MD-simulation study shows that an outward motion of S4 tightens the linker and perturbs packing of the linker-S6 helix while linker S6 repacking stabilizes the pore (Jensen et al., 2012). During relaxation the inward S4 helix motion (51 Å) of $K_V1.2/K_V2.1$ "paddle chimera" channel completes the transition. This simulation is in agreement with the helical screw model.

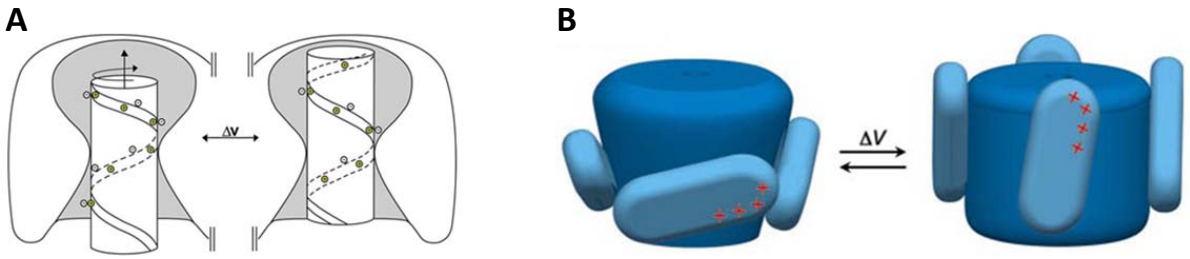

Figure 1.12: Different models of voltage sensing.
A, The sliding helix model (Catterall, 1986). Outward movement of S4 due to sequential formation of ion-pairs that pull the S4-S5-linker and open the pore.
B, The paddle model (Jiang et al., 2003). The S4-S3 paddles are nearly parallel to the membrane and need a large translocation to open the pore.

1.4 Nomenclature of Voltage-Gated Calcium Channels

An unified nomenclature of voltage-gated calcium channels has been proposed in 1994 (Birnbaumer et al., 1994). α_1-subunits were named as α_{1s}-subunit for the skeletal muscle and α_{1a}-subunit through α_{1e} according to their discovery.

Since new channels were cloned, this nomenclature created confusion because there were no structural relationships between the alphabetically grouped subunits. Therefore the sequence identity of the calcium channel family was defined and the families were divided in subfamilies. Thus a numerical nomenclature was created (see Tab. 1.1, Ertel et al., 2000a). The chemical symbol of the permeating ion with the physiological regulator as a subscript was proposed. The number after the ion describes the gene family (1-3) followed by the number of the subfamily (1-4).

The phylogenetic tree in Fig. 1.13 shows the sequence similarity of all calcium channel α_1-subunits. These are grouped into three interrelated subtypes. Interestingly, the genetic resemblance of the most primitive calcium channels from sponge and choanoflagellates (i.e. Amphimedon, Salpingoeca) to L-type channels is very strong. Ten different genes code for mammalian calcium channels.

The membrane-spanning segments and pore loops (about 350 amino acids) are compared. The sequence identities (Fig. 1.14) among the families are above eighty percent (Ca_V1, Ca_V2, and Ca_V3). The consensus sequence between the subfamilies is about 52 % (Ca_V1 vs. Ca_V2) and 28 % (Ca_V3 vs. Ca_V1 or Ca_V2, Catterall et al., 2005). Subtype specific second messenger dependent modulations occur in the highly divergent regions.

Table 1.1: Proposed nomenclature for cloned voltage-gated calcium channel α_1-subunits. In the case of different splice variants lower-case letters are put behind the subscribe of the α_1-subunit (Ertel et al., 2000a).

Name	**Gene Name**	**Splice Types**	**Tissue Distribution**
$Ca_V1.1$ ($\alpha_1 1.1$)	CACNA1S		Skeletal muscle
$Ca_V1.2$ ($\alpha_1 1.2$)	CACNA1C	$Ca_V1.2a$	Heart
		$Ca_V1.2b$	Smooth muscle
		$Ca_V1.2c$	Brain, heart, pituitary, adrenal
$Ca_V1.3$ ($\alpha_1 1.3$)	CACNA1D		Brain, pancreas, kidney, ovary, cochlea
$Ca_V1.4$ ($\alpha_1 1.4$)	CACNA1F		Retina
$Ca_V2.1$ ($\alpha_1 2.1$)	CACNA1A	$Ca_V2.1a$	Brain, cochlea, pituitary
		$Ca_V2.1b$	Brain, cochlea, pituitary
$Ca_V2.2$ ($\alpha_1 2.2$)	CACNA1B	$Ca_V2.2a$	Brain, nervous system
		$Ca_V2.2b$	Brain, nervous system
$Ca_V2.3$ ($\alpha_1 2.3$)	CACNA1E	$Ca_V2.3a$	Brain, cochlea, retina, heart, pituitary
		$Ca_V2.3b$	Brain, cochlea, retina
$Ca_V3.1$ ($\alpha_1 3.1$)	CACNA1G	$Ca_V3.1a$	Brain, nervous system
$Ca_V3.2$ ($\alpha_1 3.2$)	CACNA1H	$Ca_V3.2a$	Brain, heart, kidney, liver
$Ca_V3.3$ ($\alpha_1 3.3$)	CACNA1I	$Ca_V3.3a$	Brain

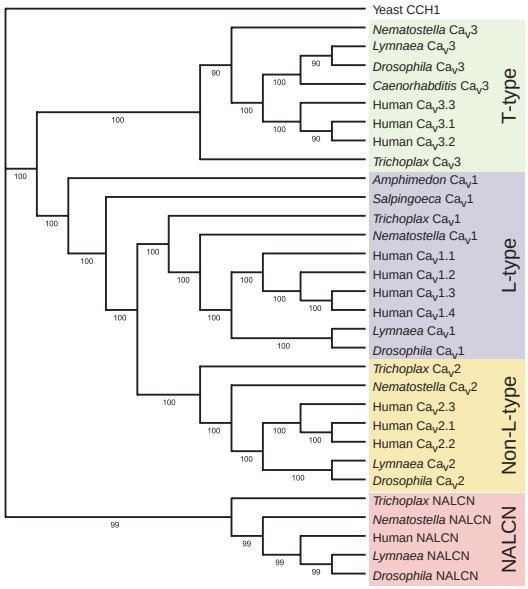

Figure 1.13: Phylogenetic tree (Senatore et al., 2012)

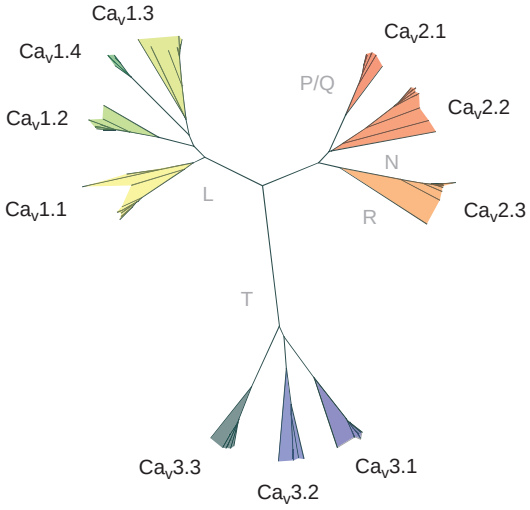

Figure 1.14: Dendrogram illustrating the genetic similarity (Perez-Reyes et al., 1992)

1.5 Classification based on Gating and Conduction

Voltage-gated calcium channels have previously been classified based on their activation threshold in high-voltage activated Ca^{2+} channels (HVA, Ca_V1 and Ca_V2 families) and low-voltage activated channels (LVA, Ca_V3 family, Hofmann et al., 1999). The complete classification can be seen in Tab. 1.2.

Low-voltage activated calcium channels (LVA) open in response to small changes from resting potentials (depolarizations) and mediate low-threshold potentials (more positive than $-70\,\mathrm{mV}$). For opening of high voltage activated calcium channels larger membrane depolarisations are required (Perez-Reyes et al., 1992, Catterall et al., 2005). Low-voltage activated channels inactivate fast and calcium independently. They are called T-type channels due to their transient (rapid) kinetics and tiny currents. T-type channels occur in pacemaking cells (Mangoni and Nargeot, 2008).

The activation of high voltage activated channels (HVA) occurs at a membrane potential more positive than $-20\,\mathrm{mV}$. Therefore they require large depolarisation pulses for opening (Catterall et al., 2005). Depending on the co-expressed β-subunits, these channels inactivate at different potentials.

L-type calcium channels are characterized by long-lasting single channel openings and large unitary barium currents (when barium is used as charge carrier). These channels are sensitive to calcium channel blockers such as Dihydropyridines, Phenylalkylamines and Benzothiazepines and have allosterically dinstinct binding sites. N-Type channels are part of the HVA channels and react with ω-Conotoxin-GVIA, while P/Q-Type channels respond to ω-Agatoxin IVA. R-Type channels respond to SNX-482. Several signalling effects of Ca_V-channels are known. Fig. 1.15 illustrates the time-scale of these effects.

1.5.1 $Ca_V1.2$ and its Role in Excitation-Contraction Coupling

The L-type channel $Ca_V1.2$ is widely expressed in our organism (i.e. in myocardial cells (as illustrated in Fig. 1.16, Catterall et al., 2005) but also in nerve cells, endocrine cells). In the myocardium $Ca_V1.2$ channels are involved in cardiac action potential generation and muscle contraction, the so called excitation-contraction coupling (EC). Initially, connexin channels open after depolarization followed by opening of voltage-gated sodium channels which lead to sodium influx. Then depolarization inactivates sodium channels and voltage-gated potassium and L-type calcium channels open. Ca^{2+} (Calcium current $I_{Ca^{2+}}$) entry through $Ca_V1.2$ channels activates Ryanodine receptors (RyR2) of the sarcoplasmatic reticulum (Bers, 2002, Tanabe et al., 1993, Clapham, 2007, Knollmann and Roden, 2008). Calcium further binds to the myofilament protein Troponin C and activates the sarcomere (actine and

Table 1.2: Classification of high and low activated calcium channels (Catterall, 2000).

Type	α_1-Subunit	Tissue Distribution	Major Cellular Functions	Inherited Diseases
L	$Ca_V1.1$	Skeletal muscle; transverse tubules	EC-coupling in skeletal muscle, regulates transcription	HypoPP1, MHS5
	$Ca_V1.2$	Cardiac myocytes; smooth muscle myocytes; endocrine cells; neuronal cell bodies; proximal dendrites	EC-coupling (cardiac, smooth muscle), endocrine secretion, neuronal Ca^{2+} flow in cell bodies and dendrites, regulates enzyme activity and transcription	Timothy syndrome: cardiac arrhythmia with developmental abnormalities and autism spectrum disorders
	$Ca_V1.3$	Endocrine cells; neuronal cell bodies and dendrites; cardiac atrial myocytes and pacemaker cells; cochlear hair cells	Endocrine secretion, cardiac pacemaking, neuronal Ca^{2+} transients in cell bodies and dendrites, auditory transduction	SANDD (sinoatrial node dysfunction and deafness)
	$Ca_V1.4$	Retinal rod and bipolar cells; spinal cord; adrenal gland; mast cells	Neurotransmitter release in visual system	Stationary night blindness
N	$Ca_V2.2$	Nerve terminals and dendrites; neuroendocrine cells	Neurotransmitter release, dendritic signalling	
P/Q	$Ca_V2.1$	Nerve terminals and dendrites; neuroendocrine cells	Neurotransmitter release, dendritic signalling	Familial hemiplegic migraine, cerebellar ataxia
R	$Ca_V2.3$	Neuronal cell bodies and dendrites	Neurotransmitter release, dendritic Ca^{2+} transients	
T	$Ca_V3.1$	Neuronal cell bodies and dendrites; cardiac and smooth muscle myocytes	Pacemaking and repetitive firing	
	$Ca_V3.2$	Neuronal cell bodies and dendrites; cardiac and smooth muscle myocytes	Pacemaking and repetitive firing	Absence seizures
	$Ca_V3.3$	Neuronal cell bodies and dendrites		

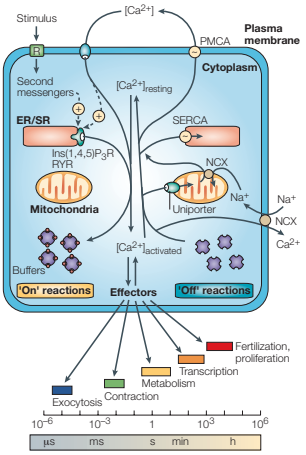

Figure 1.15: Time scale of calcium signalling effects (Berridge et al., 2003).

myosine filaments). Then calcium is transported out of the cytosol by the SERCA calcium-ATPase. Moreover the plasma-membrane calcium-ATPase (PMCA) and the sodium/calcium exchanger (NCX) of the extracellular fluid or the mitochondrial calcium uniport allow cellular relaxation (Bers, 2002).

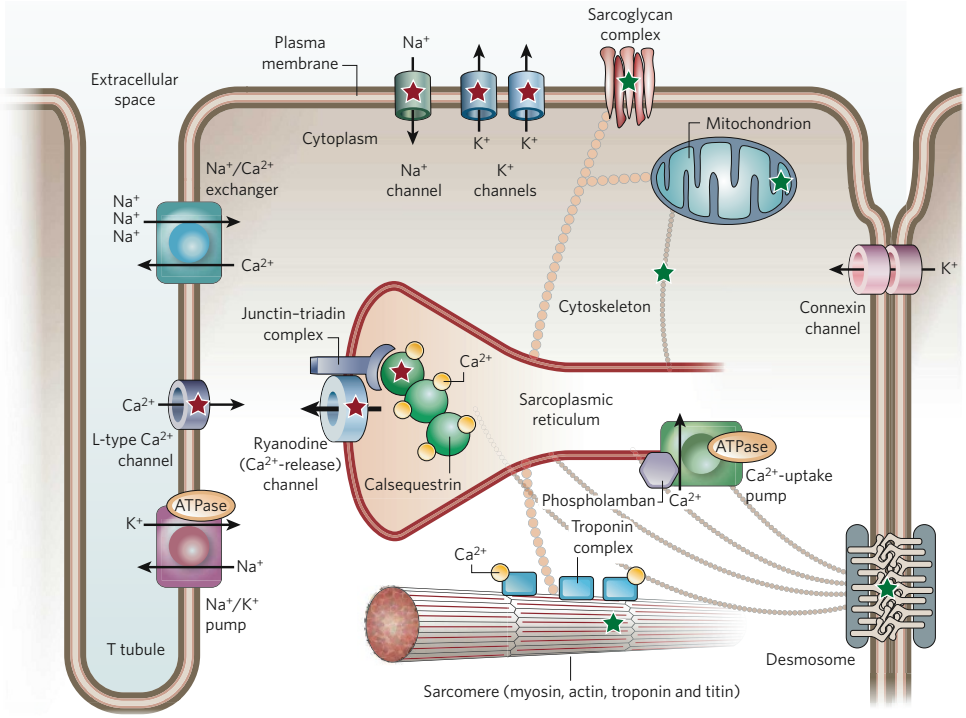

Figure 1.16: Illustration of the cardiomyocyte architecture and intracellular organelles (Knollmann and Roden, 2008).

1.6 Subunits

1.6.1 The $\alpha_2\delta$-Subunits

The highly glycosylated $\alpha_2\delta$-subunit is an auxiliary subunit of voltage-gated calcium channels and binds 1,4-DHPs (dihydropyridine). Sequence analysis showed that α_2 and δ are products of a single gene and separated by proteolytic cleavage. Gabapentin and $\alpha_2\delta$ ligands bind on defined binding sites of this subunit. It was hypothesized that this mechanism is responsible for the anticonvulsant and neurpathic-pain releasing effect of Gabapentin (Gee et al., 1996, Welty et al., 1993).

Four different genes with several splice variants of the $\alpha_2\delta$-subunit are known (Tab. 1.3 Ertel et al., 2000a, Qin et al., 2002, Gao et al., 2000, Klugbauer et al., 1999, Klugbauer et al., 2003, Barclay and Rees, 2000). α_2-1 and α_2-2 are extracellular according to topology mapping (Brodbeck et al., 2002, Gurnett et al., 1996, Brickley et al., 1995, Wiser et al., 1996, Gurnett et al., 1997). The amplitude of a $Ca_V1.2$ current increases up to three times when $\alpha_2\delta$-1 is coexpressed in tsA-201 cells. Furthermore, also activation and inactivation kinetics are found to be accelerated (Felix et al., 1997). Coexpression of the $\alpha_2\delta$-1-subunit enhances membrane trafficking of the α_1-subunit (Felix et al., 1997).

In contrast to the $\alpha_2\delta$-1-subunit, the $\alpha_2\delta$-2 subunit changes the biophysical properties (Gao et al., 2000). The δ-subunit anchors the α_2 protein in the plasma membrane (Fankhauser and Mäser, 2005, Pierleoni et al., 2008). The mechanism of the disulphide linkage of the cysteine bonds between both subunits is still not known. The α_2-subunit interacts extracellularly with the third domain of the α_1-subunit (Gurnett et al., 1997) but there is no interaction between the α_2-subunit and the β- or the γ-subunit known. The $\alpha_2\delta$-subunit contains a Von Willebrand Factor A domain, which is a metal-ion-dependent adhesion site (MIDAS, Cantí et al., 2005). This intact motif is necessary to promote trafficking of the α_1-subunit to the plasma membrane (Cantí et al., 2005). All of the listed different $\alpha_2\delta$-subunits increase the current amplitude. The different functional effects and the tissue distribution are illustrated.

Table 1.3: Effects and tissue distribution of $\alpha_2\delta$ subunits (Arikkath and Campbell, 2003).

Subunit	Functional Effects	Tissue Distribution
$\alpha_2\delta$-1	Membrane trafficking of α_1, increase in current amplitude activation/inactivation kinetics, voltage dependence of activation	Brain, heart, skeletal muscle
$\alpha_2\delta$-2	Increase in current amplitude	Lung, testis, brain, heart, pancreas, prostate, skeletal muscle, spinal cord
$\alpha_2\delta$-3	Increase in current density, voltage dependence of activation, steady state inactivation	Brain, heart, skeletal muscle
$\alpha_2\delta$-4	Increase in current amplitude	Heart, skeletal muscle, intestine, fetal liver erythroblasts, adrenal gland, pituitary

1.6.2 The β-Subunits

Four different genes with a number of splice variants of the β-subunit have been cloned (Helton and Horne, 2002). The first β-subunit was found in the skeletal muscle DHPR (Curtis and Catterall, 1984). The approximately 500 amino acid ($50 - 70$ kDa) containing β-subunit is located intracellularly.

This subunit consists of five different domains. The two central domains C1 and C2 are conserved among all β-subunits and build the functional core (Hanlon et al., 1999, Van Petegem and Minor, 2006). Additionally three variable domains V1, V2, V3 exist in this protein. An SH3 (Src homology 3 domain) and an NK (nucleotide kinase or guanylate kinase GK) domain are formed by the two conserved domains C1 and C2. These two domains are connected by a HOOK region and form the SH3-HOOK-GK module (Chen et al., 2004). β-subunits have structural features like the membrane-associated guanylate kinases (MAGUK) but miss some essential MAGUK domains and differ in the relative orientation (Opatowsky et al., 2004, Chen et al., 2004, Van Petegem et al., 2004). The conserved α-Interaction-Domain in the α_1 subunit mediates the association of the β-subunit. The AID is located in the Ca_V I-II intracellular loop of α_1-subunits (Van Petegem et al., 2004). Fig. 1.17 shows the Cavb-AID complex structure (Van Petegem and Minor, 2006). The AID binds

at the distal end of the NK domain (alpha binding pocket, ABP) through eighteen amino acids including two aromatic residues. The β-subunit has an important role for the expression of the α_1-subunit. It reverses the signal of the Ca_V I-II loop (that contains an endoplasmatic reticulum (ER) retention signal) that would restrict the plasma membrane incorporation of α_1-subunit (Bichet et al., 2000).

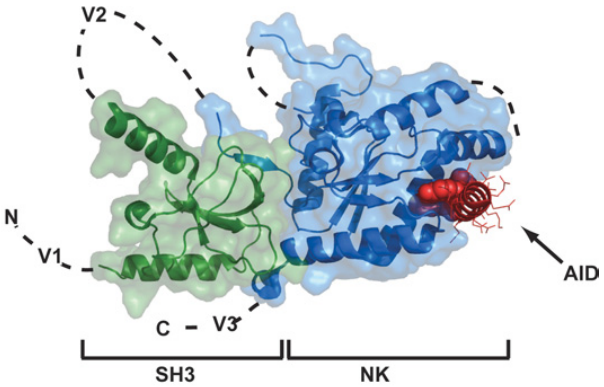

Figure 1.17: The Cavb-AID complex structure (Van Petegem and Minor, 2006).

In Tab. 1.4 different types of β-subunits are listed.

1.6.3 The γ-Subunits

In the mammalian genome eight genes encoding γ-subunits ($\gamma_1 - \gamma_8$) have been identified (Kang and Campbell, 2003). γ-subunits are associated with the voltage-gated channel complex (Jay et al., 1990). All γ-subunits have a conserved four transmembrane domain topology with an intracellular amino- and carboxyl terminus. The γ_2- and γ_4-subunits shift the voltage dependence of inactivation to hyperpolarized potentials (Klugbauer et al., 2000). γ_2, γ_3, γ_4 and γ_8 are necessary for targeting the channel to the membrane. Trafficking of AMPA receptors is modulated by γ_2-subunits which are collectively known as TARPs (transmembrane AMPA receptor regulatory proteins, Chen et al., 2007, Payne, 2008).

A structural similarity between a γ_2s and a protein named *stargazing* (located in the synaptic plasma membrane) was identified. These two proteins are encoded by the same gene. Mutated γ_2 causes the stargazer mouse phenotype including absence epilepsy, defects in the inner ear and in the cerebellum (Letts et al., 1998). Although γ-subunits are located in many tissues, the γ_1-subunit is only expressed in the skeletal muscle (Arikkath and Campbell, 2003). This table shows the tissue distribution and the functional effects of all eight different γ-subunits (Tab. 1.5).

Table 1.4: Effects and tissue distribution of β-subunits (Arikkath and Campbell, 2003, Buraei and Yang, 2010).

Subunit	Functional Effects	Tissue Distribution
β_1	Skeletal excitation–contraction coupling, membrane trafficking of α_1, targeting of $\alpha_1 1.1$ to triads, increase in current amplitude activation/inactivation kinetics, accelerates inactivation by factor $2-10$	β_{1a}-skeletal muscle, brain (other isoforms)
β_2	Accelerates activation by 2- to 4-fold, β_{2a} slows inactivation by ≈10-fold, other β_2 inactivation is accelerated except with β_{2e}, targeting of $\alpha_1 1.4$ in retina, membrane trafficking of α_1	Heart, lung, trachea, aorta, brain
β_3	Increase in current amplitude activation/inactivation kinetics, membrane trafficking of α_1	Smooth muscle, trachea, aorta, lung, brain
β_4	Increase in current amplitude, activation/inactivation kinetics, membrane trafficking of α_1	Brain

Table 1.5: Effects and tissue distribution of γ-subunits (Arikkath and Campbell, 2003, Buraei and Yang, 2010).

Subunit	**Functional Effects**	**Tissue Distribution**
γ_1	Inhibitory effect, activation/inactivation kinetics	Skeletal muscle
γ_2	Inhibitory effect, activation/inactivation kinetics, trafficking of AMPA receptor	Brain
γ_3	Activation/inactivation kinetics	Brain
γ_4	Inactivation kinetics	Heart, lung, brain, prostate, spinal cord
γ_5	Unknown	Brain
γ_6	Reduction of current amplitude (low voltage-gated calcium channel)	Heart, skeletal muscle, brain
γ_7	Reduction of current amplitude	Brain, heart, lung, testis
γ_8	Unknown	Brain, testis, spinal cord

1.7 Inactivation

1.7.1 Voltage Dependent Inactivation

Fast inactivation of $Ca_V1.2$ prevents calcium overload during depolarization of an action potential. After opening the channels enter a non-conducting state called "inactivation". In the inactivated state the binding affinity of many calcium channel blockers is higher than in the closed (resting) state (Bean, 1984). β-subunits are involved in the voltage dependence of inactivation (VDI). It is known that voltage gated calcium channels inactivate even if they do not interact with ancillary subunits. Inactivation is therefore an intrinsic mechanism of the α_1-subunit (Birnbaumer et al., 1994).

A "Ball and Chain mechanism of inactivation" model for voltage gated sodium channels was developed by Armstrong et al. (Armstrong et al., 1973). In the cytoplasmic side of the cell a ball occludes the channel pore of the α_1-subunit.

To investigate inactivation in Ca_V channels in detail, chimeras of $Ca_V1.2$ (slow inactivating) and $Ca_V2.3$ (fast inactivating) were constructed. The $Ca_V1.2/Ca_V2.3$ chimera inactivated rapidly (Stotz et al., 2000). However, $Ca_V2.3$ was only turned into a slow inactivating channel when IIS6, IIIS6 and the domain I-II linker were substituted by $Ca_V1.2$ sequences. This suggests the domain I-II linker has an important role in inactivation. This linker could function as a gating hinge because over-expression of this segment in $Ca_V2.1$ accelerates inactivation kinetics. Several studies have shown that all four S6 segments contribute to voltage dependent inactivation. Mutating M1811Q in IVS6 accelerates and V1818 slows inactivation kinetic rates in $Ca_V2.1$ (Berjukow et al., 2001). Replacement of F823 in IIS6 of $Ca_V1.2$ by residues with increasing size slows inactivation (Stotz and Zamponi, 2001).

Geib et al. suggest that interactions between the domain I-II linker and the III-IV linker of $Ca_V2.1$ are necessary for voltage dependent inactivation (Geib et al., 2002). Moreover, the N-terminal (Stephens et al., 2000) and the C-terminal region (Soldatov et al., 1998, Sandoz et al., 2001) have an important function in the regulation of inactivation.

Co-expression of β-subunits affects the voltage dependence of activation of HVA channels (Birnbaumer et al., 1994) and enhances the activation and inactivation (except of β_{2a} and β_{2e}) kinetics of these channels.

Slow inactivation of the isoform β_{2a}-subunit is determined by structural elements in the N-terminus. The slow inactivation effect can be removed when eighteen residues in this region are deleted (Olcese et al., 1994). Two cysteine residues are important for palmitoylation of the β_{2a}-subunit.

Finally it was hypothesized that the domain I-II linker acts as a hinge lid (Stotz et al., 2000, Stotz and Zamponi, 2001). The mobility of the putative "inactivation gate" is restricted when the domain I-II linker associates with the β-subunit or alternatively the β-subunit interacts indirectly with the N- and C-terminus (Stephens et al., 2000, Sandoz et al., 2001).

β_3-subunits accelerate the rate of inactivation (Hering et al., 2002).

Fig. 1.18 illustrates, that the slowest inactivation is induced by β_{2a}-subunit and the fastest inactivation by β_3- or β_{1b}-subunits.

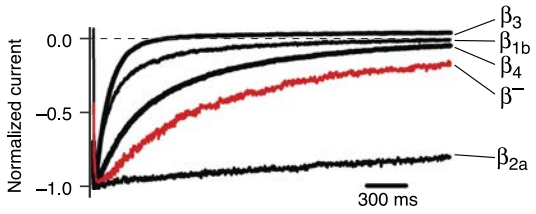

Figure 1.18: Current traces with 300 ms pulses to +30 mV showing voltage-gated inactivation kinetics (Buraei and Yang, 2010).

1.7.2 Calcium/Calmodulin Dependent Inactivation CDI

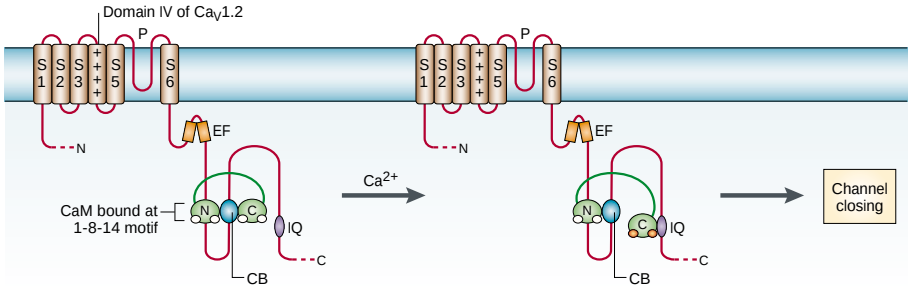

Figure 1.19: Model of CDI induction by CaM in $Ca_V1.2$ Ca^{2+} channels (Budde et al., 2002).

The calcium sensor Calmodulin plays a critical role in voltage dependent inactivation. It functions as negative calcium feedback signal facilitating inactivation in high voltage activated calcium channels. Calcium dependent inactivation (CDI) (Fig. 1.19) is a key determinant for the length of the cardiac action potential plateau. Calmodulin has a C- and an N-terminal lobe, two with low and two with high affinity for calcium ions ("EF-hands", Chin and Means, 2000). The two lobes are connected by

an eight-turn α-helix. At low concentrations of intracellular calcium, free Calmodulin (Apocalmodulin) is binding to the carboxy-terminal of calcium channels. A Calmodulin thetering-site is responsible for Ca^{2+} binding (Rhoads and Friedberg, 1997). This site contains residues of the IQ motif and other sequences that are important for CDI (Pitt et al., 2001, Zühlke et al., 1999). It is proposed that the EF-hand in the carboxy-terminal region of calcium channels is important for transduction signals of the Calmodulin binding domain (Anderson, 2001).

After channel activation the amount of intracellular calcium increases and the C-terminal lobe of Calmodulin leads to a structural rearrangement (due to the binding of calcium). A concentration above 1 μM enables binding of the calcium Calmodulin complex with the IQ motif that effects calcium dependent inactivation (Peterson et al., 1999, Alseikhan et al., 2002).

Calcium/Calmodulin dependent facilitation designates an increase in current amplitude after the first channel opening and functions as a positive feedback regulation facilitating Ca^{2+} entry. Facilitation requires the presence of Calmodulin which activates the Calmodulin-dependent kinase II. This enhances channel open probability due to phosphorylation of β_{2a} (Abiria and Colbran, 2010).

1.8 L-Type Calcium Channel Dysfunction Channelopathies

1.8.1 Hypokalemic Periodic Paralysis Type 1 (HypoPP1)

The hypokalemic periodic paralysis type 1 disorder was the first calcium channelopathy that was described in humans (Bidaud et al., 2006). Mutations of two arginine residues (R528 and R1239) in segment S4 of Domain II and IV in $Ca_V1.1$ are linked to the HypoPP1 disorder (Ptácek et al., 1994, Fontaine et al., 1994). Patients affected from HypoPP1 suffer from attacks of paralysis or generalized skeletal muscle weakness, hypotonia, hypokalemia. The disease occurs at the second decade of life (Caciotti et al., 2003). R897S and R900S are two newly identified mutations in the S4 Segment of Domain III that are linked to HypoPP1 (Matthews et al., 2009). The reason for the decrease in serum potassium is currently unclear.

1.8.2 Malignant Hyperthermia Susceptibility Type 5 (MHS5)

Mutations in the CACNA1S gene ($Ca_V1.1$) lead to malignant hyperthermia. This disorder can be provoked by anesthesia or muscle relaxants and induces skeletal muscle rigidity and high fever (MacLennan and Phillips, 1992). Rhabdomyolysis and cardiac arrhythmias, hyperkalemia, and elevation of creatinine kinase may occur (Carpenter et al., 2009). Mutations R1086H or R1086C are located at the intracellular III-IV linker. These mutants induce malignant hyperthermia susceptibility type 5 (Monnier et al., 1997). The interaction of the linker with the Ryanodine receptor (RyR1) III-IV due to conformational changes of $Ca_V1.1$ and a retrograde signalling are supposed to be the reason for the enhancement of calcium in the skeletal muscle (Grabner et al., 1999, Weiss et al., 2004). The two newly identified mutations R174W in IS4 and T1354S in the linker of domain IV are also related to MHS5 and RyR1 calcium release from SR calcium stores although they are located in a transmembrane segment or in an extracellular region (Pirone et al., 2010).

1.8.3 Incomplete Congenital Stationary Night Blindness Type 2

CSNB2 is a form of congenital stationary night blindness caused by mutations in the $Ca_V1.4$ channel (Striessnig et al., 2010). These channels control light dependent calcium influx in photoreceptors (Hoda et al., 2006). The symptoms of CSNB2 are nystagmus, myopia, low visual acuity and night blindness (Boycott et al., 2000, Weiergräber et al., 2008).

If the membrane potential changes at the ribbon synapses of retinal photoreceptors, these cells release neurotransmitter (Striessnig et al., 2010). Darkness depolarizes these channels to -40 mV, calcium influx occurs and triggers the tonic release of glutamate (Hoda et al., 2006). If light is absorbed, cGMP-gated cation channels in the photoreceptor close and the cells hyperpolarize at around -55 mV (Witkovsky et al., 1997). For tonic neurotransmitter release it appears to be important that $Ca_V1.4$ activate rapidly (below -40 mV) and inactivate slowly (Rabl and Thoreson, 2002). In the $Ca_V1.4$ gene of CSNB2 patients more than forty different mutations were discovered and some of them lead to truncated α_1-subunits. Since the CSNB2 is X-linked, all affected men have a complete loss of channel function. In contrast to these results mutation G369D leads to a gain of channel function and affects ion selectivity. Interestingly G369D corresponds to the mutated glycine in the Timothy syndrome G406R in $Ca_V1.2$ channels (Splawski et al., 2004) and affects voltage dependent inactivation (VDI, Splawski et al., 2005). However, mutations R508Q and L1364H result in decreased calcium current densities (Hoda et al., 2006). Mutations G674D, A928D and W1459X (a truncation mutation) have no effect on channel gating. S229P, L1068P and W1440X could not be expressed in Xenopus oocytes (Hoda et al., 2005).

In a New Zealand family a visual disorder with severe, non-progressive visual impairment, night blindness and in some cases autism was discovered (Hemara-Wahanui et al., 2005). The gain of function mutation I745T in $Ca_V1.4$ produces a remarkable -30 mV shift in the voltage dependence of channel activation and slower inactivation kinetics (Hemara-Wahanui et al., 2005). The shift in channel activation increases the percentage of open channels. Reduced inactivation supports calcium entry so that glutamate release is higher than normal during darkness and continues to inhibit postsynaptic cells during light stimuli (Hemara-Wahanui et al., 2005).

1.8.4 Brugada Syndrome (BrS3)

The loss of function mutations A39V and G490R occur in the $Ca_V1.2$ channel and are associated with the so called Brugada Syndrome (Antzelevitch et al., 2007). The characteristics of this arrhythmic syndrome are an ST-segment elevation in the right pericardial leas of the ECG and the development of polymorphic ventricular tachycardia that can result in sudden cardiac death (Chen et al., 1998). The QT-intervals of these patients are shorter-than-normal due to the loss of channel function (Antzelevitch et al., 2007).

1.8.5 Sinoatrial Node Dysfunction and Deafness (SANDD)

The $Ca_V1.3$ channel is expressed in the sinoatrial node, in cochlear hair cells, in neurons, adrenal chromaffin cells and pancreatic islets (Striessnig and Koschak, 2008). An insertion of a glycine residue in the highly conserved position G403 in IS6 of $Ca_V1.3$ leads to non-conducting calcium channels with abnormal voltage-dependent gating (Baig et al., 2011). This loss of channel function (insertion) was first found in a Pakistani family that suffered from deafness. Patients with the homozygous mutation (insertion) suffer from and sinoatrial node dysfunction (bradycardia and/or high heart rate variability, Baig et al., 2011, Striessnig and Koschak, 2008).

1.8.6 Timothy Syndrome

Timothy Syndrome (TS), an autosomal dominant disorder, arises from two de novo missense mutations, G402S and G406R, in $Ca_V1.2$ calcium channels (Splawski et al., 2005). This channelopathy manifests itself clinically in physical, neurological, and developmental defects and autism spectrum disorders. G406R additionally causes syndactyly (Splawski et al., 2004). Functional studies have shown that TS mutations G402S and G406R dramatically reduce voltage-dependent channel inactivation. This leads membrane depolarization and increased calcium entry during an action potential (Splawski et al., 2004). The resulting prolongation of the QT interval can induce severe arrhythmias causing sudden death in early childhood (Splawski et al., 2004). Kinetic modelling studies suggested that the increased action potential duration and enhanced calcium entry may be associated with delayed after-depolarizations in cardiac myocytes (Splawski et al., 2005). A role of G406R in calcium-dependent inactivation was established by Raybaud et al. (Raybaud et al., 2006) and Barrett and Tsien (Barrett and Tsien, 2008).

1.9 References

Abiria, S.A., and Colbran, R.J. (2010). CaMKII associates with $Ca_V1.2$ L-type calcium channels via selected beta subunits to enhance regulatory phosphorylation. J. Neurochem. 112, 150–161.

Aggarwal, S.K., and MacKinnon, R. (1996). Contribution of the S4 segment to gating charge in the Shaker K^+ channel. Neuron 16, 1169–1177.

Ahern, C.A., and Horn, R. (2004). Stirring up controversy with a voltage sensor paddle. Trends Neurosci. 27, 303–307.

Alseikhan, B.A., DeMaria, C.D., Colecraft, H.M., and Yue, D.T. (2002). Engineered calmodulins reveal the unexpected eminence of Ca^{2+} channel inactivation in controlling heart excitation. Proc. Natl. Acad. Sci. U.S.A. 99, 17185–17190.

Altschul, S.F., Gish, W., Miller, W., Myers, E.W., and Lipman, D.J. (1990). Basic local alignment search tool. J. Mol. Biol 215, 403–410.

Anderson, M.E. (2001). Ca^{2+}-dependent regulation of cardiac L-type Ca^{2+} channels: is a unifying mechanism at hand? J. Mol. Cell. Cardiol. 33, 639–650.

Antzelevitch, C., Pollevick, G.D., Cordeiro, J.M., Casis, O., Sanguinetti, M.C., Aizawa, Y., Guerchicoff, A., Pfeiffer, R., Oliva, A., Wollnik, B., et al. (2007). Loss-of-Function Mutations in the Cardiac calcium Channel Underlie a New Clinical Entity Characterized by ST-Segment Elevation, Short QT Intervals, and Sudden Cardiac Death. Circulation 115, 442–449.

Arikkath, J., and Campbell, K.P. (2003). Auxiliary subunits: essential components of the voltage-gated calcium channel complex. Curr. Opin. Neurobiol. 13, 298–307.

Armstrong, C.M. (2003). Voltage-gated K channels. Sci. STKE 2003, re10.

Armstrong, C.M., and Bezanilla, F. (1973). Currents related to movement of the gating particles of the sodium channels. Nature 242, 459–461.

Baig, S.M., Koschak, A., Lieb, A., Gebhart, M., Dafinger, C., Nürnberg, G., Ali, A., Ahmad, I., Sinnegger-Brauns, M.J., Brandt, N., et al. (2011). Loss of Ca(v)1.3 (CACNA1D) function in a human channelopathy with bradycardia and congenital deafness. Nat. Neurosci. 14, 77–84.

Barclay, J., and Rees, M. (2000). Genomic organization of the mouse and human alpha2delta2 voltage-dependent calcium channel subunit genes. Mamm. Genome 11, 1142–1144.

Barrett, C.F., and Tsien, R.W. (2008). The Timothy syndrome mutation differentially affects voltage- and calcium-dependent inactivation of $Ca_V1.2$ L-type calcium channels. Proc. Natl. Acad. Sci. U.S.A 105, 2157–2162.

Bean, B.P. (1984). Nitrendipine block of cardiac calcium channels: high-affinity binding to the inactivated state. Proc. Natl. Acad. Sci. U.S.A. 81, 6388-6392.

Berjukow, S., Marksteiner, R., Sokolov, S., Weiss, R.G., Margreiter, E., and Hering, S. (2001). Amino acids in segment IVS6 and beta-subunit interaction support distinct conformational changes during Ca(v)2.1 inactivation. J. Biol. Chem. 276, 17076–17082.

Berridge, M.J., Bootman, M.D., and Roderick, H.L. (2003). calcium signalling: dynamics, homeostasis and remodelling. Nature Reviews Molecular Cell Biology 4, 517–529.

Bers, D.M. (2002). Cardiac excitation-contraction coupling. Nature 415, 198–205.

Beyl, S., Depil, K., Hohaus, A., Stary-Weinzinger, A., Timin, E., Shabbir, W., Kudrnac, M., and Hering, S. (2011). Physicochemical properties of pore residues predict activation gating of Ca V1.2: a correlation mutation analysis. Pflugers Arch 461, 53–63.

Beyl, S., Depil, K., Hohaus, A., Stary-Weinzinger, A., Linder, T., Timin, E., and Hering, S. (2012). Neutraization of a single voltage sensor (IIS4) affects gating determinants in all four pore forming S6 segments of $Ca_V1.2$. J. Gen. Phys., in revision.

Bichet, D., Cornet, V., Geib, S., Carlier, E., Volsen, S., Hoshi, T., Mori, Y., and De Waard, M. (2000). The I-II loop of the Ca^{2+} channel alpha1 subunit contains an endoplasmic reticulum retention signal antagonized by the beta subunit. Neuron 25, 177–190.

Bidaud, I., and Lory, P. (2011). Hallmarks of the channelopathies associated with L-type calcium channels : A focus on the Timothy mutations in $Ca_V1.2$ channels. Biochimie 93, 2080–2086.

Bidaud, I., Mezghrani, A., Swayne, L.A., Monteil, A., and Lory, P. (2006). Voltage-gated calcium channels in genetic diseases. Biochim. Biophys. Acta 1763, 1169–1174.

Biel, M., Ruth, P., Bosse, E., Hullin, R., Stühmer, W., Flockerzi, V., and Hofmann, F. (1990). Primary structure and functional expression of a high voltage activated calcium channel from rabbit lung. FEBS Lett. 269, 409–412.

Birnbaumer, L., Campbell, K.P., Catterall, W.A., Harpold, M.M., Hofmann, F., Horne, W.A., Mori, Y., Schwartz, A., Snutch, T.P., and Tanabe, T. (1994). The naming of voltage-gated calcium channels. Neuron 13, 505–506.

Bokvist, K., Eliasson, L., Ammälä, C., Renström, E., and Rorsman, P. (1995). Co-localization of L-type Ca^{2+} channels and insulin-containing secretory granules and its significance for the initiation of exocytosis in mouse pancreatic B-cells. Embo J. 14, 50–57.

Boycott, K.M., Pearce, W.G., and Bech-Hansen, N.T. (2000). Clinical variability among patients with incomplete X-linked congenital stationary night blindness and a founder mutation in CACNA1F. Can. J. Ophthalmol. 35, 204–213.

Brickley, K., Campbell, V., Berrow, N., Leach, R., Norman, R.I., Wray, D., Dolphin, A.C., and Baldwin, S.A. (1995). Use of site-directed antibodies to probe the topography of the alpha 2 subunit of voltage-gated Ca^{2+} channels. FEBS Lett. 364, 129–133.

Brodbeck, J., Davies, A., Courtney, J.-M., Meir, A., Balaguero, N., Canti, C., Moss, F.J., Page, K.M., Pratt, W.S., Hunt, S.P., et al. (2002). The ducky mutation in Cacna2d2 results in altered Purkinje cell morphology and is associated with the expression of a truncated alpha 2 delta-2 protein with abnormal function. J. Biol. Chem. 277, 7684–7693.

Budde, T., Meuth, S., and Pape, H.-C. (2002). calcium-dependent inactivation of neuronal calcium channels. Nature Reviews Neuroscience 3, 873–883.

Buraei, Z., and Yang, J. (2010). The ß subunit of voltage-gated Ca^{2+} channels. Physiol. Rev. 90, 1461–1506.

Caciotti, A., Morrone, A., Domenici, R., Donati, M.A., and Zammarchi, E. (2003). Severe prognosis in a large family with hypokalemic periodic paralysis. Muscle Nerve 27, 165–169.

Cantí, C., Nieto-Rostro, M., Foucault, I., Heblich, F., Wratten, J., Richards, M.W., Hendrich, J., Douglas, L., Page, K.M., Davies, A., et al. (2005). The metal-ion-dependent adhesion site in the Von Willebrand factor-A domain of alpha2delta subunits is key to trafficking voltage-gated Ca^{2+} channels. Proc. Natl. Acad. Sci. U.S.A. 102, 11230–11235.

Carpenter, D., Ringrose, C., Leo, V., Morris, A., Robinson, R.L., Halsall, P.J., Hopkins, P.M., and Shaw, M.-A. (2009). The role of CACNA1S in predisposition to malignant hyperthermia. BMC Med. Genet. 10, 104.

Catterall, W.A. (1986). Molecular properties of voltage-sensitive sodium channels. Annu. Rev. Biochem. 55, 953–985.

Catterall, W.A. (2000). Structure and regulation of voltage-gated Ca^{2+} channels. Annu. Rev. Cell Dev. Biol. 16, 521–555.

Catterall, W.A., Perez-Reyes, E., Snutch, T.P., and Striessnig, J. (2005). International Union of Pharmacology. XLVIII. Nomenclature and structure-function relationships of voltage-gated calcium channels. Pharmacol. Rev 57, 411–425.

Chen, Q., Kirsch, G.E., Zhang, D., Brugada, R., Brugada, J., Brugada, P., Potenza, D., Moya, A., Borggrefe, M., Breithardt, G., et al. (1998). Genetic basis and molecular mechanism for idiopathic ventricular fibrillation. Nature 392, 293–296.

Chen, R.-S., Deng, T.-C., Garcia, T., Sellers, Z.M., and Best, P.M. (2007). calcium channel gamma subunits: a functionally diverse protein family. Cell Biochem. Biophys. 47, 178–186.

Chen, Y.-H., Li, M.-H., Zhang, Y., He, L.-L., Yamada, Y., Fitzmaurice, A., Shen, Y., Zhang, H., Tong, L., and Yang, J. (2004). Structural basis of the alpha1-beta subunit interaction of voltage-gated Ca^{2+} channels. Nature 429, 675–680.

Chenna, R., Sugawara, H., Koike, T., Lopez, R., Gibson, T.J., Higgins, D.G., and Thompson, J.D. (2003). Multiple sequence alignment with the Clustal series of programs. Nucleic Acids Res 31, 3497–3500.

Chin, D., and Means, A.R. (2000). Calmodulin: a prototypical calcium sensor. Trends Cell Biol. 10, 322–328.

Clapham, D.E. (2007). calcium signaling. Cell 131, 1047–1058.

Cooper, C.L., Vandaele, S., Barhanin, J., Fosset, M., Lazdunski, M., and Hosey, M.M. (1987). Purification and characterization of the dihydropyridine-sensitive voltage-dependent calcium channel from cardiac tissue. J. Biol. Chem. 262, 509–512.

Curtis, B.M., and Catterall, W.A. (1984). Purification of the calcium antagonist receptor of the voltage-sensitive calcium channel from skeletal muscle transverse tubules. Biochemistry 23, 2113–2118.

DeCaen, P.G., Yarov-Yarovoy, V., Sharp, E.M., Scheuer, T., and Catterall, W.A. (2009). Sequential formation of ion pairs during activation of a sodium channel voltage sensor. Proc. Natl. Acad. Sci. USA 106, 22498-22503.

DeCaen, P.G., Yarov-Yarovoy, V., Zhao, Y., Scheuer, T., and Catterall, W.A. (2008). Disulfide locking a sodium channel voltage sensor reveals ion pair formation during activation. Proc. Natl. Acad. Sci. USA 105, 15142-15147.

Depil, K., Beyl, S., Stary-Weinzinger, A., Hohaus, A., Timin, E., and Hering, S. (2011). Timothy mutation disrupts the link between activation and inactivation in Ca(V)1.2 protein. J. Biol. Chem. 286, 31557–31564.

Doyle, D.A., Morais Cabral, J., Pfuetzner, R.A., Kuo, A., Gulbis, J.M., Cohen, S.L., Chait, B.T., and MacKinnon, R. (1998). The structure of the potassium channel: molecular basis of K^+ conduction and selectivity. Science 280, 69–77.

Eisenberg, D., Weiss, R.M., and Terwilliger, T.C. (1984). The hydrophobic moment detects periodicity in protein hydrophobicity. Proc. Natl. Acad. Sci. U.S.A. 81, 140–144.

Ellis, S.B., Williams, M.E., Ways, N.R., Brenner, R., Sharp, A.H., Leung, A.T., Campbell, K.P., McKenna, E., Koch, W.J., and Hui, A. (1988). Sequence and expression of mRNAs encoding the alpha 1 and alpha 2 subunits of a DHP-sensitive calcium channel. Science 241, 1661–1664.

Ertel, E.A., Campbell, K.P., Harpold, M.M., Hofmann, F., Mori, Y., Perez-Reyes, E., Schwartz, A., Snutch, T.P., Tanabe, T., Birnbaumer, L., et al. (2000a). Nomenclature of voltage-gated calcium channels. Neuron 25, 533–535.

Ertel, E.A., Campbell, K.P., Harpold, M.M., Hofmann, F., Mori, Y., Perez-Reyes, E., Schwartz, A., Snutch, T.P., Tanabe, T., Birnbaumer, L., et al. (2000b). Nomenclature of Voltage-Gated calcium Channels. Neuron 25, 533–535.

Eswar, N., Webb, B., Marti-Renom, M.A., Madhusudhan, M.S., Eramian, D., Shen, M.-Y., Pieper, U., and Sali, A. (2007). Comparative protein structure modeling using MODELLER. Curr Protoc Protein Sci Chapter 2, Unit 2.9.

Fankhauser, N., and Mäser, P. (2005). Identification of GPI anchor attachment signals by a Kohonen self-organizing map. Bioinformatics 21, 1846–1852.

Felix, R., Gurnett, C.A., De Waard, M., and Campbell, K.P. (1997). Dissection of functional domains of the voltage-dependent Ca^{2+} channel alpha2delta subunit. J. Neurosci. 17, 6884–6891.

Fontaine, B., Vale-Santos, J., Jurkat-Rott, K., Reboul, J., Plassart, E., Rime, C.-S., Elbaz, A., Heine, R., Guimarães, J., Weissenbach, J., et al. (1994). Mapping of the hypokalaemic periodic paralysis (HypoPP) locus to chromosome 1q31-32 in three European families. Nature Genetics 6, 267–272.

Furini, S., and Domene, C. (2012). On conduction in a bacterial sodium channel. PLoS Comput. Biol. 8, e1002476.

Gao, B., Sekido, Y., Maximov, A., Saad, M., Forgacs, E., Latif, F., Wei, M.H., Lerman, M., Lee, J.H., Perez-Reyes, E., et al. (2000). Functional properties of a new voltage-dependent calcium channel alpha(2)delta auxiliary subunit gene (CACNA2D2). J. Biol. Chem. 275, 12237–12242.

Gee N.S., Brown J.P., Dissanayake V.U.K., Offord J., Thurlow R., Woodruff G.N. (1996). The novel anticonvulsant drug, gabapentin (Neurontin) binds to the $\alpha_2\delta$ subunit of a calcium channel. J. Biol. Chem. 271, 5768–5776.

Geib, S., Sandoz, G., Cornet, V., Mabrouk, K., Fund-Saunier, O., Bichet, D., Villaz, M., Hoshi, T., Sabatier, J.-M., and De Waard, M. (2002). The interaction between the I-II loop and the III-IV loop of $Ca_V2.1$ contributes to voltage-dependent inactivation in a beta -dependent manner. J. Biol. Chem. 277, 10003–10013.

Glossmann, H., and Striessnig, J. (1990). Molecular properties of calcium channels. Rev. Physiol. Biochem. Pharmacol. 114, 1–105.

Gottfries, J., and Eriksson, L. (2010). Extensions to amino acid description. Mol. Divers 14, 709–718.

Grabner, M., Dirksen, R.T., and Beam, K.G. (1998). Tagging with green fluorescent protein reveals a distinct subcellular distribution of L-type and non-L-type Ca^{2+} channels expressed in dysgenic myotubes. Proc. Natl. Acad. Sci. U.S.A 95, 1903–1908.

Grabner, M., Dirksen, R.T., Suda, N., and Beam, K.G. (1999). The II-III loop of the skeletal muscle dihydropyridine receptor is responsible for the Bi-directional coupling with the ryanodine receptor. J. Biol. Chem. 274, 21913–21919.

Gurnett, C.A., Felix, R., and Campbell, K.P. (1997). Extracellular interaction of the voltage-dependent Ca^{2+} channel alpha2delta and alpha1 subunits. J. Biol. Chem. 272, 18508–18512.

Gurnett, C.A., De Waard, M., and Campbell, K.P. (1996). Dual function of the voltage-dependent Ca^{2+} channel alpha 2 delta subunit in current stimulation and subunit interaction. Neuron 16, 431–440.

Guy, H.R. (1985). Amino acid side-chain partition energies and distribution of residues in soluble proteins. Biophys. J. 47, 61–70.

Guy, H.R., and Seetharamulu, P. (1986). Molecular model of the action potential sodium channel. Proc. Natl. Acad. Sci. U.S.A. 83, 508–512.

Hamill, O.P., Marty, A., Neher, E., Sakmann, B., and Sigworth, F.J. (1981). Improved patch-clamp techniques for high-resolution current recording from cells and cell-free membrane patches. Pflugers Arch 391, 85–100.

Hanlon, M.R., Berrow, N.S., Dolphin, A.C., and Wallace, B.A. (1999). Modelling of a voltage-dependent Ca^{2+} channel beta subunit as a basis for understanding its functional properties. FEBS Lett. 445, 366–370.

Hardman, R.M., Stansfeld, P.J., Dalibalta, S., Sutcliffe, M.J., and Mitcheson, J.S. (2007). Activation gating of hERG potassium channels: S6 glycines are not required as gating hinges. J. Biol. Chem 282, 31972–31981.

Harmar, A.J., Hills, R.A., Rosser, E.M., Jones, M., Buneman, O.P., Dunbar, D.R., Greenhill, S.D., Hale, V.A., Sharman, J.L., Bonner, T.I., et al. (2009). IUPHAR-DB: the IUPHAR database of G protein-coupled receptors and ion channels. Nucleic Acids Res 37, D680–685.

Hell, J.W., Westenbroek, R.E., Warner, C., Ahlijanian, M.K., Prystay, W., Gilbert, M.M., Snutch, T.P., and Catterall, W.A. (1993). Identification and differential subcellular localization of the neuronal class C and class D L-type calcium channel alpha 1 subunits. J. Cell Biol. 123, 949–962.

Helton, T.D., and Horne, W.A. (2002). Alternative splicing of the beta 4 subunit has alpha1 subunit subtype-specific effects on Ca^{2+} channel gating. J. Neurosci. 22, 1573–1582.

Hemara-Wahanui, A., Berjukow, S., Hope, C.I., Dearden, P.K., Wu, S.-B., Wilson-Wheeler, J., Sharp, D.M., Lundon-Treweek, P., Clover, G.M., Hoda, J.-C., et al. (2005). A CACNA1F mutation identified in an X-linked retinal disorder shifts the voltage dependence of $Ca_V1.4$ channel activation. Proc. Natl. Acad. Sci. U.S.A. 102, 7553–7558.

Hering, S. (2002). beta-Subunits: fine tuning of Ca^{2+} channel block. Trends Pharmacol. Sci. 23, 509-513.

Hering, S., Berjukow, S., Sokolov, S., Marksteiner, R., Weiss, R.G., Kraus, R., and Timin, E.N. (2000). Molecular determinants of inactivation in voltage-gated Ca^{2+} channels. J. Physiol. (Lond.) 528 Pt 2, 237–249.

Hering, S., Beyl, S., Stary, A., Kudrnac, M., Hohaus, A., Guy, H.R., and Timin, E. (2008). Pore stability and gating in voltage-activated calcium channels. Channels (Austin) 2, 61–69.

Hessa, T., Kim, H., Bihlmaier, K., Lundin, C., Boekel, J., Andersson, H., Nilsson, I., White, S.H., and von Heijne, G. (2005). Recognition of transmembrane helices by the endoplasmic reticulum translocon. Nature 433, 377–381.

Hockerman, G.H., Johnson, B.D., Scheuer, T., and Catterall, W.A. (1995). Molecular determinants of high affinity phenylalkylamine block of L-type calcium channels. J. Biol. Chem 270, 22119–22122.

Hoda, J.-C., Zaghetto, F., Koschak, A., and Striessnig, J. (2005). Congenital stationary night blindness type 2 mutations S229P, G369D, L1068P, and W1440X alter channel gating or functional expression of Ca(v)1.4 L-type Ca^{2+} channels. J. Neurosci. 25, 252–259.

Hoda, J.-C., Zaghetto, F., Singh, A., Koschak, A., and Striessnig, J. (2006). Effects of congenital stationary night blindness type 2 mutations R508Q and L1364H on $Ca_V1.4$ L-type Ca^{2+} channel function and expression. J. Neurochem. 96, 1648–1658.

Hofmann, F., Lacinová, L., and Klugbauer, N. (1999). Voltage-dependent calcium channels: from structure to function. Rev. Physiol. Biochem. Pharmacol. 139, 33–87.

Hohaus, A., Beyl, S., Kudrnac, M., Berjukow, S., Timin, E.N., Marksteiner, R., Maw, M.A., and Hering, S. (2005). Structural determinants of L-type channel activation in segment IIS6 revealed by a retinal disorder. J. Biol. Chem 280, 38471–38477.

Hopp, T.P., and Woods, K.R. (1981). Prediction of protein antigenic determinants from amino acid sequences. Proc. Natl. Acad. Sci. U.S.A. 78, 3824–3828.

Hu, H., and Marban, E. (1998). Isoform-specific inhibition of L-type calcium channels by dihydropyridines is independent of isoform-specific gating properties. Mol. Pharmacol. 53, 902–907.

Jay, S.D., Ellis, S.B., McCue, A.F., Williams, M.E., Vedvick, T.S., Harpold, M.M., and Campbell, K.P. (1990). Primary structure of the gamma subunit of the DHP-sensitive calcium channel from skeletal muscle. Science 248, 490–492.

Jensen, M.Ø., Jogini, V., Borhani, D.W., Leffler, A.E., Dror, R.O., and Shaw, D.E. (2012). Mechanism of Voltage Gating in Potassium Channels. Science 336, 229–233.

Jiang, Y., Ruta, V., Chen, J., Lee, A., and MacKinnon, R. (2003). The principle of gating charge movement in a voltage-dependent K^+ channel. Nature 423, 42–48.

Kang, M.-G., and Campbell, K.P. (2003). Gamma subunit of voltage-activated calcium channels. J. Biol. Chem. 278, 21315–21318.

Klugbauer, N., Dai, S., Specht, V., Lacinová, L., Marais, E., Bohn, G., and Hofmann, F. (2000). A family of gamma-like calcium channel subunits. FEBS Lett. 470, 189-97.

Klugbauer, N., Lacinová, L., Marais, E., Hobom, M., and Hofmann, F. (1999). Molecular diversity of the calcium channel alpha2delta subunit. J. Neurosci. 19, 684–691.

Klugbauer, N., Marais, E., and Hofmann, F. (2003). calcium channel alpha2delta subunits: differential expression, function, and drug binding. J. Bioenerg. Biomembr. 35, 639–647.

Knollmann, B.C., and Roden, D.M. (2008). A genetic framework for improving arrhythmia therapy. Nature 451, 929–936.

Koschak, A., Reimer, D., Huber, I., Grabner, M., Glossmann, H., Engel, J., and Striessnig, J. (2001). alpha 1D ($Ca_V1.3$) subunits can form l-type Ca^{2+} channels activating at negative voltages. J. Biol. Chem. 276, 22100–22106.

Koschak, A., Reimer, D., Walter, D., Hoda, J.-C., Heinzle, T., Grabner, M., and Striessnig, J. (2003). $Ca_V1.4$ alpha1 subunits can form slowly inactivating dihydropyridine-sensitive L-type Ca^{2+} channels lacking Ca^{2+}-dependent inactivation. J. Neurosci. 23, 6041–6049.

Kudrnac, M., Beyl, S., Hohaus, A., Stary, A., Peterbauer, T., Timin, E., and Hering, S. (2009). Coupled and independent contributions of residues in IS6 and IIS6 to activation gating of $Ca_V1.2$. J. Biol. Chem 284, 12276–12284.

Kyte, J., and Doolittle, R.F. (1982). A simple method for displaying the hydropathic character of a protein. J. Mol. Biol 157, 105–132.

Lee, S.Y., Lee, A., Chen, J., and MacKinnon, R. (2005). Structure of the KvAP voltage-dependent K^+ channel and its dependence on the lipid membrane. Proc. Natl. Acad. Sci. USA 102, 15441-15446.

Letts, V.A., Felix, R., Biddlecome, G.H., Arikkath, J., Mahaffey, C.L., Valenzuela, A., Bartlett, F.S., 2nd, Mori, Y., Campbell, K.P., and Frankel, W.N. (1998). The mouse stargazer gene encodes a neuronal Ca^{2+}-channel gamma subunit. Nat. Genet. 19, 340–347.

Logothetis, D.E., Movahedi, S., Satler, C., Lindpaintner, K., and Nadal-Ginard, B. (1992). Incremental reductions of positive charge within the S4 region of a voltage-gated K^+ channel result in corresponding decreases in gating charge. Neuron 8, 531-540.

Long, S.B., Campbell, E.B., and Mackinnon, R. (2005). Voltage sensor of $K_V1.2$: structural basis of electromechanical coupling. Science 309, 903–908.

Long, S.B., Tao, X., Campbell, E.B., and MacKinnon, R. (2007). Atomic structure of a voltage-dependent K^+ channel in a lipid membrane-like environment. Nature 450, 376–382.

MacLennan, D.H., and Phillips, M.S. (1992). Malignant hyperthermia. Science 256, 789–794.

Mangoni, M.E., and Nargeot, J. (2008). Genesis and regulation of the heart automaticity. Physiol. Rev. 88, 919–982.

Marks, M.L., Whisler, S.L., Clericuzio, C., and Keating, M. (1995). A new form of long QT syndrome associated with syndactyly. Journal of the American College of Cardiology 25, 59–64.

Matthews, E., Labrum, R., Sweeney, M.G., Sud, R., Haworth, A., Chinnery, P.F., Meola, G., Schorge, S., Kullmann, D.M., Davis, M.B., et al. (2009). Voltage sensor charge loss accounts for most cases of hypokalemic periodic paralysis. Neurology 72, 1544–1547.

Monné, M., Nilsson, I., Elofsson, A., and von Heijne, G. (1999). Turns in transmembrane helices: determination of the minimal length of a "helical hairpin" and derivation of a fine-grained turn propensity scale. J. Mol. Biol. 293, 807–814.

Monnier, N., Procaccio, V., Stieglitz, P., and Lunardi, J. (1997). Malignant-hyperthermia susceptibility is associated with a mutation of the alpha 1-subunit of the human dihydropyridine-sensitive L-type voltage-dependent calcium-channel receptor in skeletal muscle. Am. J. Hum. Genet. 60, 1316–1325.

Neher, E., and Sakmann, B. (1976). Single-channel currents recorded from membrane of denervated frog muscle fibres. Nature 260, 799–802.

Nicholas, K.B., Nicholas H.B. Jr., and Deerfield, D.W. II. (1997). Embnew.news 14.

Noda, M., Shimizu, S., Tanabe, T., Takai, T., Kayano, T., Ikeda, T., Takahashi, H., Nakayama, H., Kanaoka, Y., and Minamino, N. (1984). Primary structure of Electrophorus electricus sodium channel deduced from cDNA sequence. Nature 312, 121–127.

Olcese, R., Qin, N., Schneider, T., Neely, A., Wei, X., Stefani, E., and Birnbaumer, L. (1994). The amino terminus of a calcium channel beta subunit sets rates of channel inactivation independently of the subunit's effect on activation. Neuron 13, 1433–1438.

Opatowsky, Y., Chen, C.-C., Campbell, K.P., and Hirsch, J.A. (2004). Structural analysis of the voltage-dependent calcium channel beta subunit functional core and its complex with the alpha 1 interaction domain. Neuron 42, 387–399.

Papazian, D.M., Shao, X.M., Seoh, S.A., Mock, A.F., Huang, Y., and Wainstock, D.H. (1995). Electrostatic interactions of S4 voltage sensor in Shaker K^+ channel. Neuron 14, 1293-1301.

Payandeh, J., Scheuer, T., Zheng, N., and Catterall, W.A. (2011). The crystal structure of a voltage-gated sodium channel. Nature 475, 353–358.

Payne, H.L. (2008). The role of transmembrane AMPA receptor regulatory proteins (TARPs) in neurotransmission and receptor trafficking (Review). Mol. Membr. Biol. 25, 353–362.

Perez-Reyes, E., Castellano, A., Kim, H.S., Bertrand, P., Baggstrom, E., Lacerda, A.E., Wei, X.Y., and Birnbaumer, L. (1992). Cloning and expression of a cardiac/brain beta subunit of the L-type calcium channel. J. Biol. Chem 267, 1792–1797.

Van Petegem, F., Clark, K.A., Chatelain, F.C., and Minor, D.L., Jr (2004). Structure of a complex between a voltage-gated calcium channel beta-subunit and an alpha-subunit domain. Nature 429, 671–675.

Van Petegem, F., and Minor, D.L., Jr (2006). The structural biology of voltage-gated calcium channel function and regulation. Biochem. Soc. Trans. 34, 887–893.

Peterson, B.Z., DeMaria, C.D., Adelman, J.P., and Yue, D.T. (1999). Calmodulin is the Ca^{2+} sensor for Ca^{2+}-dependent inactivation of L-type calcium channels. Neuron 22, 549–558.

Peterson, B.Z., Johnson, B.D., Hockerman, G.H., Acheson, M., Scheuer, T., and Catterall, W.A. (1997). Analysis of the dihydropyridine receptor site of L-type calcium channels by alanine-scanning mutagenesis. J. Biol. Chem. 272, 18752–18758.

Pierleoni, A., Martelli, P.L., and Casadio, R. (2008). PredGPI: a GPI-anchor predictor. BMC Bioinformatics 9, 392.

Pirone, A., Schredelseker, J., Tuluc, P., Gravino, E., Fortunato, G., Flucher, B.E., Carsana, A., Salvatore, F., and Grabner, M. (2010). Identification and functional characterization of malignant hyperthermia mutation T1354S in the outer pore of the Ca_V alpha1S-subunit. Am. J. Physiol., Cell Physiol. 299, C1345–1354.

Pitt, G.S., Zühlke, R.D., Hudmon, A., Schulman, H., Reuter, H., and Tsien, R.W. (2001). Molecular basis of calmodulin tethering and Ca^{2+}-dependent inactivation of L-type Ca^{2+} channels. J. Biol. Chem. 276, 30794–30802.

Ptácek, L.J., Tawil, R., Griggs, R.C., Engel, A.G., Layzer, R.B., Kwiecinski, H., McManis, P.G., Santiago, L., Moore, M., Fouad, G., et al. (1994). Dihydropyridine receptor mutations cause hypokalemic periodic paralysis. Cell 77, 863–868.

Qin, N., Yagel, S., Momplaisir, M.-L., Codd, E.E., and D'Andrea, M.R. (2002). Molecular cloning and characterization of the human voltage-gated calcium channel alpha(2)delta-4 subunit. Mol. Pharmacol. 62, 485–496.

Rabl, K., and Thoreson, W.B. (2002). calcium-dependent inactivation and depletion of synaptic cleft calcium ions combine to regulate rod calcium currents under physiological conditions. Eur. J. Neurosci. 16, 2070–2077.

Raybaud, A., Dodier, Y., Bissonnette, P., Simoes, M., Bichet, D.G., Sauvé, R., and Parent, L. (2006). The role of the GX9GX3G motif in the gating of high voltage-activated Ca^{2+} channels. J. Biol. Chem 281, 39424–39436.

Reichenbach, H., Meister, E.M., and Theile, H. (1992). The heart-hand syndrome. A new variant of disorders of heart conduction and syndactylia including osseous changes in hands and feet. Kinderarztliche Praxis 60, 54–56.

Reimer, D., Huber, I.G., Garcia, M.L., Haase, H., and Striessnig, J. (2000). beta subunit heterogeneity of L-type Ca(2+) channels in smooth muscle tissues. FEBS Lett. 467, 65–69.

Rhoads, A.R., and Friedberg, F. (1997). Sequence motifs for calmodulin recognition. Faseb J. 11, 331–340.

Rottbauer, W., Baker, K., Wo, Z.G., Mohideen, M.A., Cantiello, H.F., and Fishman, M.C. (2001). Growth and function of the embryonic heart depend upon the cardiac-specific L-type calcium channel alpha1 subunit. Dev. Cell 1, 265–275.

Roullet, J.B., Spaetgens, R.L., Burlingame, T., Feng, Z.P., and Zamponi, G.W. (1999). Modulation of neuronal voltage-gated calcium channels by farnesol. J. Biol. Chem. 274, 25439–25446.

Sandoz, G., Bichet, D., Cornet, V., Mori, Y., Felix, R., and De Waard, M. (2001). Distinct properties and differential beta subunit regulation of two C-terminal isoforms of the P/Q-type Ca^{2+}-channel alpha(1A) subunit. Eur. J. Neurosci. 14, 987–997.

Schulla, V., Renström, E., Feil, R., Feil, S., Franklin, I., Gjinovci, A., Jing, X.-J., Laux, D., Lundquist, I., Magnuson, M.A., et al. (2003). Impaired insulin secretion and glucose tolerance in beta cell-selective Ca(v)1.2 Ca^{2+} channel null mice. Embo J. 22, 3844–3854.

Seisenberger, C., Specht, V., Welling, A., Platzer, J., Pfeifer, A., Kühbandner, S., Striessnig, J., Klugbauer, N., Feil, R., and Hofmann, F. (2000). Functional embryonic cardiomyocytes after disruption of the L-type alpha1C ($Ca_V1.2$) calcium channel gene in the mouse. J. Biol. Chem. 275, 39193–39199.

Senatore, A., Zhorov, B.S., and Spafford, J.D. Ca_V3 T-type calcium channels. Wiley Interdisciplinary Reviews: Membrane Transport and Signaling.

Seoh, S.A., Sigg, D., Papazian, D.M., and Bezanilla, F. (1996). Voltage-sensing residues in the S2 and S4 segments of the Shaker K^+ channel. Neuron 16, 1159–1167.

Shafrir, Y., Durell, S.R., and Guy, H.R. (2008a). Models of the structure and gating mechanisms of the pore domain of the NaChBac ion channel. Biophys. J 95, 3650–3662.

Shafrir, Y., Durell, S.R., and Guy, H.R. (2008b). Models of voltage-dependent conformational changes in NaChBac channels. Biophys. J 95, 3663–3676.

Sinnegger-Brauns, M.J., Hetzenauer, A., Huber, I.G., Renström, E., Wietzorrek, G., Berjukov, S., Cavalli, M., Walter, D., Koschak, A., Waldschütz, R., et al. (2004). Isoform-specific regulation of mood behavior and pancreatic beta cell and cardiovascular function by L-type Ca^{2+} channels. J. Clin. Invest. 113, 1430–1439.

Snutch, T.P. (2009). Encyclopedia of Neuroscience.

Snutch, T.P., Tomlinson, W.J., Leonard, J.P., and Gilbert, M.M. (1991). Distinct calcium channels are generated by alternative splicing and are differentially expressed in the mammalian CNS. Neuron 7, 45–57.

Soldatov, N.M., Oz, M., O'Brien, K.A., Abernethy, D.R., and Morad, M. (1998). Molecular determinants of L-type Ca^{2+} channel inactivation. Segment exchange analysis of the carboxyl-terminal cytoplasmic motif encoded by exons 40-42 of the human alpha1C subunit gene. J. Biol. Chem. 273, 957–963.

Splawski, I., Timothy, K.W., Decher, N., Kumar, P., Sachse, F.B., Beggs, A.H., Sanguinetti, M.C., and Keating, M.T. (2005). Severe arrhythmia disorder caused by cardiac L-type calcium channel mutations. Proc. Natl. Acad. Sci. U.S.A 102, 8089–8096; discussion 8086–8088.

Splawski, I., Timothy, K.W., Sharpe, L.M., Decher, N., Kumar, P., Bloise, R., Napolitano, C., Schwartz, P.J., Joseph, R.M., Condouris, K., et al. (2004). Ca(V)1.2 calcium channel dysfunction causes a multisystem disorder including arrhythmia and autism. Cell 119, 19–31.

Stary, A., Shafrir, Y., Hering, S., Wolschann, P., and Guy, H.R. (2008). Structural model of the Ca V 1.2 pore. Channels (Austin) 2, 210–215.

Stephens, G.J., Page, K.M., Bogdanov, Y., and Dolphin, A.C. (2000). The alpha1B Ca^{2+} channel amino terminus contributes determinants for beta subunit-mediated voltage-dependent inactivation properties. J. Physiol. (Lond.) 525 Pt 2, 377–390.

Stotz, S.C., Hamid, J., Spaetgens, R.L., Jarvis, S.E., and Zamponi, G.W. (2000). Fast inactivation of voltage-dependent calcium channels. A hinged-lid mechanism? J. Biol. Chem. 275, 24575–24582.

Stotz, S.C., and Zamponi, G.W. (2001). Identification of inactivation determinants in the domain IIS6 region of high voltage-activated calcium channels. J. Biol. Chem. 276, 33001–33010.

Striessnig, J. (1999). Pharmacology, structure and function of cardiac L-type Ca^{2+} channels. Cell. Physiol. Biochem. 9, 242–269.

Striessnig, J., Bolz, H.J., and Koschak, A. (2010). Channelopathies in $Ca_V1.1$, $Ca_V1.3$, and $Ca_V1.4$ voltage-gated L-type Ca^{2+} channels. Pflugers Arch. 460, 361–374.

Striessnig, J., and Koschak, A. (2008). Exploring the function and pharmacotherapeutic potential of voltage-gated Ca^{2+} channels with gene-knockout models. Channels 2, 233–251.

Stühmer, W., Conti, F., Suzuki, H., Wang, X.D., Noda, M., Yahagi, N., Kubo, H., and Numa, S. (1989). Structural parts involved in activation and inactivation of the sodium channel. Nature 339, 597-603.

Tanabe, T., Mikami, A., Niidome, T., Numa, S., Adams, B.A., and Beam, K.G. (1993). Structure and function of voltage-dependent calcium channels from muscle. Ann. N. Y. Acad. Sci. 707, 81–86.

Tang, Z.Z., Liang, M.C., Lu, S., Yu, D., Yu, C.Y., Yue, D.T., and Soong, T.W. (2004). Transcript scanning reveals novel and extensive splice variations in human l-type voltage-gated calcium channel, $Ca_V1.2$ alpha1 subunit. J. Biol. Chem. 279, 44335–44343.

Tsien, R.W., Hess, P., McCleskey, E.W., and Rosenberg, R.L. (1987). calcium channels: mechanisms of selectivity, permeation, and block. Annu Rev Biophys Biophys Chem 16, 265–290.

Vriend, G. (1990). WHAT IF: a molecular modeling and drug design program. J Mol Graph 8, 52–56, 29.

Webster, S.M., Del Camino, D., Dekker, J.P., and Yellen, G. (2004). Intracellular gate opening in Shaker K+ channels defined by high-affinity metal bridges. Nature 428, 864–868.

Weiergräber, M., Hescheler, J., and Schneider, T. (2008). [Human calcium channelopathies. Voltage-gated Ca(2+) channels in etiology, pathogenesis, and pharmacotherapy of neurologic disorders]. Nervenarzt 79, 426–436.

Weiss, R.G., O'Connell, K.M.S., Flucher, B.E., Allen, P.D., Grabner, M., and Dirksen, R.T. (2004). Functional analysis of the R1086H malignant hyperthermia mutation in the DHPR reveals an unexpected influence of the III-IV loop on skeletal muscle EC coupling. Am. J. Physiol., Cell Physiol. 287, C1094–1102.

Welling, A., Ludwig, A., Zimmer, S., Klugbauer, N., Flockerzi, V., and Hofmann, F. (1997). Alternatively spliced IS6 segments of the alpha 1C gene determine the tissue-specific dihydropyridine sensitivity of cardiac and vascular smooth muscle L-type Ca^{2+} channels. Circ. Res. 81, 526–532.

Welty D.F., Schielke G.P., Vartanian M.G., Taylor C.P. (1993). Gabapentin anticonvulsant action in rats: disequilibrium with peak drug concentrations in plasma and brain microdialysate. Epilepsy Res. 16, 175–181.

Werry, D. (2009). Single Channel Properties of the Slow Cardiac Potassium Current, I_{KS}. Master Thesis. University of British Columbia, Vancouver, Canada.

William A. Catterall (2010). Ion Channel Voltage Sensors: Structure, Function, and Pathophysiology. Neuron 67, 915-928.

Wiser, O., Trus, M., Tobi, D., Halevi, S., Giladi, E., and Atlas, D. (1996). The alpha 2/delta subunit of voltage sensitive Ca^{2+} channels is a single transmembrane extracellular protein which is involved in regulated secretion. FEBS Lett. 379, 15–20.

Witkovsky, P., Schmitz, Y., Akopian, A., Krizaj, D., and Tranchina, D. (1997). Gain of rod to horizontal cell synaptic transfer: relation to glutamate release and a dihydropyridine-sensitive calcium current. J. Neurosci. 17, 7297–7306.

Xu, W., and Lipscombe, D. (2001). Neuronal Ca(V)1.3alpha(1) L-type channels activate at relatively hyperpolarized membrane potentials and are incompletely inhibited by dihydropyridines. J. Neurosci. 21, 5944–5951.

Zhao, Y., Scheuer, T., and Catterall, W.A. (2004). Reversed voltage-dependent gating of a bacterial sodium channel with proline substitutions in the S6 transmembrane segment. Proc. Natl. Acad. Sci. U.S.A. 101, 17873–17878.

Zühlke, R.D., Pitt, G.S., Deisseroth, K., Tsien, R.W., and Reuter, H. (1999). Calmodulin supports both inactivation and facilitation of L-type calcium channels. Nature 399, 159–162.

2 Timothy Mutation Disrupts the Link between Activation and Inactivation in $Ca_V1.2$ Protein

Depil K, Beyl S, Stary-Weinzinger A, Hohaus A, Timin E, Hering S.

Published in the Journal of Biological Chemistry, 2011, Sep;

286(36):31557-64

2.1 Introduction

Timothy syndrome (TS), an autosomal dominant disorder, arises from two de novo missense mutations, G402S and G406R, in $Ca_V1.2$ calcium channels. This channelopathy manifests itself clinically in physical, neurological, and developmental defects and autism spectrum disorders. G406R additionally causes syndactyly (1). Functional studies have shown that TS mutations G402S and G406R dramatically reduce voltage-dependent channel inactivation, resulting in sustained membrane depolarization and increased calcium entry during an action potential (1). The resulting prolongation of the QT interval can induce severe arrhythmias causing sudden death in early childhood (1). Kinetic modeling studies suggested that the increased action potential duration and enhanced calcium entry may be associated with delayed after-depolarizations in cardiac myocytes (2).

A role of G406R in calcium-dependent inactivation was established by Raybaud et al. (3) and Barrett and Tsien (4). Systematic mutations of Gly-436 in rabbit $Ca_V1.2$ (corresponding to Gly-406 in the human $Ca_V1.2$) to Ala, Pro, Tyr, Glu, Arg, His, Lys, or Asp all substantially slow channel inactivation (3). A large number of amino acids involved in Ca^{2+} channel inactivation have been identified, and several molecular mechanisms for this process have been proposed ($5 - 7$).

We have previously shown that mutations in the lower third of S6 segments in $Ca_V1.2$ in most cases shift the channel inactivation and activation in a coupled manner. This is evident from similar shifts of channel activation and inactivation curves (8, 9), suggesting a serial gating scheme (R)est $\rightarrow$ (O)pen $\rightarrow$ (I)nactivated where a shift in R $\rightarrow$ O transitions would automatically shift the inactivation curve. However, Raybaud et al. (3) reported that mutations of the TS Gly-436 that suppressed inactivation in $Ca_V1.2$ induced only minor changes in activation gating.

The functional impact and structural basis of amino acid substitutions of the TS Gly-432 (corresponding to Timothy Gly-402 in human $Ca_V1.2$) are less understood. Our homology model suggests that Gly-432 forms part of a conserved group of small amino acids, Gly-432(IS6), Ala-780(IIS6), Gly-1193(IIIS6), and Ala-1503(IVS6), near the inner channel mouth of $Ca_V1.2$ (Fig. 1), which we call the G/A/G/A motif. A corresponding Gly-657 in hERG (Human Ether-a-go-go related Gene) potassium channels was found to be important for close helix packing (10), and in KcsA, replacement of the corresponding small and hydrophobic Ala-108 by a polar serine or threonine (A108S/T) dramatically increased channel open probability (11, 12). Small gating-sensitive residues at this position thus seem to be essential for helix-helix interactions in a number of ion channels.

To clarify the role of Gly-432 as part of the apparent G/A/G/A motif of $Ca_V1.2$, we have asked several questions. First, do mutations of the homologous small residues

in the other domains, Ala-780(IIS6), Gly-1193(IIIS6), and Ala-1503(IVS6), have similar effects on channel gating to substitutions of Gly-432? Second, how do amino acid substitutions in these positions affect the link between activation and inactivation? Third, is an essential role of the G/A/G/A residues in helix packing and closed-state stability supported by functional data? Answers to these questions will help to understand the interactions of residues in the bundle crossing region and help to clarify the specific impact of pore residues on activation and inactivation.

2.2 Experimental Procedures

2.2.1 Conservation Analysis

Sequences of voltage-gated calcium channels (13) were downloaded from the International Union of Basic and Clinical Pharmacology data base (14). Sequences of all channels from Homo sapiens were used to search NCBI BLAST (blastp) (15). Initial sequence alignment was performed using ClustalW (16). Sequences of selected potassium channel crystal structures (KcsA, MthK, K_VAP, $K_V1.2$, and MlotiK) were aligned manually with Ca_V channels using GENEDOC (17).

2.2.2 Homology Modeling

The homology model of the open $Ca_V1.2$ channels, based on the K_VAP crystal structure and a NaChBac model, incorporating an insertion at the position of the conserved asparagines, was published previously (8). A model of the closed conformation using the same alignment as for the open conformation (indel at Asn) was generated using Modeller9v7 (18). The KcsA crystal structure and the NaChBac model were used as templates. Coordinates of the model can be found in the supplemental material.

2.2.3 Accessibility Calculations

Amino acid accessibilities were calculated using the WHAT IF webserver (19). The accessible surface area in this program is defined as the area at the Van der Waals surface that is accessible by a water molecule (1.4 Å). The units of accessible surface are $Å^2$. Re-entrant surfaces are not considered by WHAT IF.

2.2.4 Mutagenesis

The $Ca_V1.2$ α_1-subunit coding sequence (GenBank™ X15539) in-frame 3′ to the coding region of a modified green fluorescent protein was kindly donated by Dr. M. Grabner (20). Substitutions in segment IS6, IIS6, and IVS6 of the $Ca_V1.2$ α_1-subunit were introduced using the QuikChange® Lightning site-directed mutagenesis kit (Stratagene) with mutagenic primers according to the manufacturer's instructions. Mutations were introduced in segment IS6 in position 432 (G432A/S/V/N/M/W), in helix IIS6 in position 780 (A780G/N/P/T/V/W), in IVS6 in position 1503

(A1503G/P/M/N/T/V/W), and one double mutation in IS6 (G432S/S435G). All constructs were checked by restriction site mapping and sequencing.

2.2.5 Cell Culture and Transient Transfection

Human embryonic kidney tsA-201 cells were grown at 5 % CO_2 and 37 °C to 80 % confluence in Dulbecco's modified Eagle's/F-12 medium supplemented with 10 % (v/v) fetal calf serum and 100 units/ml penicillin/streptomycin. Cells were split with trypsin/EDTA and plated on 35 mm Petri dishes (Falcon) at $30-50$ % confluence 16 h before transfection. Subsequently tsA-201 cells were co-transfected with cDNAs encoding wild-type or mutant $Ca_V1.2$ α_1-subunits with auxiliary β_{2a} and β_{2c} (21) as well as α_2-δ_1 (22) subunits. The transfection of tsA-201 cells was performed using the FuGENE 6 transfection reagent (Roche Applied Science) following standard protocols. tsA-201 cells were used until passage number 15. No variation in channel gating related to different cell passage numbers was observed.

2.2.6 Ionic Current Recordings and Data Acquisition

Barium currents (I_{Ba}) through voltage-gated Ca^{2+} channels were recorded at $22-25$ °C by patch-clamping (23) using an Axopatch 200A patch clamp amplifier (Axon Instruments, Foster City) $36-48$ h after transfection. The extracellular bath solution (5 mM $BaCl_2$, 1 mM $MgCl_2$, 10 mM HEPES, 140 mM choline chloride) was titrated to pH 7.4 with methanesulfonic acid. Patch pipettes with resistances of $1-4$ MΩ were made from borosilicate glass (Clark Electromedical Instruments) and filled with pipette solution (145 mM CsCl, 3 mM $MgCl_2$, 10 mM HEPES, 10 mM EGTA 10), titrated to pH 7.25 with CsOH. All data were digitized using a DIGIDATA 1200 interface (Axon Instruments), smoothed by means of a four-pole Bessel filter, and saved to disk. 100 ms current traces were sampled at 100 kHz and filtered at 5 kHz; tail currents were sampled at 50 kHz and filtered at 10 kHz. Leak currents were subtracted digitally using average values of scaled leakage currents elicited by a 10 mV hyperpolarizing pulse or electronically by means of an Axopatch 200 amplifier (Axon Instruments). Series resistance and offset voltage were routinely compensated for. The pClamp software package (Version 7.0 Axon Instruments) was used for data acquisition and preliminary analysis. Microcal Origin 7.0 was used for analysis and curve-fitting.

The voltage dependence of activation was determined from I-V curves and fitted to

$$m_\infty = \frac{1}{1+\exp\frac{V_{0.5,act}-V}{k_{act}}} \tag{2.1}$$

The time course of current activation was fitted to a mono-exponential function,

$$I(t) = A \cdot \exp\left(\frac{t}{\tau}\right) + C \tag{2.2}$$

where $I(t)$ is current at time t, A is the amplitude coefficient, τ is the time constant, and C is the steady-state current. Data are given as the mean $\pm S.E.$

2.2.7 Calculation of Amino Acid Descriptors

Physicochemical descriptors were calculated for amino acids using the Molecular Operating Environment (MOE; Version 2008.10, Chemical Computing Group, Inc., Montreal, QC, Canada) (24).

2.3 Results

2.3.1 The "Timothy Gly-432" Is Part of a Motif of Small Residues at the Inner Channel Mouth

To analyze the degree of conservation of the TS Gly-402, a sequence alignment was performed. Sequences of the 10 different voltage-gated calcium channels genes encoded in the human genome were downloaded from the International Union of Basic and Clinical Pharmacology data base. The human sequences were used to search NCBI BLAST using the blastp program. The pore-forming segments of Ca_V channels (S5, P, S6) from different species were aligned using standard parameters in ClustalW. Fig. 2.1 shows the multiple sequence alignment of selected Ca_V channels, and the complete alignment of all human S6 segments can be found in supplemental Fig. 2.7. Fig. 2.1 shows that Gly-432 is part of a motif of small amino acids (Gly-432(IS6)-Ala-780(IIS6)-Gly-1193(IIIS6)-Ala-1503(IVS6)) at the inner channel mouth. The conservation analysis reveals that these positions either have a glycine or an alanine. The only exceptions are T-type channels, which have a valine at this position in IS6. We will refer to this structural motif of Ca_V as G/A/G/A.

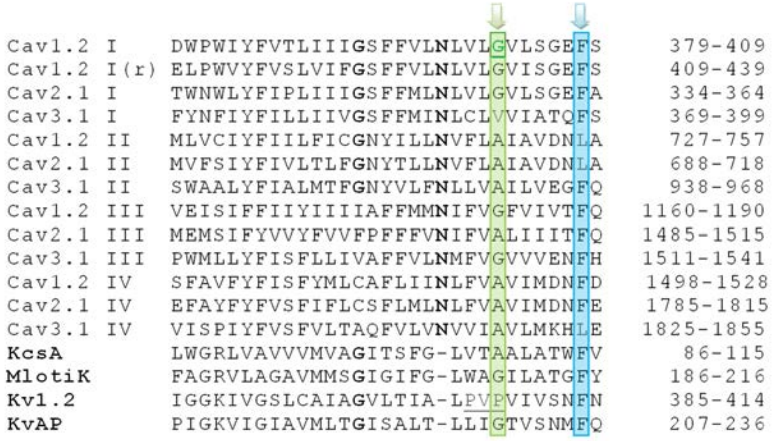

Figure 2.1: Multiple sequence alignment of S6 helices of Ca_V channels with selected K^+ channels. Conserved G/A/G/A residues are shaded green, interacting phenylalanines (neighboring domains) are shaded blue. The Timothy glycine is underlined green and the PVP motif of $K_V1.2$ is underlined black.

2.3.2 Mutations of Gly-432 Shift the Activation Curve

In the absence of experimentally determined structures of calcium channels, homology models have been used successfully to explain experimental data and to suggest new experiments (25–29). Our modeling data on $Ca_V1.2$ suggest that G/A/G/A plays an essential role in helix packing. In light of this hypothesis, we investigated whether replacement of Gly-432 by residues with different properties (e.g. size and hydrophobicity) would affect the voltage dependence of channel activation. Fig. 2.2, A and B, illustrate the corresponding effects on the steady-state activation curves. Replacement of Gly-432 by methionine, asparagine, and tryptophan shifts channel activation toward hyperpolarization. Interestingly, G432A and G432V shifted the curve to the right, suggesting a stabilization of the closed or a destabilization of the open states. Changes in activation and deactivation gating for selected mutants are illustrated by current traces shown in Fig. 2.2, C and D. The slowing of channel activation and deactivation (voltage dependences of activation and deactivation time constants) for G432N accompanying the leftward shift of the activation curve and fast activation/deactivation kinetics of G432A inducing a rightward shift are exemplified (Fig. 2.2, E and F).

2.3.3 Substitutions of Gly-432 Remove Channel Inactivation

In contrast to the differing effects on channel activation (Fig. 2.2, Tab. 2.1), all mutations of Gly-432 tested reduced inactivation regardless of the properties of the new side chain. This is evident from current traces under long-lasting depolarizations for all mutants Fig. 2.3. The changes in the steady-state inactivation curves for mutation to alanine (G432A) and asparagines (G432N) are exemplified in Fig. 2.3 A. The remaining currents after 3000 ms depolarizations to the peak current voltage of the current voltage activation curves are given in Tab. 2.1.

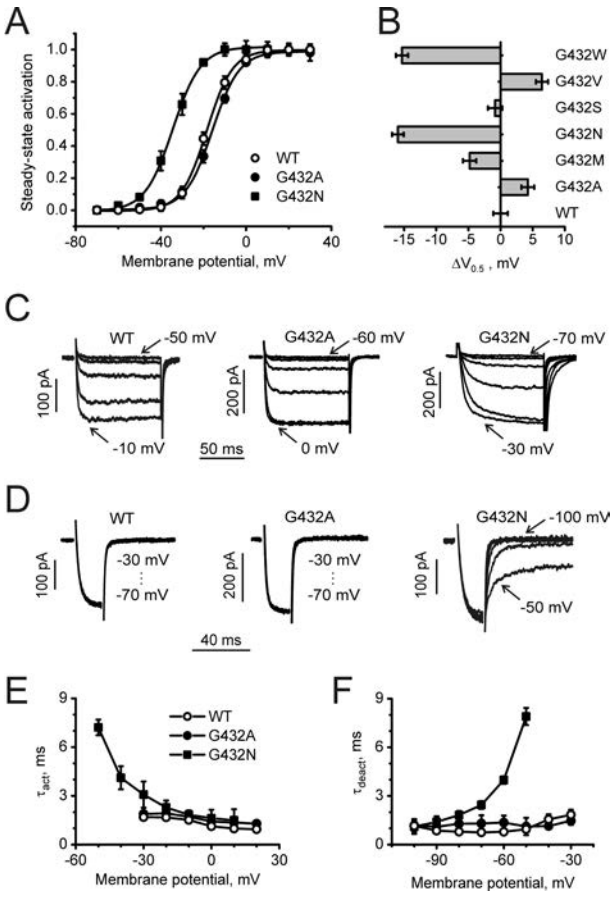

Figure 2.2: Gating changes induced by mutations of G432 in segment IS6 of $Ca_V1.2$.
A, Averaged activation curves of wild-type (n=9) and mutants G432A (n=7) and G432N (n=7).
B, Shift of activation curves induced by substitutions of G432 by residues of different physico-chemical properties.
C, Representative families of I_{Ba} through wild-type and indicated mutant channels during depolarizing test pulses from -100 mV in 10 mV increments (first and last potentials are indicated).
D, Representative tail currents of WT and indicated mutant channels. Currents were activated during a 20 mV conditioning depolarization to -10 mV for wild-type, 0 mV for G432A and -20 mV for G432N. Deactivation was recorded during subsequent repolarizations in 10 mV increments starting from -100 mV.
E, Mean time constants of channel activation of WT (n=9) and mutants G432A (n=7) and G432N (n=7) are plotted against test potential.
F, Mean time constants of channel deactivation of wild-type (n=8) and mutants G432A (n=6) and G432N (n=6) are plotted against test potential. Time constants were estimated by fitting current activation and deactivation to a mono-exponential function.

Table 2.1: Pore mutations affect voltage-dependent gating of $Ca_V1.2$
Midpoints, slope factors of the activation, inactivation curves and fractions of non inactivated channels after a 3 s depolarization to the peak current potential of the current voltage relationship (I-V curve).

Construct	$\mathbf{V_{0.5}}$ [mV]	$\mathbf{k_{act}}$ [mV]	$\mathbf{V_{0.5,inact}}$ [mV]	$\mathbf{k_{inact}}$ [mV]	$\mathbf{r_{3000}}$
WT	-18.4 ± 0.8 (9)	6.0 ± 0.7	-41.5 ± 0.9 (5)	6.4 ± 0.9	0.35 ± 0.03
IS6 G432[1]					
G432A	-14.2 ± 0.6 (7)	6.2 ± 0.5			0.77 ± 0.05
G432M	-23.2 ± 0.6 (7)	7.7 ± 0.6			0.68 ± 0.07
G432N	-34.4 ± 0.4 (7)	6.5 ± 0.5			0.72 ± 0.04
G432S	-19.2 ± 0.7 (7)	5.9 ± 0.7			0.74 ± 0.07
G432V	-12.0 ± 0.6 (6)	5.7 ± 0.5			0.86 ± 0.04
G432W	-33.7 ± 0.6 (8)	4.7 ± 0.4			0.58 ± 0.04
IIS6 A780					
A780G	-29.4 ± 0.6 (5)	6.2 ± 0.6	-54.4 ± 1.3 (4)	6.2 ± 1.1	0.11 ± 0.06
A780N	-43.8 ± 1.0 (7)	6.8 ± 0.9	-67.4 ± 0.7 (4)	4.6 ± 0.9	0.25 ± 0.04
A780P	-45.0 ± 0.7 (5)	5.9 ± 0.8	-39.4 ± 1.2 (4)	5.2 ± 1.9	0.34 ± 0.07
A780T	-44.0 ± 0.6 (5)	5.1 ± 0.6	-59.8 ± 0.9 (4)	7.5 ± 0.9	0.24 ± 0.04
A780V	-34.6 ± 0.8 (8)	6.6 ± 0.7	-54.3 ± 0.8 (4)	4.8 ± 0.8	0.10 ± 0.05
A780W	-49.3 ± 0.6 (7)	5.9 ± 0.5	-68.0 ± 0.8 (4)	6.3 ± 0.9	0.16 ± 0.05
IIIS6 G1193[2]					
G1193A	-12.1 ± 1.0 (6)	5.7 ± 0.7	-25.2 ± 1.1 (6)	8.8 ± 0.9	0.27 ± 0.07
G1193M	-33.6 ± 0.7 (8)	6.4 ± 0.6	-52.8 ± 1.0 (4)	6.1 ± 0.9	0.34 ± 0.08
G1193N	-46.5 ± 1.0 (5)	5.6 ± 0.8	-61.3 ± 0.9 (4)	6.9 ± 0.9	0.38 ± 0.08
G1193P	-37.7 ± 0.7 (7)	6.3 ± 0.6	-64.6 ± 1.0 (4)	6.1 ± 0.8	0.18 ± 0.07
G1193Q	-39.2 ± 0.8 (5)	7.0 ± 0.7	-64.4 ± 1.2 (4)	8.4 ± 1.1	0.29 ± 0.08
G1193T	-49.8 ± 1.0 (7)	5.1 ± 0.6	-70.0 ± 1.1 (5)	5.4 ± 1.1	0.16 ± 0.07
G1193V	-38.1 ± 0.7 (8)	5.6 ± 0.6	-60.4 ± 0.8 (5)	7.5 ± 0.6	0.14 ± 0.08
IVS6 A1503					
A1503G	-41.4 ± 0.8 (5)	5.8 ± 0.5	-54.0 ± 1.0 (4)	4.9 ± 0.8	0.31 ± 0.07
A1503M	-29.2 ± 0.7 (8)	5.9 ± 0.7	-60.1 ± 1.0 (4)	5.5 ± 1.0	0.26 ± 0.08
A1503N	-31.5 ± 0.7 (5)	6.3 ± 0.6	-45.1 ± 1.1 (4)	6.0 ± 1.0	0.32 ± 0.09
A1503T	-17.9 ± 0.8 (7)	8.7 ± 0.8	-38.0 ± 1.2 (4)	6.9 ± 1.1	0.29 ± 0.09
A1503V	-11.4 ± 0.8 (5)	7.2 ± 0.6	-37.2 ± 1.2 (4)	6.8 ± 1.2	0.24 ± 0.06
A1503W	-16.9 ± 0.6 (9)	6.6 ± 0.6	-38.9 ± 1.3 (4)	7.5 ± 0.8	0.33 ± 0.09
A1503P	no current				
Double mutations					
G432S/S435G	-19.8 ± 0.9 (5)	6.3 ± 0.7	-39.2 ± 1.2 (4)	5.7 ± 1.1	0.54 ± 0.07

[1] $V_{0.5,inact}$ lack of inactivation prevented quantitative estimations.
[2] $V_{0.5,act}$ data are from Beyl et al. (24).

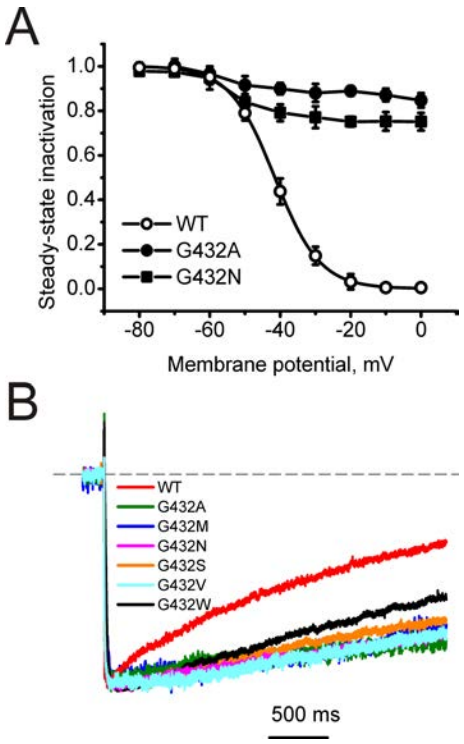

Figure 2.3: Inactivation changes induced by mutations of G432 in segment IS6 of $Ca_V1.2$.
A, Averaged inactivation curves of wild-type (n=5) and mutants G432A (n=4) and G432N (n=4).
B, Representative I_{Ba} through wild-type and indicated mutant channels during depolarizing test pulses from -100 mV to the peak potential of the I-V curve.

2.3.4 Mutations of Ala-780, Gly-1193, and Ala-1503 (Homologous to Gly-432) Affect Channel Activation but Preserve Inactivation

None of the mutations in positions Ala-780, Gly-1193, and Ala-1503 slowed channel inactivation, as observed with substitutions of Gly-432. The modulatory effects of mutations in these positions are illustrated in Fig. 2.4. We observed a strong correlation between the shifts of the activation and inactivation curves (Fig. 2.5, $r = 0.91$, $p < 0.001$) in domains II, III, and IV (see also Tab. 2.1), suggesting that the coupling between the two processes was intact. These data indicate a special role of Gly-432 in inactivation gating, in that only mutations of Gly-432 diminished inactivation, whereas substitutions in homologous positions in other segments either had no effect on inactivation or even made it faster.

2.3.5 Structural Analysis of the G/A/G/A Motif

To visualize the location of G/A/G/A, homology models of $Ca_V1.2$ in open and closed conformation were analyzed. The open channel conformation has been published previously (30). A model of the closed $Ca_V1.2$ channel, including an insertion at the highly conserved asparagines, was developed by basing the structures of P-helices and selectivity filter segments on the NaChBac model (31), as both channels possess the same selectivity signature sequence. The S5 and S6 segments are based on the KcsA crystal structure. The alignment is shown in Fig. 2.1.

Residues in closed K^+ channel crystal structures of KcsA and MlotiK that align with the G/A/G/A motif are positioned at the M2 helix-helix interface (Fig. 2.6, A and B). These helices correspond to S6 helices in calcium channels. The small amino acids in positions homologous to $Ca_V1.2$ G/A/G/A motif interact with bulky hydrophobic residues from the adjacent M2 helices. Interestingly, in both crystal structures the small Ala-108/Gly-208 are in close contact with a conserved phenylalanine (see alignment, Fig. 2.1) located two turns below in the neighbouring pore helix. Our homology model of the closed conformation suggests similar interactions in $Ca_V1.2$ (Fig. 2.6, C – F). Small amino acids Gly-432, Ala-780, Gly-1193, and Ala-1503 are located at the S6-S6 interface, tightly surrounded by hydrophobic residues from the adjacent S6 segments. A structural hypothesis (Fig. 2.6, C–F) illustrates putative interactions of the G/A/G/A residues with adjacent bulky residues, e.g. phenylalanines in domains I, III, and IV and leucine in domain II. All residues that are located within a short distance (< 7 [Å] of $C\beta$ atom) of G/A/G/A according to our homology model are given in Tab. 2.2.

To further characterize this putative packing motif, the accessibility of the surrounding residues was calculated with the WHAT IF online server (19) (see Tab. 2.3). Cal-

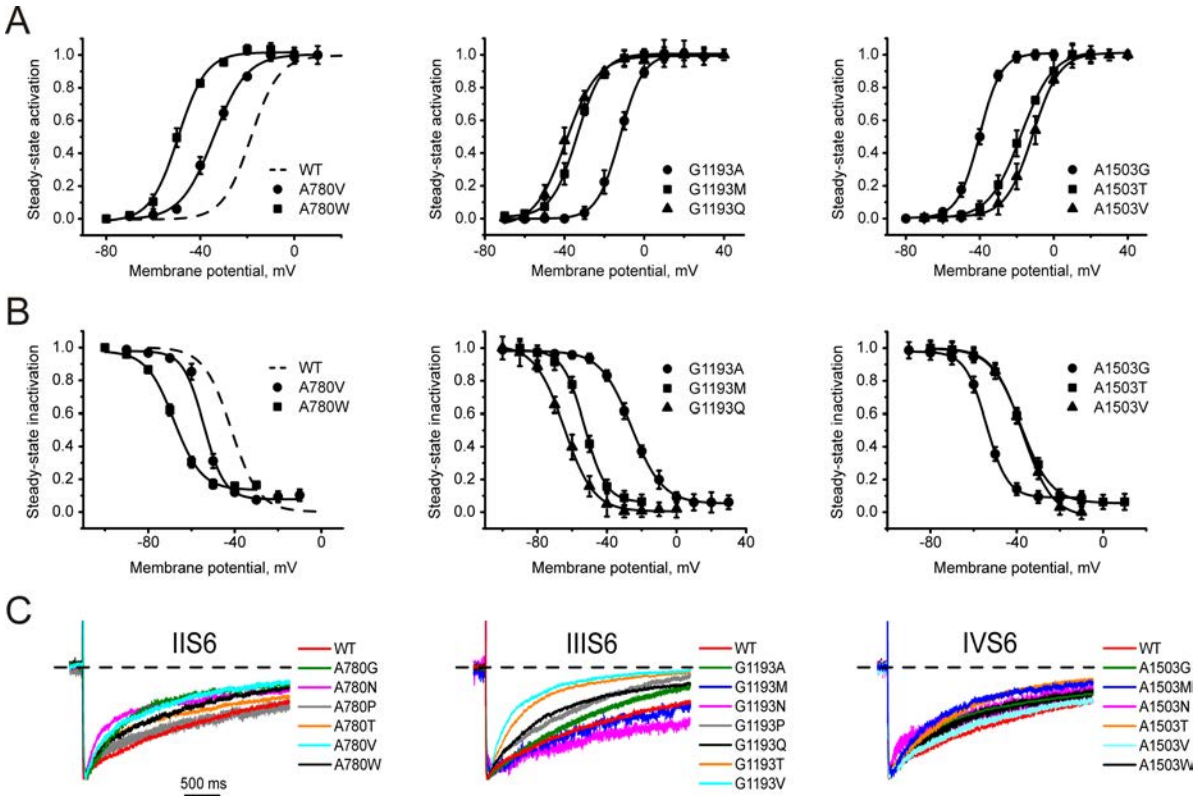

Figure 2.4: Mutations in the pore segments IIS6, IIIS6 and IVS6 in positions homologous to G432 in IS6 induce significant shifts of activation and inactivation curves.
A and B, Averaged activation (A) and inactivation (B) curves of wild-type and mutations of A780 in segment IIS6 (left), G1193 in segment IIIS6 (middle) and A1503 in segment IVS6 (right). All mutations are summarized in Tab. 2.1.
C, Representative I_{Ba} through wild-type and indicated mutant channels in segments IIS6-IVS6 during depolarizing test pulses from -100 mV to the peak potentials of the current-voltage relationships. No deceleration of inactivation was observed (compare with G432 in IS6, Fig. 2.3).

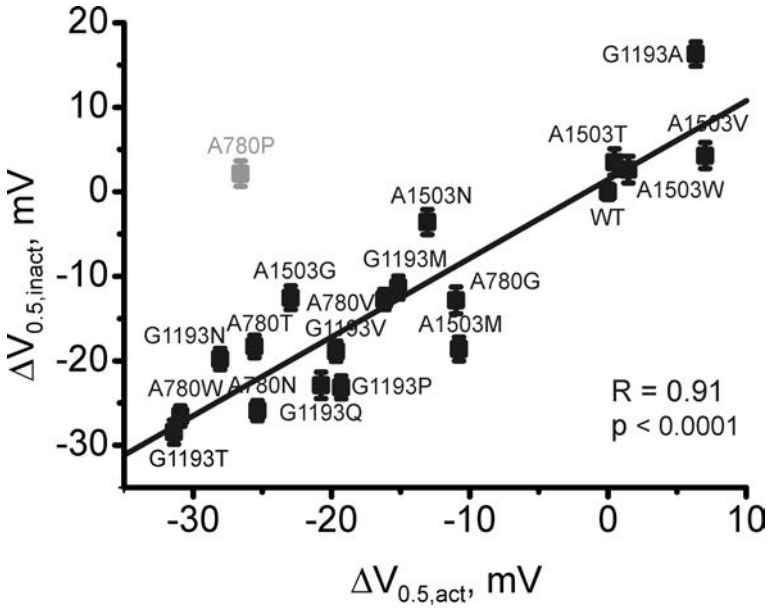

Figure 2.5: Correlation between shifts of the midpoint of the inactivation and activation curves for G/A/G/A mutations in segments IIS6-IVS6. A proline mutation of A780 (shaded) was excluded from correlation analysis as this residue is likely to disturb the link between voltage sensor and the channel pore (9, 24).

Table 2.2: Potential interactions of G/A/G/A residues in the closed channel state (see model in Fig. 2.6).

Member of G/A/G/A	**Neighbouring residues (β-carbons < 7 Å apart)**
G432 (IS6)	IS6: **N428**, L429, L431, V433, S435, G436, IVS6: V1502, I1505, M1506, F1509
A780 (IIS6)	IS6: L431, G432, L434, S435, G436, F438 IIS6: **N776**, V776, V777, L779, I781, V783, D784
G1193 (IIIS6)	IIS6: L779, A782, V783, L786 IIIS6: **N1189**, I1190, V1192, F1194, V1195, I1196, V1197 IVS6: **N1499**, A1503
A1503 (IVS6)	IIIS6: G1193, V1195, I1196, F1199 IVS5: K1385 IVS6: **N1499**, L1500, V1502, V1504, M1506, D1507

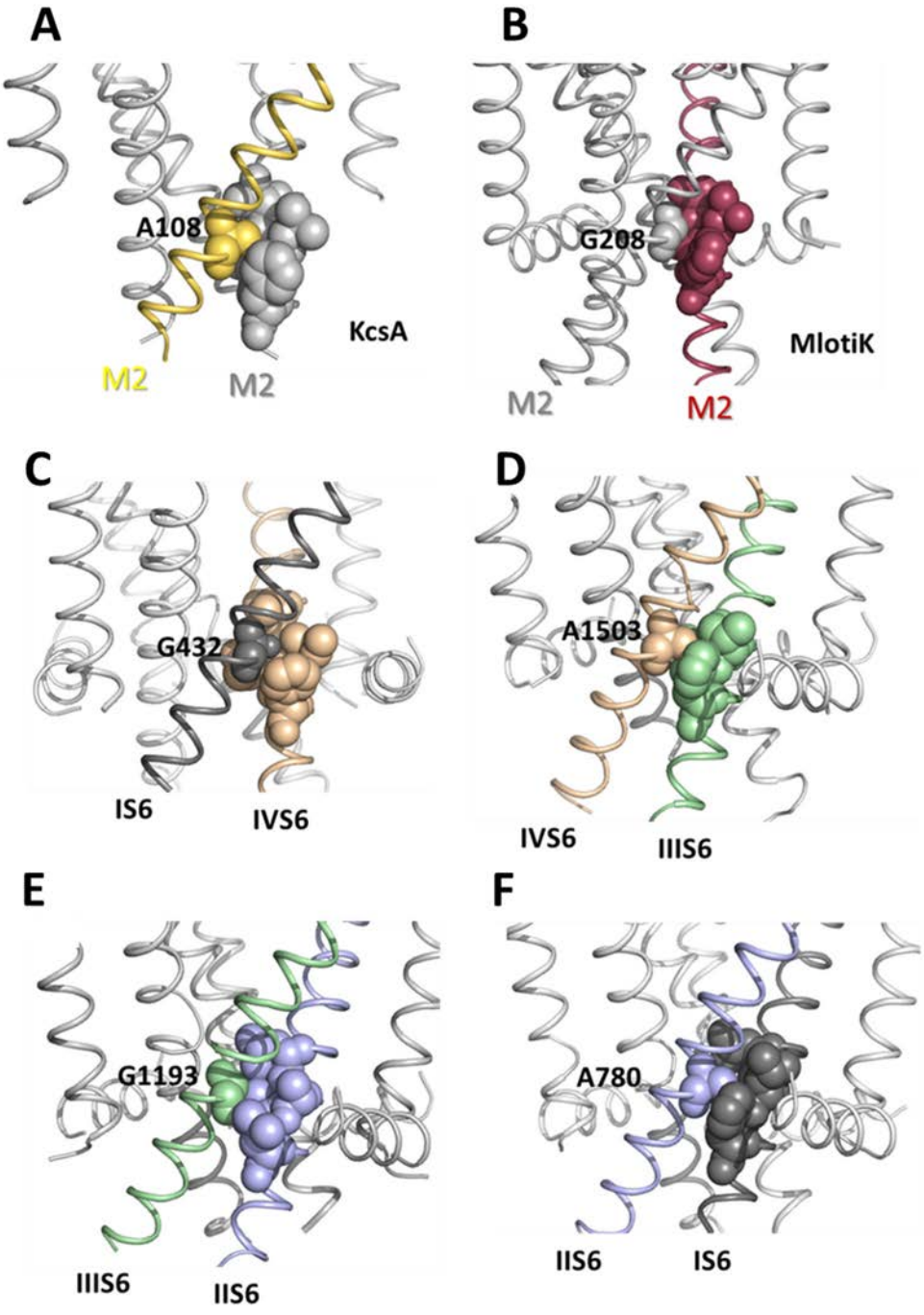

Figure 2.6: Hypothetical role of small amino acids in helix-helix packing of voltage gated ion channels.
Location of an alanine (A) in the closed conformation crystal structures of KcsA and the location of a corresponding glycine (B) in Mlotik (34). C-F illustrate the location of the G/A/G/A residues interacting with bulky hydrophobic residues from the neighboring S6 segments (shown as spheres).

culations using KcsA and MlotiK crystal structures show that the amino acids corresponding to the G/A/G/A motif are inaccessible. Similar results are obtained when calculating the accessible molecular surface in our closed $Ca_V1.2$ homology model. The conserved phenylalanines are also generally inaccessible, with the exception of Phe-114 from the KcsA crystal structure. This might be due to incompleteness of the crystal structure, which lacks the slide helices.

Table 2.3: Accessibility of residues at the contact interface between S6 (M2) helices. G/A/G/A motif shown in bold, conserved phenylalanines are underlined.

Channel	**Accessibilities of amino acids in the bundle crossing region [Å^2]**
KcsA (1k4c)	T107 (5.9); **A108 (0.17)**; A109 (14.19); L110 (10.1); A111 (2.44); T112 (11.5); W113 (56.8); F114 (20.2)
MlotiK (3beh)	A207 (1.7); **G208 (0)**; I209 (0.1); L210 (1.2); A211 (4.1); T212 (2.4); G213 (0); F114 (1.9)
$Ca_V1.2$ I	L431 (0); **G432 (0)**; V433 (0.6); L434 (1.2); S435 (0); G436 (0); E437 (17.1); F438 (1.5)
$Ca_V1.2$ II	L779 (0.3); **A780 (0)**; I781 (7.3); A782 (1.7); V783 (1.5); D784 (1.5); N785 (21.5); L786 (2.9)
$Ca_V1.2$ III	V1192 (0.1); **G1193 (0)**; F1194 (13.9); V1195 (6.9); I1196 (0.1); V1197 (19.8); T1198 (19.8); F1199 (3.4)
$Ca_V1.2$ IV	V1502 (0); **A1503 (0)**; V1504 (5.5); I1505 (9.7); M1506 (0.3); D1507 (1.0); N1508 (17.6); F1509 (1.6)

A comparison of closed and open crystal structure conformations of the bacterial potassium channel KcsA reveals large conformational changes upon gating, resulting in a displacement of this amino acid by more than 7 Å. Accessibility calculations show that this residue is accessible to water in the open channel conformation. Because several open and open-inactivated crystal structures are available, we calculated values for three different KcsA crystal structures (32) with the PDB identifiers 3f5w, 3fb7, and 3f7v. The obtained accessibility values (range $9.9 - 17.2$ Å^2) might reflect different degrees of channel opening. Similar accessibilities are obtained when calculating the accessible molecular surface in our open $Ca_V1.2$ homology model. The values are 14.4 Å^2 (Gly-432), 11.8 Å^2 (Ala-780), 11.1 Å^2 (G1193), and 18.5 Å^2 (A1503).

2.4 Discussion

Reduced inactivation by TS mutations G406R and G402S results in sustained membrane depolarization and enhanced calcium entry through L-type channels into neuronal, myocardial, and other cell types (2). This slowing of channel inactivation is the key to understanding the wide spectrum of developmental abnormalities and pathological changes in different organs leading to cardiac arrhythmias, autism spectrum disorders, and other diseases (2). TS mutations affect the mechanism of calcium-dependent inactivation that occurs irrespective of expression of a fast (β_{1c}-) or slow β_{2a}-subunit (3, 4). Later studies revealed that mutation G436R (corresponding to the TS mutation G406R in humans) slows channel activation and deactivation, which may augment the arrhythmogenic effects of this mutation (33). Splawski et al. (2) emphasize that substitution of Gly-406 by different amino acids reduces inactivation similar to G406R. This finding was supported by data of Raybaud et al. (3) who substituted 11 different residues for the corresponding Gly-436 in the rabbit channel and found that all these mutations reduced voltage-dependent inactivation. However, the role of these residues in stabilization of the different conformational states of $Ca_V1.2$ remained elusive.

Splawski et al. (2) hypothesized, in analogy to potassium channels, that Gly-406 and Gly-402 may act as the hinge points during channel activation. Raybaud et al. (3) discussed a potential role of G402S and G406R in helix packing. In continuation of the work by Splawski et al. (2) and Raybaud et al. (3), we have substituted Gly-432 by residues of different physicochemical properties. Our homology model suggests that the Timothy Gly-432 is part of a motif of tightly packed small amino acids (Fig. 2.6, A–F). It was, therefore, interesting to compare gating changes induced by mutations in these positions of all four S6 segments.

2.4.1 Mutations of G/A/G/A Residues Affect Activation Gating

All mutations of the TS Gly-432 and homologous Ala-780, Gly-1193, and Ala-1503 affected the stability of the channel pore. The majority of mutations induced leftward shifts of the activation curves that were always accompanied by a slowing down of channel deactivation, suggesting a stabilization of the open and destabilization of the closed state (9, 24). Four mutations, G432A, G432V, G1193A, and A1503V, induced rightward shifts of the steady-state curve and exhibited corresponding fast activation and deactivation (Fig. 2.2 and Fig. 2.4), indicating a stabilization of the closed channel state.

To test the structural hypothesis that size is an important determinant of pore stability (supplemental Fig. 2.8) in the G/A/G/A positions, we applied mutation-

correlation analysis (24). In all four positions the insertion of larger residues disturbed pore stability, as evident from shifts of the activation curve. In line with these data, characteristics of amino acid size (either molecular weight or Van der Waals volume) correlated in combination with hydrophobicity or flexibility indices with the shifts of the activation curve (supplemental Fig. 2.8). Despite their common impact on activation gating (all residues of G/A/G/A contribute to closed state stability), these residues interact in a domain-specific manner with their surrounding residues. As illustrated in supplemental Fig. 2.8, descriptors characterizing the size of the substituting residues (either molecular weight in domains I-III or Van der Waals volume in domain IV) correlate with the shifts of the activation curves. Domain-specific (asymmetric) contributions are evident from different impacts of hydrophobicity indices (domains I-III) and side chain flexibility (domain IV). Interestingly, mutating a small and flexible Gly-432 to a small but more rigid alanine or valine in domain I stabilized the closed state by shifting the activation curve by $5-7$ mV. In domain IV, replacing a rigid Ala-1503 by a flexible glycine destabilizes the closed state by shifting the activation curve by -20 mV. The asymmetric impact of pore mutations (i.e. domain specific contributions of G/A/G/A substitutions) on $Ca_V1.2$ gating warrants further research.

2.4.2 Structural Model of the G/A/G/A Region

To illustrate the structural location of the TS Gly-432 and the G/A/G/A motif residues, we refer to crystal structures of potassium channels and designed a homology model. The model supports the idea that the small amino acids are in close contact with bulky hydrophobic residues from neighboring S6 segments, thereby providing domain-domain interfaces (Fig. 2.6). In other words, these homologous residues are likely to be involved in tight S6-S6 packing of the closed channel conformation. If we see these interactions as stabilizing the closed conformation, then the insertion of larger residues would be expected to disrupt the packing and destabilize the closed state, as illustrated in supplemental Fig. 2.9.

2.4.3 Exclusive Role of Gly-432 in Channel Inactivation

In this study we asked the question of how structural changes in Gly-432 and homologous residues Ala-780, Gly-1193, and Ala-1503 affect channel inactivation. Our data revealed a high degree of positional specificity for mutations in position Gly-432. All mutations of Gly-432 slowed down or prevented inactivation (Fig. 2.3, Tab. 2.1), whereas substitutions in domains II-IV did either not affect, or even accelerated inactivation (Fig. 2.4 C). Parallel shifts of the activation and inactivation

curves (Fig. 2.5) indicate that mutations in these three domains do not affect the coupling between activation and inactivation supporting a gating scheme (R)est $\rightarrow$ (O)pen $\rightarrow$ (I)nactivated.

However, mutations in position Gly-432 suppress inactivation regardless of the stability of the activation gates. Any mutation that either stabilizes (e.g. G432A/V) or destabilizes (G432S/M/N/W) the closed resting state prevents channel inactivation, supporting a gating scheme R $\rightarrow$ O $\not\rightarrow$ I. This is evident from Fig. 2.2 and Fig. 2.3, illustrating the observed stabilization of the closed state (shifts of activation curve to the right) and destabilization of the closed state (different shifts of the curve to the left or to the right, see supplemental Fig. 2.8 A). Thus, despite the similar impact of Gly-432 and other residues of the G/A/G/A ring in channel activation, only Gly-432 (IS6) is essential for inactivation in an "all or none" manner.

2.4.4 Conclusions and Outlook

Our structure-activity studies suggest that the TS Gly-432 in domain I of $Ca_V1.2$ forms part of a ring of small and tightly packed residues (G/A/G/A) interacting with adjacent bulky hydrophobic amino acids. The identification of the particular interaction partners of the G/A/G/A ring in adjacent segments remains a challenge for future experimental studies (see Tab. 2.3). These small residues in the lower third of the $Ca_V1.2$ S6 segments are homologous to a ring of small residues in MlotiK and KcsA crystal structures. Systematic mutational studies and correlation analysis of Ca_V revealed that hydrophobic interactions in this region stabilize the channel closed state. The small size is apparently required for tight-fitting interactions with neighbouring bulky residues of $Ca_V1.2$. The apparent structural homologies between KcsA and MlotiK and Ca_V in the pore region provide a guideline for the alignment of S6 segments. Only mutations of the TS Gly-432 disrupted the link between activation and inactivation, whereas substitution of the other alanines or the IIIS6 glycine in most cases simultaneously shifted activation and inactivation. The mechanism behind the unique effect of Gly-432 mutations on inactivation remains to be elucidated.

Ca^{2+} channels are expressed as a single polypeptide assembling into four pseudo-subunits. Although the pseudo-4-fold symmetry might be maintained in S6 helices, it is not preserved in the intracellular domains, where sequence length and interaction partners vary.

It is tempting to speculate that flexibility in IS6 is required for proper transmission of β-subunit-mediated effects on inactivation. Only Gly-432 in segment IS6 is linked to the β interaction domain (BID) located on I-II linker (35, 36). Mutations in position Gly-432 disrupt inactivation irrespective whether the $Ca_V1.2$ comprises

a "fast-inactivating" β_1 or a "slow-inactivating" β_{2a}-subunit (exemplified in supplemental Fig. 2.10), suggesting that the mutated $Ca_V1.2$ α-subunits (G432X) interact with their β-subunits. Similar findings were previously reported for the Timothy mutations G406R (4). We have therefore substituted a flexible glycine for a serine one turn below Gly-432. The introduction of helix flexibility next to the TS mutation G432S partially rescued channel inactivation (supplemental Fig. 2.10). Flexibility in the lower third of segment IS6 may thus be a molecular determinant of β-subunit-mediated inactivation.

2.5 Supplemental Data

```
Cav1.1 I      EWPWIYFVTLILLGSFFILNLVLGVLSGEFT
Cav1.2 I      ELPWVYFVSLVIFGSFFVLNLVLGVISGEFS
Cav1.3 I      ELPWVYFVSLVIFGSFFVLNLVLGVLSGEFS
Cav1.4 I      ELPWVYFVSLVIFGSFFVLNLVLGVLSGEFS
Cav2.1 I      TWNWLYFIPLIIIGSFFMLNLVLGVLSGEFA
Cav2.2 I      TWNWLYFIPLIIIGSFFMLNLVLGVLSGEFA
Cav2.3 I      TWNWLYFIPLIIIGSFFVLNLVLGVLSGEFA
Cav3.1 I      FYNFIYFILLIIVGSFFMINLCLVVIATQFS
Cav3.2 I      FYNFIYFILLIIVGSFFMINLCLVVIATQFS
Cav3.3 I      FYNFIYFILLIIVGSFFMINLCLVVIATQFS
Cav1.1 II     MLVCIYFIILFVCGNYILLNVFLAIAVDNLA
Cav1.2 II     MLVCIYFIILFICGNYILLNVFLAIAVDNLA
Cav1.3 II     MIVCIYFIILFICGNYILLNVFLAIAVDNLA
Cav1.4 II     MLVCIYFIILFICGNYILLNVFLAIAVDNLA
Cav2.1 II     MVFSIYFIVLTLFGNYTLLNVFLAIAVDNLA
Cav2.2 II     MFSSFYFIVLTLFGNYTLLNVFLAIAVDNLA
Cav2.3 II     MWSAIYFIVLTLFGNYTLLNVFLAIAVDNLA
Cav3.1 II     SWAALYFIALMTFGNYVLFNLLVAILVEGFQ
Cav3.2 II     SWAALYFIALMTFGNYVLFNLLVAILVEGFQ
Cav3.3 II     PWASLYFVALMTFGNYVLFNLLVAILVEGFQ
Cav1.1 III    VEMAIFFIIYIILIAFFMMNIFVGFVIVTFQ
Cav1.2 III    VEISIFFIIYIIIIAFFMMNIFVGFVIVTFQ
Cav1.3 III    VEISIFFIIYIIIVAFFMMNIFVGFVIVTFQ
Cav1.4 III    VEISVFFIVYIIIIAFFMMNIFVGFVIITFR
Cav2.1 III    MEMSIFYVVYFVVFPFFFVNIFVALIIITFQ
Cav2.2 III    MELSIFYVVYFVVFPFFFVNIFVALIIITFQ
Cav2.3 III    MEMSIFYVVYFVVFPFFFVNIFVALIIITFQ
Cav3.1 III    PWMLLYFISFLLIVAFFVLNMFVGVVVENFH
Cav3.2 III    PWMLLYFISFLLIVSFFVLNMFVGVVVENFH
Cav3.3 III    PWMLLYFISFLLIVSFFVLNMFVGVVVENFH
Cav1.1 IV     NFAYYYFISFYMLCAFLVINLFVAVIMDNFD
Cav1.2 IV     SFAVFYFISFYMLCAFLIINLFVAVIMDNFD
Cav1.3 IV     NFAIVYFISFYMLCAFLIINLFVAVIMDNFD
Cav1.4 IV     NFAIAYFISFFMLCAFLIINLFVAVIMDNFD
Cav2.1 IV     EFAYFYFVSFIFLCSFLMLNLFVAVIMDNFE
Cav2.2 IV     DFAYFYFVSFIFLCSFLMLNLFVAVIMDNFE
Cav2.3 IV     DLAYVYFVSFIFFCSFLMLNLFVAVIMDNFE
Cav3.1 IV     VISPIYFVSFVLTAQFVLVNVVIAVLMKHLE
Cav3.2 IV     ALSPVYFVTFVLVAQFVLVNVVVAVLMKHLE
Cav3.3 IV     FVSPLYFVSFVLTAQFVLINVVVAVLMKHLD
```

Figure 2.7: Alignment of S6 helices from all ten human Ca_V channels

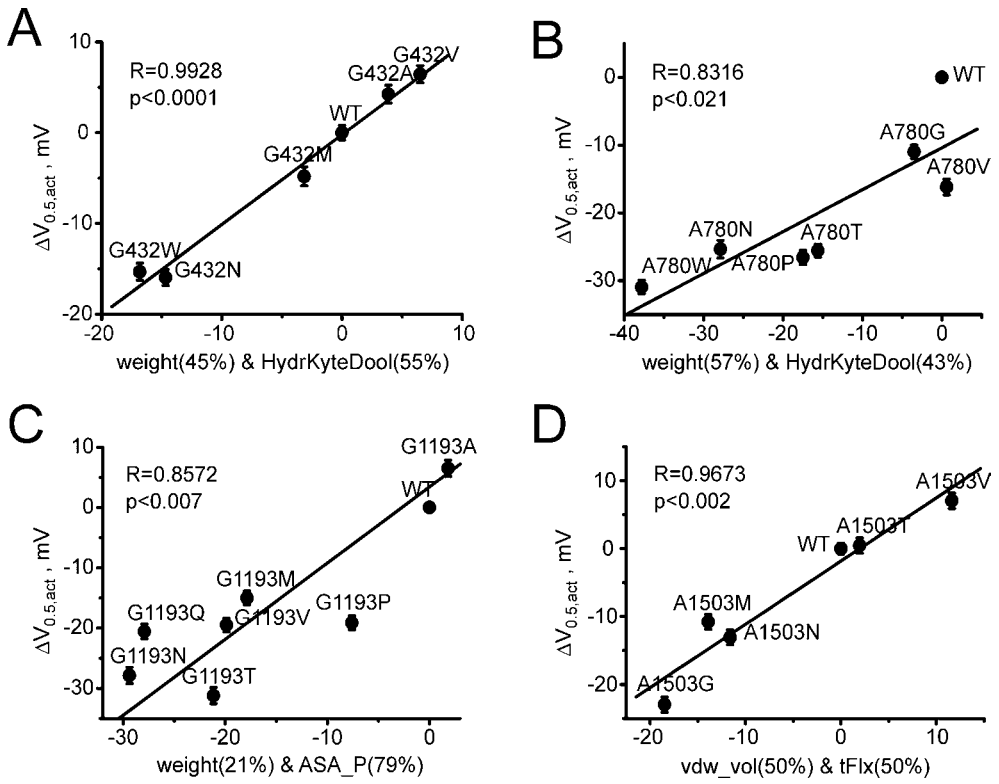

Figure 2.8: Role of residue size in channel activation in S6 segments of $Ca_V1.2$.
Correlation between the shifts of the activation curves (ΔV_{act}) and a linear combination of descriptors characterizing the size of amino acids (either molecular weight (A, B, C) or Van der Waals volume[1] (D)) in combination with hydrophobicity indices such as HydrKyteDool[2] or ASA_P[3] (A, B, C) or a flexibility index[4] (D) with the shifts of the activation curve.

1 vdw_vol – Van der Waals volume
2 HydrKyteDool – hydrophobicity (Kyte and Doolittle (1982))
3 ASA_P – Water accessible surface area of all polar atoms. Accessible surface area refers to the water accessible surface area using a probe radius of 1.4 Å.
4 tFlx - Amino acid side chain flexibility (Gottfries and Eriksson (2009))

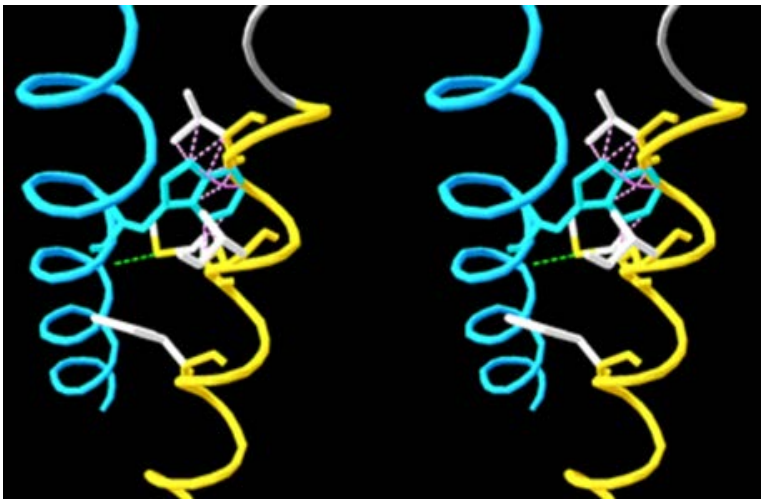

Figure 2.9: Schematic illustration of packing distortions due to insertion of bulky hydrophobic residues in position G432.
Stereo view of helices IS6 (cyan) neighboring IVS6 (yellow). G432 was mutated to W432 using Deep View software (37). Unfavorable steric interactions are shown as pink dots.

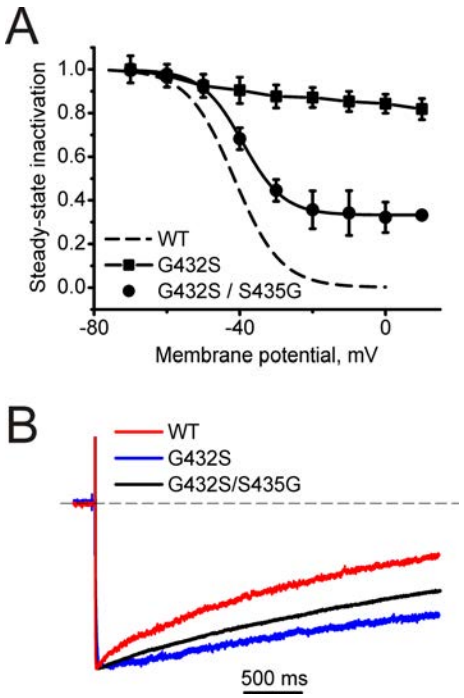

Figure 2.10: Mutation S435G partially rescue channel inactivation.
A, Averaged inactivation curves of double mutation G432S/S435G in comparison with wild-type.
B, Representative I_{Ba} through wild-type and indicated mutant channels during depolarizing test pulses from -100 mV to the peak potentials of the current-voltage relationships (see Tab. 2.1 for mean r_3000 and $V_{0.5,inact}$).

2.6 References

1. Splawski, I., Timothy, K. W., Sharpe, L. M., Decher, N., Kumar, P., Bloise, R., Napolitano, C., Schwartz, P. J., Joseph, R. M., Condouris, K., Tager-Flusberg, H., Priori, S. G., Sanguinetti, M. C., and Keating, M. T. (2004) Cell 119, 19-31
2. Splawski, I., Timothy, K. W., Decher, N., Kumar, P., Sachse, F. B., Beggs, A. H., Sanguinetti, M. C., and Keating, M. T. (2005) Proc. Natl. Acad. Sci. U.S.A 102, 8089-8096; discussion 8086-8088
3. Raybaud, A., Dodier, Y., Bissonnette, P., Simoes, M., Bichet, D. G., Sauvé, R., and Parent, L. (2006) J. Biol. Chem 281, 39424-39436
4. Barrett, C. F., and Tsien, R. W. (2008) Proc. Natl. Acad. Sci. U.S.A 105, 2157-2162
5. Shi, C., and Soldatov, N. M. (2002) J. Biol. Chem 277, 6813-6821
6. Hering, S., Berjukow, S., Sokolov, S., Marksteiner, R., Weiss, R. G., Kraus, R., and Timin, E. N. (2000) J. Physiol. (Lond.) 528 Pt 2, 237-249
7. Stotz, S. C., and Zamponi, G. W. (2001) Trends Neurosci 24, 176-181
8. Kudrnac, M., Beyl, S., Hohaus, A., Stary, A., Peterbauer, T., Timin, E., and Hering, S. (2009) J. Biol. Chem 284, 12276-12284
9. Hohaus, A., Beyl, S., Kudrnac, M., Berjukow, S., Timin, E. N., Marksteiner, R., Maw, M. A., and Hering, S. (2005) J. Biol. Chem 280, 38471-38477
10. Hardman, R. M., Stansfeld, P. J., Dalibalta, S., Sutcliffe, M. J., and Mitcheson, J. S. (2007) J. Biol. Chem 282, 31972-31981
11. Irizarry, S. N., Kutluay, E., Drews, G., Hart, S. J., and Heginbotham, L. (2002) Biochemistry 41, 13653-13662
12. Paynter, J. J., Sarkies, P., Andres-Enguix, I., and Tucker, S. J. (2008) Channels (Austin) 2, 413-418
13. Catterall, W. A., Perez-Reyes, E., Snutch, T. P., and Striessnig, J. (2005) Pharmacol. Rev 57, 411-425
14. Harmar, A. J., Hills, R. A., Rosser, E. M., Jones, M., Buneman, O. P., Dunbar, D. R., Greenhill, S. D., Hale, V. A., Sharman, J. L., Bonner, T. I., Catterall, W. A., Davenport, A. P., Delagrange, P., Dollery, C. T., Foord, S. M., Gutman, G. A., Laudet, V., Neubig, R. R., Ohlstein, E. H., Olsen, R. W., Peters, J., Pin, J.-P., Ruffolo, R. R., Searls, D. B., Wright, M. W., and Spedding, M. (2009) Nucleic Acids Res 37, D680-685

15. Altschul, S. F., Gish, W., Miller, W., Myers, E. W., and Lipman, D. J. (1990) J. Mol. Biol 215, 403-410

16. Chenna, R., Sugawara, H., Koike, T., Lopez, R., Gibson, T. J., Higgins, D. G., and Thompson, J. D. (2003) Nucleic Acids Res 31, 3497-3500

17. Nicholas, K.B., Nicholas H.B. Jr., and Deerfield, D.W. II. (1997) EMBNEW.NEWS, 14

18. Eswar, N., Webb, B., Marti-Renom, M. A., Madhusudhan, M. S., Eramian, D., Shen, M.-Y., Pieper, U., and Sali, A. (2007) Curr Protoc Protein Sci Chapter 2, Unit 2.9

19. Vriend, G. (1990) J Mol Graph 8, 52-56, 29

20. Grabner, M., Dirksen, R. T., and Beam, K. G. (1998) Proc. Natl. Acad. Sci. U.S.A 95, 1903-1908

21. Perez-Reyes, E., Castellano, A., Kim, H. S., Bertrand, P., Baggstrom, E., Lacerda, A. E., Wei, X. Y., and Birnbaumer, L. (1992) J. Biol. Chem 267, 1792-1797

22. Ellis, S. B., Williams, M. E., Ways, N. R., Brenner, R., Sharp, A. H., Leung, A. T., Campbell, K. P., McKenna, E., Koch, W. J., and Hui, A. (1988) Science 241, 1661-1664

23. Hamill, O. P., Marty, A., Neher, E., Sakmann, B., and Sigworth, F. J. (1981) Pflugers Arch 391, 85-100

24. Beyl, S., Depil, K., Hohaus, A., Stary-Weinzinger, A., Timin, E., Shabbir, W., Kudrnac, M., and Hering, S. (2010) Pflugers Arch 461, 53-63

25. Huber, I., Wappl, E., Herzog, A., Mitterdorfer, J., Glossmann, H., Langer, T., and Striessnig, J. (2000) Biochem. J 347 Pt 3, 829-836

26. Stary, A., Kudrnac, M., Beyl, S., Hohaus, A., Timin, E. N., Wolschann, P., Guy, H. R., and Hering, S. (2008) Channels (Austin) 2, 216-223

27. Bruhova, I., and Zhorov, B. S. (2010) J. Gen. Physiol 135, 261-274

28. Tikhonov, D. B., and Zhorov, B. S. (2011) J. Biol. Chem 286, 2998-3006

29. Lipkind, G. M., and Fozzard, H. A. (2001) Biochemistry 40, 6786-6794

30. Stary, A., Shafrir, Y., Hering, S., Wolschann, P., and Guy, H. R. (2008) Channels (Austin) 2, 210-215

31. Shafrir, Y., Durell, S. R., and Guy, H. R. (2008) Biophys. J 95, 3650-3662

32. Cuello, L. G., Jogini, V., Cortes, D. M., Pan, A. C., Gagnon, D. G., Dalmas, O., Cordero-Morales, J. F., Chakrapani, S., Roux, B., and Perozo, E. (2010) Nature 466, 272-275

33. Yarotskyy, V., Gao, G., Peterson, B. Z., and Elmslie, K. S. (2009) J. Physiol. (Lond.) 587, 551-565

34. Clayton, G. M., Altieri, S., Heginbotham, L., Unger, V. M., and Morais-Cabral, J. H. (2008) Proc. Natl. Acad. Sci. U.S.A 105, 1511-1515

35. Van Petegem F, Clark K.A., Chatelain F.C. and Minor D.L. Jr. (2004) Nature 429, 671-675

36. Vitko I., Shcheglovitov A., Baumgart J.P., Arias-Olguín I.I., Murbartián J., Arias J.M. and Perez-Reyes E. (2008) PLoS One 3:e3560.

37. Guex, N. and Peitsch, M.C. (1997) Electrophoresis 18, 2714-2723.

3 Physicochemical Properties of Pore Residues Predict Activation Gating of $Ca_V1.2$: A Correlation Mutation Analysis

Beyl S[1], Depil K[1], Hohaus A, Stary-Weinzinger A, Timin E, Shabbir W, Kudrnac M, Hering S.

Published in Pflügers Archiv – European Journal of Physiology, 2011 Jan; 461(1):53-63

[1] **authors contributed equally to this work**

3.1 Introduction

Calcium entry through voltage-gated calcium channels (Ca_V) initiates and controls a large variety of cellular functions such as generation and propagation of electrical impulses, sensory processes, muscle contraction, secretion of hormones and neurotransmitters, cell differentiation and gene expression [1]. Mammalian Ca^{2+} channel α_1-subunits are encoded by at least ten genes [7]. Depending on the potential where voltage-gated Ca^{2+} channels first open during a depolarisation (so-called threshold potential), they can be subdivided in high-voltage-activated (Ca_V1 – Ca_V2) or low-voltage-activated (Ca_V3) Ca^{2+} channels. Different thresholds of activation were also reported for different isoforms of high-voltage-activated Ca^{2+} channels [7].

We have recently shown that a point mutation (I/T) in segment IIS6 of $Ca_V1.2$ that is associated with a channelopathy transforms the high-voltage-activated $Ca_V1.2$ channel into a low-voltage-activated channel [16, 19]. Additional gating-sensitive residues were identified in other S6 segments of $Ca_V1.2$ [22, 28].

The molecular mechanisms underlying channelopathy mutations in $Ca_V1.2$ are currently unknown. $Ca_V1.2$ are heterooligomeric protein complexes composed of an α_1-subunit and auxiliary β and $\alpha_2\delta$ subunits (see [7] for review). Their pore-forming/voltage-sensing α_1-subunit is composed of four homologous domains formed by six transmembrane segments (S1–S6) each [6].

Compared to K_V, the pore of $Ca_V1.2$ is asymmetric. The 'helix-bending' PXP motif of $K_V1.2$ is absent and the conserved glycine (corresponding to position 220 in K_VAP and 83 in MthK, see [21]) is only present in segments IS6 and IIS6 (see review by Hering et al. [17]). We have shown that substituting proline for this glycine in IIS6 of $Ca_V1.2$ has minor effects on gating of $Ca_V1.2$ [19].

There is evidence, however, that Ca_V α_1-subunits share a common architecture with voltage-gated potassium channels. A cysteine scan of the pore-lining S6 segments of $Ca_V2.1$ by Zhen et al. [36] revealed that opening and closing of the channel changes the accessibility of cysteines in a pattern consistent with a gate localised on the intracellular side. This view is supported by pharmacological studies. On one hand, the inner channel mouth of $Ca_V1.2$ has to open to enable access of the charged (quaternary) phenylalkylamine devapamil (qDev) from the cytosolic side [3]. Interestingly, qDev has unrestricted (voltage independent) access to its binding pocket in the vestibule, suggesting a 'widely open' inner channel mouth in the open state that is in line with Poisson distribution of voltage in the open conformation of a potassium channel [21]. On the other hand, pore-forming S6 segments are apparently able to close the channel vestibule thereby restricting dissociation of organic $Ca_V1.2$ inhibitors such as qDev [3].

Scanning the pore-forming S6 segments with mutations to alanine [4], a bulky tryptophan, a 'helix kinking' proline, a small flexible glycine, a small polar threonine or aspartate or a small cysteine which can form disulfide bonds enabled the identification of gating-sensitive positions in the pore of various voltage-gated ion channels (e.g. [14, 19, 22, 27, 33, 35, 36]).

In the present study, we ask the question how physicochemical properties of amino acids in gating-sensitive positions of $Ca_V1.2$ S6 segments affect the threshold of channel activation (i.e. the open-closed equilibrium).

In continuation of our previous work, we focus on the 'bundle-crossing region' of segments IS6, IIS6 and IIIS6 where the channel is likely closed by tight sealing. G1193 was identified as a novel strong gating determinant in segment IIIS6. Systematic substitution of this residue with amino acids with different properties affected pore stability. A common kinetic phenotype was a leftward shift of the activation curve that is accompanied by decelerated channel deactivation (see also [3, 35]).

Pivotal physicochemical properties of mutated gating determinants in segments IS6, IIS6 and IIIS6 were identified by correlating magnitudes of the shifts of the activation curves with descriptors of the amino acids. By means of this 'mutation correlation analysis', we discovered significant links between activation gating and physicochemical properties in positions L434 (IS6), I781 (IIS6) and G1193 (IIIS6).

3.2 Materials and Methods

3.2.1 Mutagenesis

The $Ca_V1.2$ α_1-subunit coding sequence (GenBank™ X15539) in-frame 3′ to the coding region of a modified green fluorescent protein was kindly donated by Dr. M. Grabner [12]. Substitutions in segment IS6, IIS6, and IVS6 of the $Ca_V1.2$ α_1-subunit were introduced using the QuikChange® Lightning site-directed mutagenesis kit (Stratagene) with mutagenic primers according to the manufacturer's instructions. Mutations were introduced in segment IIIS6 in position 1193 (G1193T/V/N/M/A/Q/W/P) and positions F1191T, V1192T, F1194T, V1195T and I1196T and in IS6 in position 434 (L434A/G/T/V/N/S/W/M).

We systematically introduced residues of different sizes, polarity/hydrophobicity, and aromaticity. All constructs were checked by restriction site mapping and sequencing.

3.2.2 Cell Culture and Transient Transfection

Human embryonic kidney tsA-201 cells were grown at 5 % CO_2 and 37 °C to 80 % confluence in Dulbecco's modified Eagle's/F-12 medium supplemented with 10 % (v/v) fetal calf serum and 100 units/ml penicillin/streptomycin. Cells were split with trypsin/EDTA and plated on 35 mm Petri dishes (Falcon) at $30-50$ % confluence 16 h before transfection. Subsequently tsA-201 cells were co-transfected with cDNAs encoding wild-type or mutant $Ca_V1.2$ α_1-subunits with auxiliary β_{2a} [26] as well as α_2-δ_1 [10] subunits. The transfection of tsA-201 cells was performed using the FuGENE 6 transfection reagent (Roche Applied Science) following standard protocols. tsA-201 cells were used until passage number 15. No variation in channel gating related to different cell passage numbers was observed.

3.2.3 Ionic Current Recordings and Data Acquisition

Barium currents (I_{Ba}) through voltage-gated Ca^{2+} channels were recorded at $22-25$ °C using the patch-clamp technique [15] by means of an Axopatch 200A patch-clamp amplifier (Axon Instruments, Foster City, CA, USA) $36-48$ h after transfection. The extracellular bath solution contained (in millimoles) $BaCl_2$ 5 , $MgCl_2$ 1 , HEPES 10 , choline chloride 140 , titrated to pH 7.4 with methanesulfonic acid. Patch pipettes with resistances of $1-4$ MΩ were made from borosilicate glass (Clark

Electromedical Instruments, UK) and filled with pipette solution containing (in millimoles) CsCl 145 , $MgCl_2$ 3 , HEPES 10 , EGTA 10 , titrated to pH 7.25 with CsOH. All data were digitized using a DIGIDATA 1200 interface (Axon Instruments, Foster City, CA, USA), smoothed by means of a four-pole Bessel filter and saved to disk. One hundred-millisecond current traces were sampled at 10 kHz and filtered at 5 kHz; tail currents were sampled at 50 kHz and filtered at 10 kHz. Holding potential of -100 mV was applied to exclude effects of inactivation on measured parameters. Peak current at more positive holding potentials (-90 mV) was routinely measured to confirm complete recovery from inactivation. Leak currents were subtracted digitally using average values of scaled leakage currents elicited by a 10 mV hyperpolarizing pulse or electronically by means of an Axopatch 200 amplifier (Axon Instruments, Foster City, CA, USA). Capacity currents were not subtracted. When the pipettes were filled with pipette solution, their input resistance ranged between 1 and 4 MΩ. The mean cell capacity was 33 $\pm$ 5 pF ($n = 12$). The mean series resistance was 4.7 $\pm$ 1.9 MΩ. It was compensated ($60 - 85$ % compensation) by the following procedure: The depth of the positive feedback was gradually increased until oscillations (small overcompensation) appear. Even in large cells, the time constant of the capacity current τ_{capacity}) did not exceed 0.25 ms. The early current phase was excluded from data processing (at least $3 \cdot \tau_{\text{capacity}} \approx 0.75$ ms). The pClamp software package (Version 7.0 Axon Instruments, Inc.) was used for data acquisition and preliminary analysis. Microcal Origin 7.0 was used for analysis and curve fitting.

Current–voltage (I–V) relationships for individual cells were normalized to the maximal current. Normalized I–V curves were averaged and the mean I–V curve was fitted to the modified Boltzmann equation:

$$I = \frac{G_{max} \cdot (V - V_{rev})}{1 + \exp \frac{V_{0.5} - V}{k_{act}}} \tag{3.1}$$

where I is the peak current, V is the membrane potential, V_{rev} is the reversal potential, G_{max} is the maximal membrane conductance, $V_{0.5}$ is the voltage for half-maximal activation and k_{act} is the slope factor.

The values of $V_{0.5}$ and k_{act} were used for calculation of the steady-state activation:

$$m_\infty = \frac{1}{1 + \exp \frac{V_{0.5,act} - V}{k_{act}}} \tag{3.2}$$

Data points for activation were calculated dividing the averaged peak currents at given potential by $G_{max} \cdot (V - V_{rev})$.

The time course of current activation was fitted to a mono-exponential function:

$$I(t) = A \cdot \exp\left(\frac{t}{\tau}\right) + C \tag{3.3}$$

where $I(t)$ is current at time t, A is the amplitude coefficient, τ is the time constant, and C is the steady-state current. Data are given as the mean $\pm S.E.$

3.2.4 Calculation of Amino Acid Descriptors

Physicochemical descriptors were calculated for amino acids substituted in positions L434 (IS6), I781 (IIS6) and G1193 (IIIS6) using the Molecular Operating Environment (MOE; version 2008.10, Chemical Computing Group, Inc., Montreal, QC, Canada). This software package calculates more than 300 descriptors. Examples include polarity measures, size and shape indices, flexibility, accessible surface area and others. Seventeen out of 327 possible descriptors were selected to analyse their potential role in channel gating (see supplementary Tab. 3.4 and supplementary Tab. 3.5 for list of descriptors and calculated values).

A turn propensity scale describing the relative turn preferences of the different amino acids in formation of transmembrane helical hairpins was taken from Monné et al. [25] (see also [34]). The hydrophobicity scales were taken from Kyte and Doolittle [23], Hessa et al. [18], White and Wimley [32], Guy [13], Eisenberg et al. [9] and Hopp and Woods [20]. Rigidity and flexibility indices accounting for a series of descriptors, i.e. number of bonds, number of rings, number of rings per atoms in molecule, number of rotatable bonds, number of rotatable bonds per atoms in molecule, number of rigid bonds (i.e. aromatic or double bonds), number of rigid bonds per atoms in molecule, longest flexible chain, ditto per atoms in molecule, number of rigid fragments, ditto per atoms in molecule, number of partial flexible chains and ditto per atoms in molecule, were taken from Gottfries and Eriksson [11].

3.2.5 Correlating Amino Acid Properties with ΔV_{act}

The capability of a given descriptor to predict the shift of the activation curve was established by ranking the correlation coefficients and its significance (t-test). This approach enabled the identification of a 'leading descriptor', i.e. the one with the largest correlation coefficient (r) and the highest significance. Linear regressions were calculated using the ORIGIN subroutine which also yielded correlation coefficients and their statistical significance.

Subsequently, we correlated weighted linear combinations of all 17 descriptors with ΔV_{act}. Combined descriptors were calculated as $\Delta D = a\Delta D_1 + b\Delta D_2$ where ΔD_i represent the difference between descriptor values for mutant and wild-type $Ca_V1.2$. Weighting factors (a and b) were used to estimate the contribution of each descriptor

to correlation (see Tab. 3.3). For mutations in positions I781 (IIS6) and G1193 (IIIS6), this approach enabled us to establish a second descriptor of relevance by ranking the combined correlations with respect to the lowest root mean square error and the highest r (see Tab. 3.2).

3.2.6 Correlating Amino Acid Properties with ΔG

ΔG in the mutant channels relative to WT channel was calculated according to the equation:

$$\Delta G = RT \left(\frac{V_{0.5,mut}}{k_{mut}} - \frac{V_{0.5,WT}}{k_{WT}} \right) \tag{3.4}$$

with $V_{0.5}$ representing the voltage of half activation and k the slope of the curve at $V_{0.5}$ (see Tab. 3.1). The shifts of the steady-state activation curves (ΔV_{act}) of the $Ca_V1.2$ mutants compared to wild-type channels and the calculated changes in free energy ΔG were plotted against the descriptor values and analyzed as described above for ΔV_{act} (see supplemental data).

Table 3.1: Pore mutations affect voltage-dependent gating of $Ca_V1.2$
Midpoints and slope factors of the activation curves, maximal peak current densities and free energies of channel opening (ΔG) of the mutant channels are indicated. Numbers of experiments are indicated in parentheses.

Mutant	$\mathbf{V_{act}}$ [mV]	**k** [mV][1]	Δ**G** [kcal/mol]	$\mathbf{I_{max}}$ [pA/pF]
Wild-type	-18.6 ± 0.9 (8)	5.9 ± 0.6		15.1 ± 2.8
IS6 segment				
L434A	-39.3 ± 0.9 (5)	5.9 ± 0.8	-2.03 ± 0.57	13.3 ± 2.5
L434G	-32.3 ± 0.7 (7)	7.6 ± 0.7	-0.63 ± 0.31	15.7 ± 2.8
L434N	-22.0 ± 0.8 (6)	6.5 ± 0.7	-0.11 ± 0.30	12.3 ± 2.1
L434T	-30.8 ± 1.3 (6)	6.9 ± 0.9	-0.76 ± 0.41	17.1 ± 3.0
L434V	-32.6 ± 0.8 (5)	5.9 ± 0.7	-1.37 ± 0.44	12.6 ± 2.7
L434M	-23.0 ± 1.2 (6)	4.6 ± 0.7	-1.08 ± 0.51	14.3 ± 3.2
L434S	-28.9 ± 0.7 (6)	5.0 ± 0.5	-1.55 ± 0.42	13.7 ± 2.2
L434W	No current			
L434P[2]	No current			
IIIS6 segment				
F1191T	-25.7 ± 1.0 (6)	7.1 ± 0.8	-0.26 ± 0.32	9.6 ± 2.5
V1192T	-16.4 ± 0.9 (7)	6.9 ± 0.9	0.45 ± 0.28	9.1 ± 2.2
G1193T	-49.8 ± 1.0 (7)	5.1 ± 0.6	-3.89 ± 0.72	17.5 ± 3.2
G1193V	-38.1 ± 0.7 (8)	5.6 ± 0.6	-2.14 ± 0.48	12.3 ± 2.7
G1193N	-46.5 ± 1.0 (5)	5.6 ± 0.8	-2.99 ± 0.73	11.2 ± 2.9
G1193M	-33.6 ± 0.7 (8)	6.4 ± 0.6	-1.22 ± 0.36	8.4 ± 2.0
G1193A	-12.1 ± 1.0 (6)	5.7 ± 0.7	0.60 ± 0.28	9.3 ± 1.8
G1193Q	-39.2 ± 0.8 (5)	7.0 ± 0.7	-1.42 ± 0.39	9.8 ± 2.1
G1193P	-37.7 ± 0.7 (7)	6.3 ± 0.6	-1.63 ± 0.39	11.3 ± 2.7
G1193W	No current			
F1194T	-16.5 ± 0.9 (7)	7.8 ± 0.9	0.61 ± 0.26	17.3 ± 3.2
V1195T	-28.9 ± 0.7 (7)	5.1 ± 0.7	-1.48 ± 0.51	18.7 ± 3.4
I1196T	-26.6 ± 0.6 (9)	4.9 ± 0.6	-1.31 ± 0.44	18.4 ± 2.7

[1] Changes of slope factors of mutated channels are statistically not significant ($p > 0.05$) compared to WT
[2] Data from Kudrnac et al. [22]

3.3 Results

3.3.1 G1193 is a Gating-Sensitive Residue in IIIS6

We have recently shown that gradual changes in hydrophobicity in the bundle-crossing region of transmembrane segment IIS6 gradually shift the activation curve of $Ca_V1.2$ [17]. To investigate whether hydrophobic interactions play a similar role in the equivalent section of segment IIIS6, we substituted the small and polar threonine for each of several hydrophobic residues (F1191–I1196) of the $Ca_V1.2$ α_1-subunit (Fig. 3.1, A). Barium (Ba^{2+}) currents were subsequently measured with the patch-clamp technique after co-expression of the auxiliary β_{2a} and α_2-δ_1 subunits in tsA-201 cells. All six threonine mutants (F1191T–I1196T) conducted ionic currents. The largest shift in channel activation ($\Delta V_{act} = -31.2 \pm 1.3$ mV) and the correspondingly slowest kinetics of current activation and deactivation were observed for mutation G1193T, suggesting a potentially important role of this glycine in $Ca_V1.2$ gating (Tab. 3.1; G1193 is ten residues downstream from the putative glycine hinge position). A family of inward Ba^{2+} currents and the corresponding activation curve of mutant G1193T are shown in Fig. 3.1. The activation time constant of G1193T ranged between 14.5 ms (-60 mV) and 1.8 ms (10 mV; Fig. 3.1, D) and the deactivation time constant between 1.8 ms (-100 mV) and 14.2 ms (-60 mV).

Smaller kinetic changes were observed for mutations V1195T ($\Delta V_{act} = -10.3 \pm 1.1$ mV), I1196T ($\Delta V_{act} = -8.0 \pm 1.1$ mV) and F1191T ($\Delta V_{act} = -7.1 \pm 1.3$ mV). Other threonine substitutions had negligible effects (Tab. 3.1; see Fig. 3.1, D and F for corresponding changes in current activation and deactivation kinetics of representative mutants V1192T, G1193T and I1196T compared to wild-type $Ca_V1.2$).

3.3.2 Mutating G1193 to Residues with Different Properties

To gain insight into the structural requirements for stabilisation of the closed state of the channel at this position, we then replaced G1193 with a series of residues of different hydrophobicity, size and polarity. The resulting changes in voltage dependence of $Ca_V1.2$ are illustrated in Fig. 3.2, A. Replacement of G1193 by threonine, asparagine, glutamine, valine, methionine, proline and alanine shifts channel activation ranging from ΔV_{act} of -27.9 ± 1.3 mV for G1193N to $\Delta V_{act} = 6.5 \pm 1.3$ mV for G1193A (Fig. 3.2, A; Fig. 3.1). Interestingly, the mutation G1193A shifted the activation curve towards more depolarised voltages ($\Delta V_{act} = 6.5 \pm 1.3$ mV). Replacement of G1193 by tryptophan results in a non-functional channel. The larger shifts in channel activation in the hyperpolarising direction were accompanied by slower kinetics of current activation and deactivation (Fig. 3.2, B and C). We observed no significant

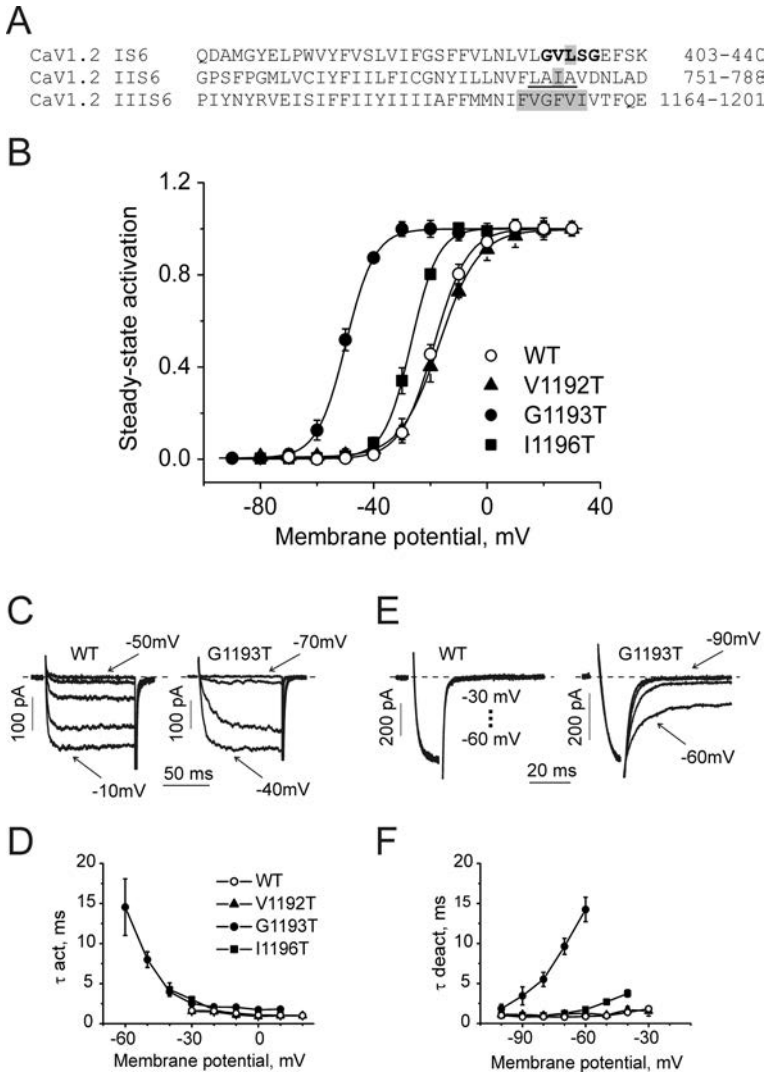

Figure 3.1: Gating changes induced by threonine mutations in segment IIIS6 of $Ca_V1.2$.
A, Alignment of pore-lining S6 segments of $Ca_V1.2$. Mutated residues are shaded grey. Previously identified gating determinants are underlined. GxxxG motif is shown in bold.
B, Averaged activation curves of wild-type ($n = 8$) and mutants V1192T ($n = 7$), G1193T ($n = 7$) and I1196T ($n = 9$).
C, Representative families of I_{Ba} through wild-type and G1193T mutant channels during depolarising test pulses from -100 mV. Zero current levels are indicated as dotted lines.
D, Mean time constants of channel activation of WT ($n = 8$) and mutants V1192T ($n = 7$), G1193T ($n = 7$) and I1196T ($n = 9$) are plotted against test potential.
E, Representative tail currents of WT and G1193T channels. Currents were activated during a 20 ms conditioning depolarisation to -10 mV for wild-type and -40 mV for G1193T. Deactivation was recorded during subsequent repolarisations with 10 mV increments starting from -100 mV.
F, Mean time constants of channel deactivation of wild-type ($n = 7$) and mutants V1192T ($n = 6$), G1193T ($n = 6$) and I1196T ($n = 7$) are plotted against test potential. Time constants were estimated by fitting current activation and deactivation to a mono-exponential function.

effects on the reversal potential (data not shown) suggesting that the studied deep pore mutations did not affect selectivity.

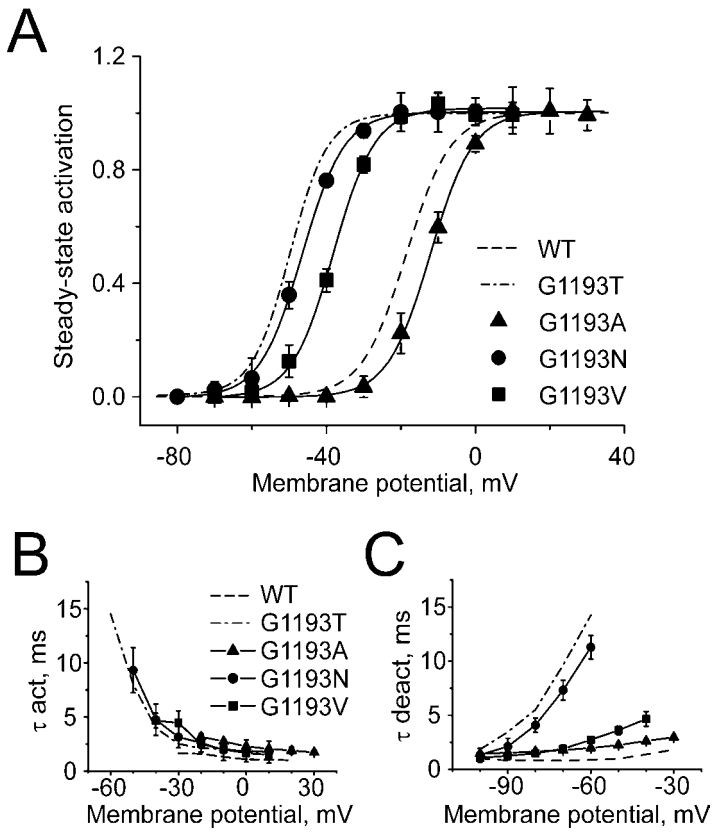

Figure 3.2: Gating changes induced by mutations of G1193 in segment IIIS6 of $Ca_V1.2$.
A, Averaged activation curves of the WT ($n = 8$) and mutants G1193T ($n = 7$), G1193A ($n = 6$), G1193N ($n = 5$) and G1193V ($n = 8$).
B, C Mean time constants of channel activation (B) and deactivation (C) for WT and mutants G1193T, G1193A, G1193N and G1193V are plotted against test potential ($n = 5 - 8$). Time constants were estimated by fitting current activation and deactivation to a mono-exponential function.

3.3.3 Mutation Correlation Analysis in Position G1193

In order to get insights into possible links between channel activation and physicochemical properties of amino acids, regression analysis was performed for selected descriptors (see "Materials and methods" section and supplementary Tab. 3.4), including size, hydrophobicity, flexibility and rigidity indices, propensity to van der

Waals interactions and others.

Descriptor values were calculated with MOE or taken from the literature (see "Materials and methods") and plotted against the corresponding shifts of the activation curves or calculated changes in free energy (ΔG). The correlations were ranked by correlation coefficient and significance. The best correlation with ΔV_{act} in position G1193, with the highest statistical significance (t test, $p < 0.009$), was obtained with the accessible surface area of all polar atoms (ASA_P; Fig. 3.3). Tab. 3.2 shows the correlation coefficients (r) for the linear regression plots of physicochemical descriptors against the measured ΔV_{act}. In contrast to our findings in segment IIS6 [17], ΔV_{act} did not correlate with hydrophobicity (Tab. 3.2). We subsequently searched for optimal two-descriptor correlations by combining all 17 descriptors in pairs (see "Materials and methods"). The most significant correlation was observed for the combination of ASA_P (leading descriptor) and the number of rotatable bonds (Tab. 3.3). Potentially modulating effects of other physicochemical properties are summarised in Tab. 3.3.

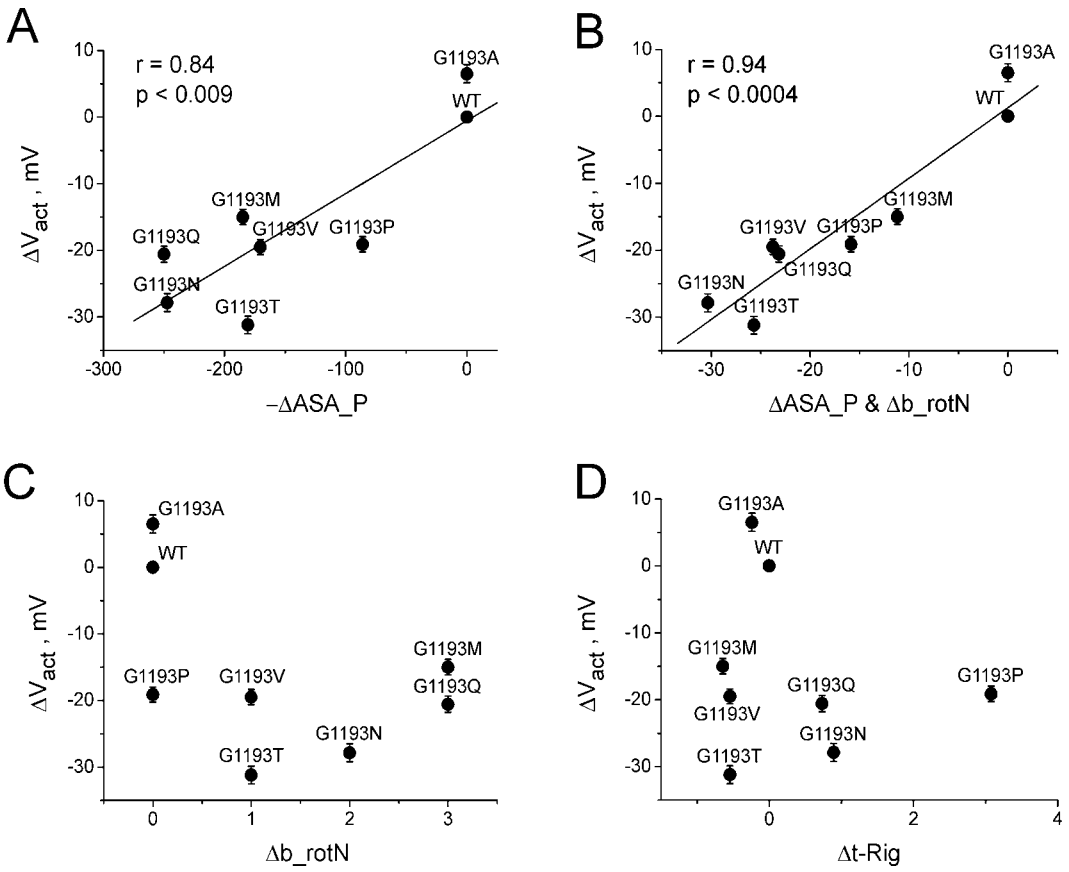

Figure 3.3: The accessible surface area of all polar atoms in position G1193 (IIIS6) predicts the shift of the activation curve.
A, Correlation between the shifts of the activation curves (ΔV_{act}) and the changes in accessible surface area of all polar atoms (ΔASA_P).
B, Correlation between ΔV_{act} and the best linear combination of two descriptors ASA_P and b_rotN (the number of rotatable bonds, see Tab. 3.3 for ranking).
C, D No correlation between ΔV_{act} and Δb_rotN or ΔV_{act} and Δt-Rig (an amino acid side-chain rigidity index). See complete list of descriptors in supplementary Fig. 3.7

Table 3.2: Identification of leading descriptors predicting ΔV_{act}.
The capability of a given descriptor to predict the shift of the activation curve was established by ranking the correlation coefficients (*r*) and its significance (t-test). This approach enabled the identification of a "leading descriptor" (L434- b_rotN; I781-hydrophobicity; G1193-ASA_P, see "Materials and methods").

Descriptor	r	p
L434 substitutions in segments IS6		
b_rotN	0.8695	0.0050
t-Flx	0.8690	0.0050
b_rotR	0.8551	0.0068
a_heavy	0.7793	0.0226
Weight	0.7761	0.0235
ASA	0.7685	0.0258
vdw_area	0.7533	0.0309
vdw_vol	0.7273	0.0408
...		
I781 substitutions in segments IIS6		
Hydrophobicity[1]	0.8679[3]	0.0042
t-Rig	-0.6910	0.0577
vdw_area	0.6648	0.0720
a_count	0.6538	0.0786
b_rotR	0.6378	0.0888
vdw_vol	0.6149	0.1047
...		
G1193 substitutions in segments IIIS6		
ASA_P	-0.8438	0.0084
a_heavy	-0.7567	0.0297
b_count	-0.6928	0.0567
a_count	-0.6890	0.0587
Weight	-0.6862	0.0602
lip_don	-0.6834	0.0616
vdw_vol	-0.6609	0.0743
...		
Hydrophobicity	0.38397	0.34769
Helix turn propensity[2]	-0.1713	0.6849

[1] Hydrophobicity scale from Kyte and Doolittle [23]. Similar correlations were obtained with other scales [9, 13, 18, 20, 32]
[2] Monné et al. [25]
[3] Data from Hering et al. [17]

Table 3.3: Combined descriptor analysis.
Correlations of weighted linear combinations of all 17 descriptors (see Tab. 3.4 in Supplemental Data) with ΔV_{act}. Combined descriptors were calculated as $\Delta D = a\Delta D_1 + b\Delta D_2$ (see "Materials and methods"). Weighting factors (a and b) were used to estimate the contribution of each descriptor to correlation. The fractional impacts of two amino acid descriptors in regression are indicated in percent. The capability of a given descriptor combination to predict the shift of the activation curve was established by ranking the correlation coefficients (r) and its significance (t-test).

Best linear combination of descriptors	**R**	**p**
L434 substitutions in segments IS6		
None of the 136 tested linear combinations improved the prediction of the leading descriptor		
I781 substitutions in segments IIS6		
Hydrophobicity (68%) + lip_acc (32%)	0.9733	<0.0001
Hydrophobicity (68%) + b_rotN (32%)	0.9567	0.0001
Hydrophobicity (68%) + t-Flx (32%)	0.9477	0.0003
Hydrophobicity (73%) + ASA_P (27%)	0.9343	0.0006
Hydrophobicity (63%) + vdw_area (37%)	0.9266	0.0009
G1193 substitutions in segments IIIS6		
−ASA_P (67%) + b_rotN (33%)	0.9455	0.0003
−ASA_P (67%) + t-Flx (33%)	0.9232	0.0010

3.3.4 Correlation Analysis in Gating-Sensitive Position L434 (IS6)

A similar methodological approach was used to estimate the predictive value of amino acid properties for mutations in position L434. This amino acid was previously identified as a gating-sensitive residue in segment IS6 [22]. Mutating L434 to eight amino acids with different properties (compare with mutations in segment IIIS6) resulted in different shifts of the activation curve (Fig. 3.4).

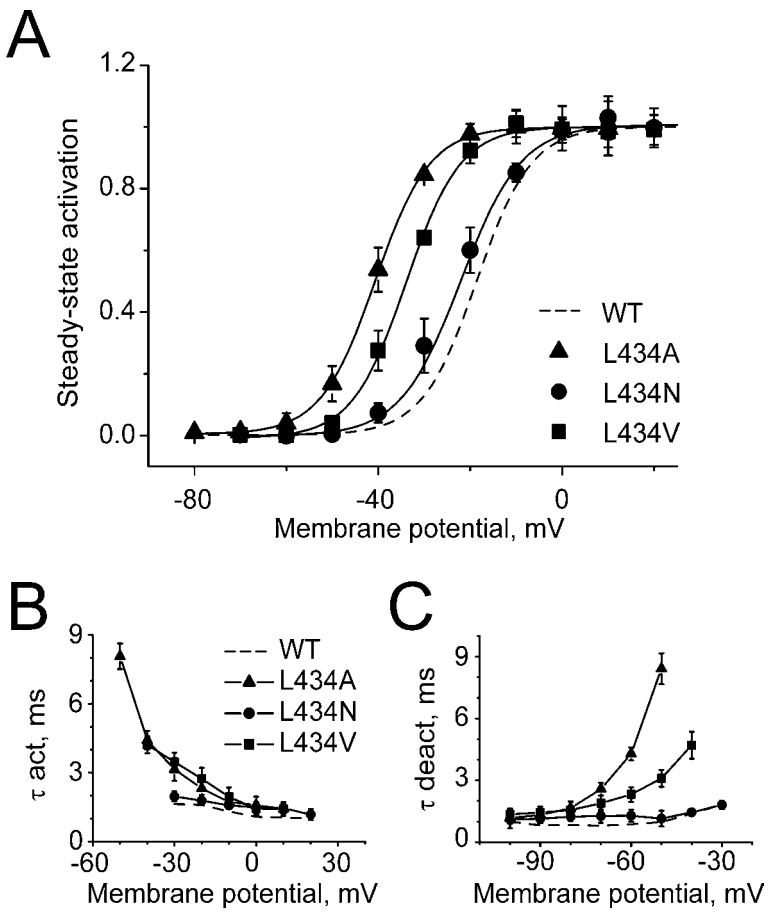

Figure 3.4: Gating changes induced by mutations of L434 in segment IS6 of $Ca_V1.2$.
A, Averaged activation curves of the WT ($n = 8$) and mutants L434A ($n = 5$), L434N ($n = 6$) and L434V ($n = 5$).
B, C Mean time constants of channel activation (B) and deactivation (C) for WT and mutants L434A, L434N and L434V are plotted against test potential ($n = 5$–8). Time constants were estimated by fitting current activation and deactivation to a mono-exponential function

The best prediction of ΔV_{act} was observed for the number of rotatable bonds (b_RotN, see Tab. 3.2). A rotatable bond is defined as any single non-ring bond to a non-

terminal heavy atom within the amino acid molecule. The regression line for b_RotN is illustrated in Fig. 3.5 ($r = 0.86$, $p < 0.006$). No improvement was observed for any combined descriptor correlation (Tab. 3.3).

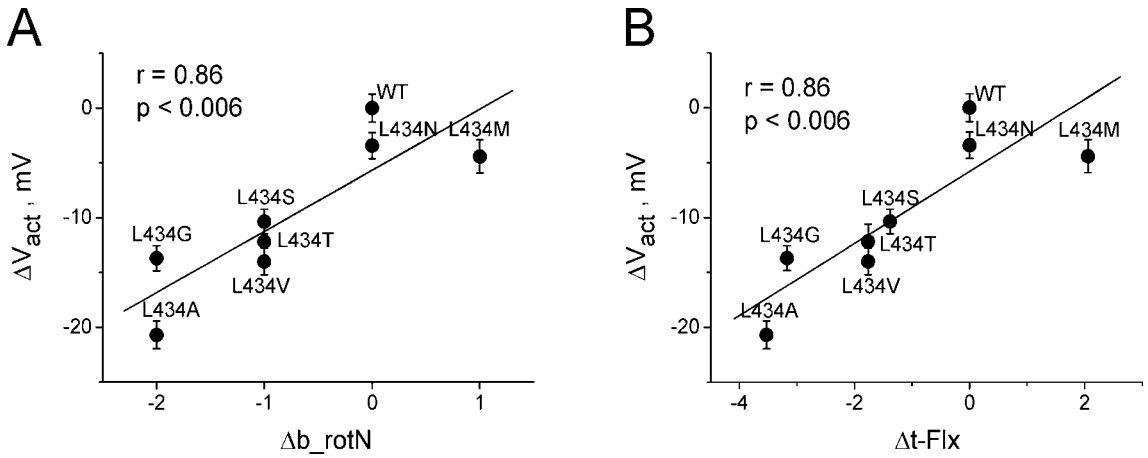

Figure 3.5: Side-chain flexibility in position L434 (IS6) predicts the shifts of the activation curve.
A, Correlation between ΔV_{act} and Δb_rotN (number of rotatable bonds).
B, Correlation with the amino acid flexibility index Δt-Flx (see Supplementary Tab. 3.4)

3.3.5 Modulation of Hydrophobic Interactions in I781 (IIS6) by other Amino Acid Properties

In a previous study, we found a highly significant correlation between changes in hydrophobicity (ΔH) and ΔV_{act} for mutations in position I781 of segment IIS6 [17]. This correlation suggested that either the closed channel state is stabilised by hydrophobic interactions with neighbouring residue or a stabilisation of the open state by exposure of more polar residues in this position to water, or both. Here we confirmed the leading role of hydrophobicity in this position by accounting for all 17 descriptors in this position ($r = 0.86$ and $p < 0.005$; see Tab. 3.3). Improved correlations were obtained for several descriptor combinations (e.g. hydrophobicity and the number of O and N atoms, with $r = 0.97$ and $p < 0.0001$; see Tab. 3.3 for improved correlations for other amino acid properties).

3.4 Discussion

We have previously reported that the shift of the activation curve induced by point mutations in segment IIS6 correlates with changes in hydrophobicity in a cluster of residues in segment IIS6 (779–784: LAIA) and particularly in position I781 (see [17] for review). Mutations of I781 in the α_1-subunit of $Ca_V1.2$ to residues of different hydrophobicity, size and polarity all shifted channel activation in the hyperpolarising direction with I781P causing the most severe (-37 mV shift) effect [19]. Mutations in position I781 decelerated activation and deactivation, and the shifts to more hyperpolarized voltages usually correlate with slower activation kinetics. Similar shifts of the activation curve and even more dramatic slowing of the activation and deactivation kinetics were observed in NaChBac when a conserved glycine 219 (corresponding to a putative hinge glycine in S6 of most K^+ channels) was mutated to a helix breaking proline [35]. Furthermore, when a locus of conserved hydrophobic residues in pore/gate-forming segment IVS6 of $Ca_V2.3$ (1718–1722: VAVIM) was systematically replaced by flexible glycines, slow deactivation of mutants A1719G and V1720G was accompanied by a -20 mV shift of the activation curve [27]. Thus, leftward shifts of the activation curve and slowing down of current activation in Ca_V are induced by mutations to amino acids with different physicochemical properties. Interestingly, the leftward shifts in the steady-state activation curves and the deceleration of the activation and deactivation resemble very much the action of L-type Ca^{2+} channel agonists such as BayK 8644 (see also [19]). Here we investigate whether these properties (descriptors) predict the measured shifts of the activation curve.

3.4.1 G1193 is a Gating-Related Residue in Segment IIIS6

Mutating the hydrophobic residues of the 'bundle-crossing' region of segment IIIS6 (Fig. 3.1 A) to the small and polar threonine revealed a gating-sensitive residue at position G1193. Mutations of G1193 caused the largest changes in gating of $Ca_V1.2$ as measured by activation curves and current deactivation kinetics (Fig. 3.1 B-F and Fig. 3.2).

3.4.2 Changes in the accessible surface area of all polar atoms in position G1193 (IIIS6) predict the shifts of the activation curve

Crystal structures of KcsA, K_VAP and MthK potassium channels revealed that a flexible glycine at analogous positions 99, 220 and 83 provides a hinge point for helix bending of K_V during channel opening [21, 24, 35]. Mutation of the analogous

glycine in NaChBac (G219P) to proline, which forces an α-helix into a bent conformation, substantially slowed deactivation and shifted the activation curve [36]. The functional role of S6 glycines and the positions for helix bending during channel activation of Ca_V remain unclear. No correlations either with side-chain rigidity or with helix turn propensity were observed for mutations of G1193 (Fig. 3.3 D; Tab. 3.2; localised ten residues downstream from the putative glycine hinge position). We then examined the effect of side-chain size because we suspected that if the structure around G1193 were tightly packed, the small size of glycine might be functionally important. No significant correlation with the mass of the substituted residues was found ($p > 0.05$; Tab. 3.3). However, a significant correlation between ΔV_{act} and the accessible surface area of all polar atoms was observed (ASA_P; Fig. 3.3 A and B). Since ASA_P would indicate more favourable energy for solvation in water [8, 29, 31] than packing in the interior of a protein, this relationship suggests that the open gate conformation either exposes this position to more water than the closed conformation or allows the side chain to avoid unfavourable interactions with other residues, or both.

3.4.3 Number of Rotatable Bonds and a Side-Chain Amino Acid Flexibility Index Predict the Shift of the Activation Curve by Mutations in Position L434 (IS6)

A strong correlation ($r = 0.86$, $p < 0.006$) between the number of rotatable bonds and ΔV_{act} was observed for mutations of L434 in segment IS6 (Fig. 3.4 and Fig. 3.5). These data suggest that a certain degree of side-chain flexibility of residues in this position of the 'bundle-crossing region' is necessary for normal channel gating. A flexibility index introduced by Gottfries and Eriksson [11] for amino acids confirms the role of side-chain flexibility in this position. Interestingly, the gating-sensitive L434 occupies the central position of a GxxxG motif (Fig. 3.1 A) which is known to allow backbone–backbone helix interactions in a hydrophobic environment [5]. The GxxxG motif participates in helix packing typically in a way where glycines allow close contacts between helices crossing at angles atypical of 'knobs-into-holes' packing. Other larger residues in these positions would probably tend to clash with atoms of the adjacent helix. L434 is located in the middle of this pattern (i.e. on the opposite face) and thus would not be involved in the helix–helix interactions that involve the glycines. We speculate that L434 is involved in interactions with other helices (e.g. if the glycines are involved with S6–S6 interactions than L434 could interact with S5 or L45 linker).

3.4.4 Co-Correlations Provide Additional Insight into Modulatory Properties of Amino Acid Residues

In positions L434 (IS6), I781 (IIS6) and G1193 (IIIS6), we identified different leading descriptors providing the highest correlations with a single amino acid descriptor. A side-chain flexibility index, hydrophobicity and the accessible surface area of polar atoms predicted the shifts of the activation curves induced by mutations in the corresponding positions (Fig. 3.3, Fig. 3.5 and Fig. 3.6). We performed a co-correlation analysis where ΔV_{act} was correlated with any of the 136 weighted linear combination of two descriptors (see supplementary Tab. 3.4 for complete list of descriptors combined for co-correlations). The predictive capability of side-chain flexibility in position L434 (i.e. number of rotatable bonds or the related amino acid descriptor Δt-Flx) was not improved by any of the 136 co-correlations tested.

Analysing all linear combinations between two descriptors for mutations in position I781 and G1193 revealed some very strongly linear predictions of ΔV_{act}. The leading descriptor was found to be always one out of the best correlating descriptor pairs. The fractional weighting of the leading descriptors in the best-ranking combinations ranged from 60 % to 83 % (see Tab. 3.3, examples are illustrated in Fig. 3.3 B and Fig. 3.6 B and D). The second descriptors alone had no predictive capability (Fig. 3.3 C and Fig. 3.6 D). The best prediction of ΔV_{act} for mutations in position I781 was obtained for a combination of ΔHydrophobicity and the number of hydrogen bound acceptors (N and O atoms) with second best ranking of the combination ΔHydrophobicity and a side-chain flexibility index. These data suggest that hydrogen bonding and side-chain flexibility in this position affect the closed-open equilibrium. The same analysis for mutations in position G1193 revealed better correlations for the combination of the accessible surface area of all polar atoms with one of the side-chain flexibility.

The improved predictive capability of combined descriptors suggests that the dominating interaction (leading descriptor) in selected positions can be modulated by additional interactions (see Tab. 3.3 for other potentially modulating interactions in position I781, e.g. side-chain flexibility, van der Waals interactions and others).

3.4.5 Link between ΔV_{act} and Changes in Free Energy (ΔG)

Replacing pore residues by amino acids with different physicochemical properties affects the free energy of $Ca_V1.2$ gating. Estimation of changes in free energies and cycle mutant analyses in voltage-gated ion channels enabled important insights into the energetics of channel opening (e.g. [30, 33]; see [22] for a study on $Ca_V1.2$). Accordingly, we have calculated the changes of free energy during the activation

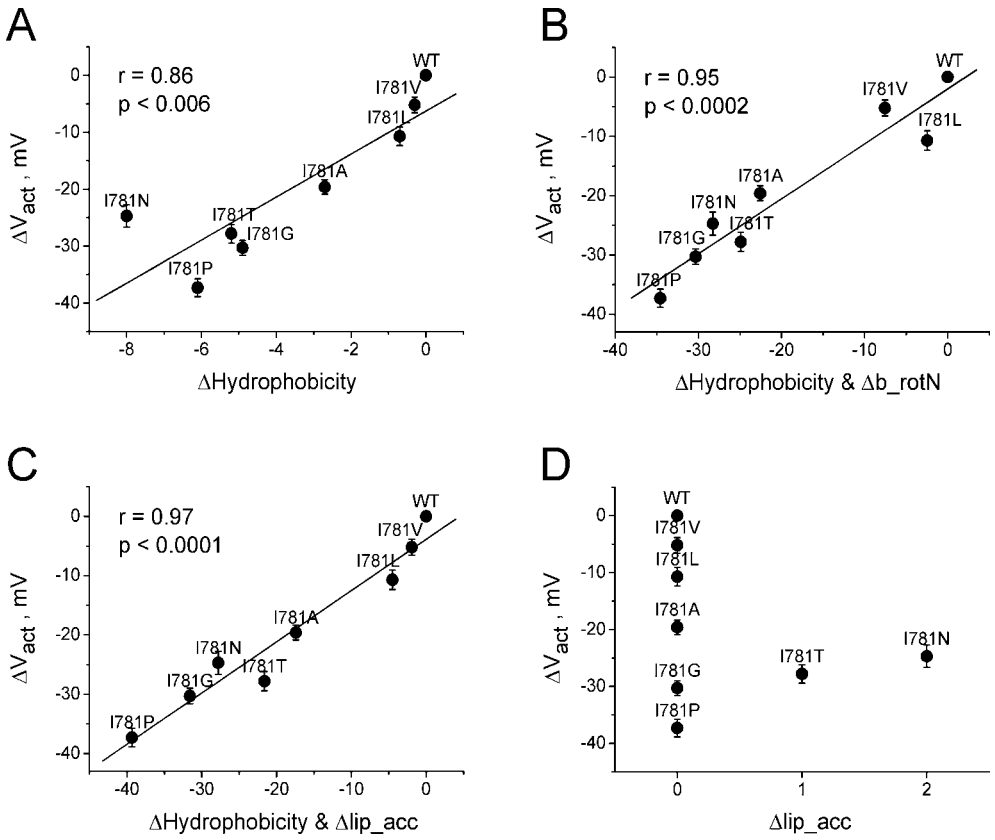

Figure 3.6: Hydrophobicity in position I781 (IIS6) predicts the shifts of the activation curve.
A, Correlation between ΔV_{act} and changes in hydrophobicity.
B, The best prediction of ΔV_{act} by a linear combination of two descriptors was obtained for ΔHydrophobicity and Δlip_acc (number of O and N atoms; hydrogen bond acceptors).
C, Second best co-correlation was observed for ΔHydrophobicity and Δb_rotN (see also Tab. 3.3).
D, No correlation between ΔV_{act} and Δlip_acc (see supplementary Tab. 3.4).

of wild-type and all IS6, IIS6 and IIIS6 $Ca_V1.2$ mutants. ΔV_{act} and ΔG correlate strongly (supplementary Fig. 3.7). Nevertheless, ΔG deduced from a Boltzmann distribution reflects not only the energy of pore opening but also the energy of voltage sensor transition. In general, it can be assumed that mutations in the pore region do not disturb the voltage sensor transition and that ΔG of S6 mutations reflects the changes in the pore. However, some mutations apparently affect the transition of the voltage-sensing machinery from the resting to the activated state (e.g. I780P (IIS6) in [2]). Changes in the slope factor reflect changes in $\delta \cdot Z$, where Z is the charge and δ is a fraction of membrane potential that the voltage sensors cross during their movement. Obviously the mutations in the pore are unable to change the charge Z. They may, however, modify the fraction of the effective membrane potential by releasing or restricting voltage sensor movements. Minor changes in the slope factor (see Tab. 3.1) have effects on the calculated ΔG and may affect correlations. For the studied S6 mutations, ΔG and ΔV_{act} appeared to be equivalent measures of the pore energetics. This may, however, not always be the case and care has to be taken with pore mutations that significantly change the slope factor (e.g. I1196T; Tab. 3.1) or significantly change the kinetics of channel opening and closure (A780P [2]).

3.5 Conclusions and Outlook

Mutations in the bundle-crossing region of pore-forming S6 segments frequently shift the activation curves along the voltage axis and affect the kinetics of channel gating. Making use of mutation correlation analysis, we identified descriptors of side chains at specific positions that predict these changes in channel activation gating. In segment IS6 (L434), ΔV_{act} correlated with the number of rotatable bonds reflecting side-chain flexibility. In position G1193 in segment IIIS6, ΔV_{act} depended on the accessible surface area of all polar atoms, and in position I781, ΔV_{act} correlated with hydrophobicity. Leading descriptors were identified by single and combined correlation analysis (i.e. correlations between ΔV_{act} and all possible pairs of amino acid descriptors were analysed). Correlation analysis emerges thus as a useful tool to unravel the importance of particular amino acid properties in pore-lining S6 segments. Different leading descriptors in different S6 segments indicate individual contributions of four homologous but not identical domains in $Ca_V1.2$ gating.

3.6 Supplemental Data

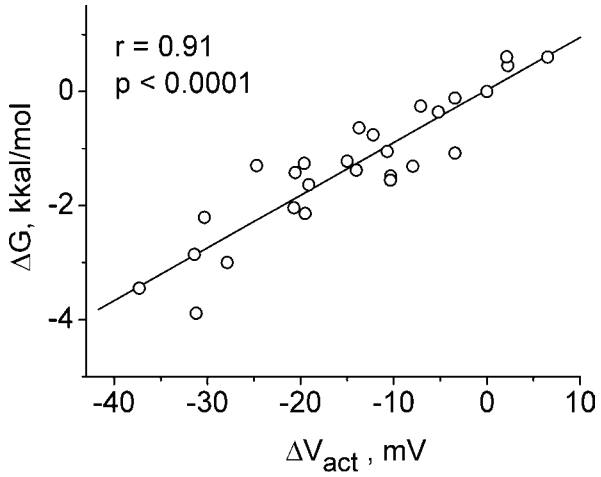

Figure 3.7: Correlation between ΔV_{act} and changes in free energy (ΔG).
Each point represents the mean value of ΔV_{act} and ΔG ($n \geq 5$) of all studied mutants.

Table 3.4: Amino acid descriptors.
List of descriptors and their abbreviations used for correlation analysis.

Descriptors	**Abbreviation**
Number of atoms (including implicit hydrogens)	a_count
Number of heavy atoms	a_heavy
Number of hydrophobic atoms	a_hyd
Water accessible surface area calculated using a radius of 1.4 Å for the water molecule	ASA
Water accessible surface area of all polar atoms. Accessible surface area refers to the water accessible surface area using a probe radius of 1.4 Å	ASA_P
Number of bonds (including implicit hydrogens)	b_count
Number of rotatable bonds. Topological parameter is a measure of molecular flexibility. A bond is rotatable if it has order 1, is not in a ring, and has at least two heavy neighbors	b_rotN
Hydropathy index of an amino acid (number representing the hydrophobic or hydrophilic properties of its side-chain)	Hydrophobicity[1]
Turn propensity scale for transmembrane helices	Helix turn propensity[2]
The number of O and N atoms	lip_acc
The number of OH and NH atoms	lip_don
Log of the octanol/water partition coefficient	logP(o/w)
Amino acid side chain flexibility	t-Flx[3]
Amino acid side chain rigidity	t-Rig[3]
Area of van der Waals surface	vdw_area
Van der Waals volume	vdw_vol
Molecular weight	weight

[1] Kyte and Doolittle (1982)
[2] Monne et al. (1999)
[3] Gottfries and Eriksson (2009)

Table 3.5: Calculated amino acid descriptors.Calculated values of descriptors for each amino acid.

Amino acid	a_count	a_heavy	a_hyd	ASA [Å^2]	ASA_P [Å^2]	b_count
A	13	6	2	242.74324	0	12
C	14	7	2	273.85648	224.60548	13
D	15	9	2	278.12979	225.49535	14
E	18	10	3	313.17535	235.8358	17
F	23	12	8	360.759	135.49438	23
G	10	5	1	217.82974	0	9
H	20	11	4	332.29614	208.60524	20
I	22	9	5	310.68332	143.2991	21
K	25	10	5	361.34518	217.77553	24
L	22	9	5	322.46146	181.95142	21
M	20	9	5	337.17654	184.87408	19
N	17	9	2	291.38504	247.48032	16
P	17	8	4	279.61813	86.08024	17
Q	20	10	3	323.83051	249.88791	19
R	27	12	4	389.96347	291.78641	26
S	14	7	2	259.00809	200.8197	13
T	17	8	3	280.57605	180.75769	16
V	19	8	4	289.1181	170.4135	18
W	27	15	10	393.14545	202.4926	28
Y	24	13	8	372.37411	232.85223	24

Amino acid	b_rotN	lip_acc	lip_don	logP(o/w)	vdw_area [Å^2]	vdw_vol [Å^3]
A	1	3	1	-0.538	107.75999	111.04782
C	2	3	1	-0.428	129.56839	132.36894
D	3	5	1	-1.165	135.29059	140.78549
E	4	5	1	-0.723	152.52267	165.21468
F	3	3	1	0.997	178.25824	226.02168
G	1	3	1	-1	90.52791	86.61864
H	3	5	2	-1.307	161.0999	190.2766
I	3	3	1	0.876	160.8013	184.33536
K	5	4	2	-0.469	176.59799	202.89105

L	3	3	1	0.876	160.8013	184.33536
M	4	3	1	0.117	165.9369	182.28906
N	3	5	2	-2.02	143.85384	151.32716
P	1	3	1	0.178	122.67898	147.62587
Q	4	5	2	-1.578	161.08592	175.75635
R	5	6	4	-0.542	204.6192	227.01431
S	2	4	2	-1.573	117.78994	119.57003
T	2	4	2	-1.111	135.02202	143.99921
V	2	3	1	0.434	143.56921	159.90617
W	3	4	2	1.363	200.41324	271.36938
Y	3	4	2	0.689	188.28818	234.5439

3.7 References

1. Berridge MJ (2003) Cardiac calcium signalling. Biochem Soc Trans 31:930–933
2. Beyl S, Kügler P, Kudrnac M, Hohaus A, Hering S, Timin E (2009) Different pathways for activation and deactivation in $Ca_V1.2$: a minimal gating model. J Gen Physiol 134:231–241
3. Beyl S, Timin EN, Hohaus A, Stary A, Kudrnac M, Guy RH, Hering S (2007) Probing the architecture of an L-type calcium channel with a charged phenylalkylamine: evidence for a widely open pore and drug trapping. J Biol Chem 282:3864–3870
4. Blaber M, Zhang XJ, Matthews BW (1993) Structural basis of amino acid alpha helix propensity. Science 260:1637–1640
5. Brosig B, Langosch D (1998) The dimerization motif of the glycophorin A transmembrane segment in membranes: importance of glycine residues. Protein Sci 7:1052–1056
6. Catterall WA (2000) Structure and regulation of voltage-gated Ca^{2+} channels. Annu Rev Cell Dev Biol 16:521–555
7. Catterall WA, Perez-Reyes E, Snutch TP, Striessnig J (2005) International Union of Pharmacology. XLVIII. Nomenclature and structure–function relationships of voltage-gated calcium channels. Pharmacol Rev 57:411–425
8. Chothia C (1974) Hydrophobic bonding and accessible surface area in proteins. Nature 248:338–339
9. Eisenberg D, Weiss RM, Terwilliger TC (1984) The hydrophobic moment detects periodicity in protein hydrophobicity. Proc Natl Acad Sci U S A 81:140–144
10. Ellis SB, Williams ME, Ways NR, Brenner R, Sharp AH, Leung AT, Campbell KP, McKenna E, Koch WJ, Hui A et al (1988) Sequence and expression of mRNAs encoding the alpha 1 and alpha 2 subunits of a DHP-sensitive calcium channel. Science 241:1661–1664
11. Gottfries J, Eriksson L (2009) Extensions to amino acid description. Mol Divers. doi:101007/s11030-009-9204-2
12. Grabner M, Dirksen RT, Beam KG (1998) Tagging with green fluorescent protein reveals a distinct subcellular distribution of L-type and non-L-type Ca^{2+} channels expressed in dysgenic myotubes. Proc Natl Acad Sci U S A 95:1903–-1908

13. Guy HR (1985) Amino acid side-chain partition energies and distribution of residues in soluble proteins. Biophys J 47:61–70

14. Hackos DH, Chang TH, Swartz KJ (2002) Scanning the intracellular S6 activation gate in the shaker K^+ channel. J Gen Physiol 119:521–532

15. Hamill OP, Marty A, Neher E, Sakmann B, Sigworth FJ (1981) Improved patch-clamp techniques for high-resolution current recording from cells and cell-free membrane patches. Pflugers Arch 391:85–100

16. Hemara-Wahanui A, Berjukow S, Hope CI, Dearden PK, Wu SB, Wilson-Wheeler J, Sharp DM, Lundon-Treweek P, Clover GM, Hoda JC, Striessnig J, Marksteiner R, Hering S, Maw MA (2005) A CACNA1F mutation identified in an X-linked retinal disorder shifts the voltage dependence of $Ca_V1.4$ channel activation. Proc Natl Acad Sci U S A 102(21):7553–7558

17. Hering S, Beyl S, Stary A, Kudrnac M, Hohaus A, Guy HR, Timin E (2008) Pore stability and gating in voltage-activated calcium channels. Channels 2:61–69

18. Hessa T, Kim H, Bihlmaier K, Lundin C, Boekel J, Ersson H, Nilsson I, White SH, von Heijne G (2005) Recognition of transmembrane helices by the endoplasmic reticulum translocon. Nature 433:377–381

19. Hohaus A, Beyl S, Kudrnac M, Berjukow S, Timin EN, Marksteiner R, Maw MA, Hering S (2005) Structural determinants of L-type channel activation in segment IIS6 revealed by a retinal disorder. J Biol Chem 280:38471–38477

20. Hopp TP, Woods KR (1981) Prediction of protein antigenic determinants from amino acid sequences. Proc Natl Acad Sci U S A 78:3824–3828

21. Jiang Y, Lee A, Chen J, Cadene M, Chait BT, MacKinnon R (2002) The open pore conformation of potassium channels. Nature 417:523–526

22. Kudrnac M, Beyl S, Hohaus A, Stary A, Peterbauer T, Timin E, Hering S (2009) Coupled and independent contributions of residues in IS6 and IIS6 to activation gating of $Ca_V1.2$. J Biol Chem 284:12276–12284

23. Kyte J, Doolittle RF (1982) A simple method for displaying the hydropathic character of a protein. J Mol Biol 157:105–132

24. Magidovich E, Yifrach O (2004) Conserved gating hinge in ligand- and voltage-dependent K^+ channels. Biochemistry 43:13242–13247

25. Monné M, Nilsson I, Elofsson A, von Heijne G (1999) Turns in transmembrane helices: determination of the minimal length of a "helical hairpin" and derivation of a fine-grained turn propensity scale. J Mol Biol 293:807–814

26. Perez-Reyes E, Castellano A, Kim HS, Bertrand P, Baggstrom E, Lacerda AE, Wei XY, Birnbaumer L (1992) Cloning and expression of a cardiac/brain beta subunit of the L-type calcium channel. J Biol Chem 267:1792–1797

27. Raybaud A, Baspinar EE, Dionne F, Dodier Y, Sauvé R, Parent L (2007) The role of distal S6 hydrophobic residues in the voltage-dependent gating of $Ca_V2.3$ channels. J Biol Chem 282:27944–27952

28. Raybaud A, Dodier Y, Bissonnette P, Simoes M, Bichet DG, Sauvé R, Parent L (2006) The role of the GX9GX3G motif in the gating of high voltage-activated Ca^{2+} channels. J Biol Chem 281(51):39424–39436

29. Rose GD, Geselowitz AR, Lesser GJ, Lee RH, Zehfus MH (1985) Hydrophobicity of amino acid residues in globular proteins. Science 229:834–838

30. Sadovsky E, Yifrach O (2007) Principles underlying energetic coupling along an allosteric communication trajectory of a voltage-activated K^+ channel. Proc Natl Acad Sci U S A 104:19813–19818

31. Sharp KA, Nicholls A, Friedman R, Honig B (1991) Extracting hydrophobic free energies from experimental data: relationship to protein folding and theoretical models. Biochemistry 30:9686–9697

32. White SH, Wimley WC (1999) Membrane protein folding and stability: physical principles. Annu Rev Biophys Biomol Struct 28:319–365

33. Yifrach O, MacKinnon R (2002) Energetics of pore opening in a voltage-gated K^+ channel. Cell 111:231–239

34. Zhao Y, Scheuer T, Catterall WA (2004) Reversed voltage-dependent gating of a bacterial sodium channel with proline substitutions in the S6 transmembrane segment. Proc Natl Acad Sci U S A 101:17873–17878

35. Zhao Y, Yarov-Yarovoy V, Scheuer T, Catterall WA (2004) A gating hinge in Na^+ channels; a molecular switch for electrical signaling. Neuron 41:859–865

36. Zhen XG, Xie C, Fitzmaurice A, Schoonover CE, Orenstein ET, Yang J (2005) Functional architecture of the inner pore of a voltage-gated Ca^{2+} channel. J Gen Physiol 126:193–204

4 Neutralization of a Single Voltage Sensor (IIS4) Affects Gating Determinants in all Four Pore Forming S6 Segments of $Ca_V1.2$

Beyl S, Depil K, Hohaus A, Stary-Weinzinger A, Linder T, Timin E, Hering S.

Submitted to Journal of General Physiology, 2012 Jun

4.1 Introduction

Hodgkin and Huxley (1952) hypothesized that activation of voltage-gated ion channels is initiated by movement of charged particles across the membrane. This charge movement (called "gating current") was later directly measured for sodium channels (Armstrong & Bezanilla, 1973). Crystal structures of ion channels revealed that four domains in Na_V or in K_V comprise 6 transmembrane segments (S1-S6) that are assembled in a way that S1-S4 form the voltage-sensing module and the remaining S5 and S6 segments form the ion-conducting pore (Payandeh et al., 2010; Long et al., 2005). In principle, the voltage-sensing and ion-conducting modules can function independently of one another (Long et al., 2005): voltage sensors can exist without ion pores (Murata et al., 2005; Ramsey et al., 2006; Sasaki et al., 2006) and 2-transmembrane-segment channels (2 TM) function without voltage sensors (Catterall, 2010).

Gating-sensitive positions in the pore of Ca_V have been identified through extensive site-directed mutagenesis studies (Hohaus et al., 2005; Zhen et al., 2005; Raybaud et al., 2006, 2007; Kudrnac et al., 2009; Wall-Lacelle et al., 2011). Changes in stability of the open and/or closed states induced by pore mutations (Zhao et al., 2004a,b; Hohaus et al. 2005) or e.g. Zn^{2+} bridges constraining the S4 movement (Phillips and Swartz, 2010) are manifested in shifts of the activation curve and accompanying deceleration of deactivation kinetics. Interestingly, such gating distortions are characteristic of a CACNA1F mutation identified in an X-linked retinal disorder (Hemara-Wahanui et al., 2005) and the Timothy syndrome (Splawski et al., 2004; Splawski et al., 2005; Depil et al., 2011). Biophysical models describe voltage sensor movements and pore opening in K_V as separate transitions (Schoppa & Sigworth, 1998c; Ledwell & Aldrich, 1999; Horn et al., 2000; Yifrach & MacKinnon, 2002, Bezanilla, 2000 for review). Based on these assumptions, the kinetic properties of mutants with gating disturbances in pore-forming S6 segments of Na_V (e.g. NaChBac, Zhao et al., 2004a,b) and Ca_V (Beyl et al, 2009) have successfully been quantified.

The opening of the Shaker K_V channel involves multiple activation steps as the S4 segments move from the resting state towards the activated state, which is followed by a concerted opening transition of the S6 gate. This concept of Ledwell and Aldrich (1999) is supported by biophysical studies in Shaker K_V (Bezanilla et al., 1994; Hoshi et al., 1994; Stefani et al., 1994; Zagotta et al., 1994a,b; Schoppa & Sigworth, 1998a,b,c; Smith-Maxwell et al., 1998a,b; Ledwell & Aldrich, 1999; Hackos et at., 2002, Sukhareva et al., 2003; del Camino et al., 2005; Pathak et al., 2005).

Surprisingly, in a concatenated Shaker K_V, a single voltage sensor is sufficient to open and close the channel (Gagnon and Bezanilla, 2009). Furthermore, a recent molecular dynamics simulation of a potassium channel revealed that the downward movement of a single S4 segment can initiate channel closure (Jensen et al. 2012).

Thus, if channel closure is a concerted movement of all four S6 gates then one S_4 segment either directly or allosterically controls gating structures in all four domains.

Here we analyze the link between a voltage sensor and gating structures by combining pore mutations in all four S6 segments in a calcium channel ($Ca_V1.2$) with a voltage sensing S_4 segment where the charged residues were replaced by neutral glutamines. Our results suggest that conformational changes in a single S_4 segment (IIS_4) are transmitted to specific residues (GAGA ring, Depil et al. 2011) in all four pore-forming S6 segments.

4.2 Methods

4.2.1 Mutagenesis

Substitutions in S4 and S6 segments of the $Ca_V1.2$ α_1-subunit (GenBank™ X15539) were introduced using the QuikChange® Lightning Site-Directed Mutagenesis Kit (Stratagene) with mutagenic primers according to the manufacturer's instructions. All constructs were checked by restriction site mapping and sequencing.

4.2.2 Cell Culture and Transient Transfection

Human embryonic kidney tsA-201 cells were grown at 5 % CO_2 and 37 °C to 80 % confluence in Dulbecco's modified Eagle's/F-12 medium supplemented with 10 % (v/v) fetal calf serum and 100 units/ml penicillin/streptomycin. Cells were split with trypsin/EDTA and plated on 35 mm Petri dishes (Falcon) at $30-50$ % confluence 16 h before transfection. Subsequently tsA-201 cells were co-transfected with cDNAs encoding wild-type or mutant $Ca_V1.2$ α_1-subunits with auxiliary β_{2a} (Perez-Reyes et al., 1992) as well as α_2-δ_1 (Ellis et al., 1988) subunits.

The transfection of tsA-201 cells was performed using the FuGENE 6 Transfection reagent (Roche) following standard protocols. tsA-201 cells were used until passage number 15. No variation in channel gating related to different cell passage numbers was observed.

4.2.3 Ionic Current Recordings and Data Acquisition

Barium currents (I_{Ba}) through voltage-gated Ca^{2+} channels were recorded at $22-25$ °C by patch-clamping (Hamill et al., 1981) using an Axopatch 200A patch clamp amplifier (Axon Instruments, Foster City) $36-48$ h after transfection. The extracellular bath solution (in mmol: $BaCl_2$ 5 , $MgCl_2$ 1 , HEPES 10 , choline-Cl 140) was titrated to pH 7.4 with methanesulfonic acid. Patch pipettes with resistances of $1-4$ MΩ were made from borosilicate glass (Clark Electromedical Instruments, UK) and filled with pipette solution containing (in mmol: CsCl 145 , $MgCl_2$ 3 , HEPES 10 , EGTA 10), titrated to pH 7.25 with CsOH. All data were digitized using a DIGIDATA 1200 interface (Axon Instruments, Foster City), smoothed by means of a four-pole Bessel filter and saved to disk. 100 ms current traces were sampled at 10 kHz and filtered at 5 kHz; tail currents were sampled at 50 kHz and filtered at 10 kHz. Leak currents were subtracted digitally using average values of scaled leakage currents elicited by a 10 mV hyperpolarizing pulse or electronically by means of

an Axopatch 200 amplifier (Axon Instruments, Foster City). Series resistance and offset voltage were routinely compensated for. The pClamp software package (Version 7.0 Axon Instruments, Inc.) was used for data acquisition and preliminary analysis. Microcal Origin 7.0 was used for analysis and curve fitting.

The voltage dependence of activation was determined from I-V curves and fitted to

$$m_\infty = \frac{1}{1 + \exp \frac{V_{0.5,act} - V}{k_{act}}} \tag{4.1}$$

The time course of current activation was fitted to a mono-exponential function:

$$I(t) = A \cdot \exp\left(\frac{t}{\tau}\right) + C \tag{4.2}$$

where $I\,(t)$ is current at time t, A is the amplitude coefficient, τ is the time constant, and C is the steady-state current. Data are given as the mean $\pm S.E$. Time constants were plotted versus voltage (e.g. Fig. 4.1 C). The left branch of the bell-shaped curve of the time constants corresponds to channel deactivation and the right branch to the activation (see Hodgkin and Huxley, 1952). At voltages where channel activation and deactivation overlap (peak of the bell-shaped dependence) the data are given as averaged values of both time constants.

4.2.4 Confocal Imaging

Images were obtained 30 h after transfection. The images were acquired with a Zeiss Axiovert 200 M microscope equipped with an LSM 510 laser scanning module, using a 63× (1.4 NA) oil immersion objective. Fluorescence from GFP-tagged $Ca_V1.2$ α_1-subunits was excited at 488 nm using an argon laser, and emitted light was recorded with a $505 - 530$ nm bandpass filter. The plasma membrane was stained with 2 µm FM4-64 (an amphiphilic styryl dye, Molecular Probes). The dye was detected with a helium-neon laser (excitation, 543 nm) in combination with a 650 nm long pass filter. The instrument was operated in the multitracking mode to minimize channel cross-talk. Pinholes were adjusted to obtain optical slices of 1 µm thickness for each channel.

4.2.5 Modeling

The homology model of $Ca_V1.2$ is based on the NavAb crystal structure (Payandeh et al., 2011) (protein databank identifier: 3RVY). Modeller 9v7 (Eswar et al., 2006) was used to generate the model. Modeling criteria have been published previously (Stary et al., 2008).

4.2.6 Online Supplemental Material

The role of individual arginines (R650Q, R653Q, R656Q, R662Q) and lysine (K659Q) in segment IIS4 in $Ca_V1.2$ gating is presented in Supplemental Materials.

Localization of wild-type and mutant $Ca_V1.2$ α_1-subunits within tsA-201cells is presented in Supplemental Materials (Fig. 4.7). Additional substitutions of residues 431-434 in segment IS6 and effect of IIS4 neutralization on gating perturbations are presented in Supplemental Materials (Fig. 4.8).

4.3 Results

4.3.1 Charge Neutralization in IIS4 Induces Only Small Gating Disturbances in $Ca_V1.2$

The location of the arginine and lysine residues (which we refer to as R1-R5) in the $S4$ segments is shown in Fig. 4.1 (A and B). We will use the designation $S4_N$ for a mutant with a "charge-neutralized" $S4$ segment in which all the positions R1-R5 are replaced by glutamines. Currents were measurable only through construct $IIS4_N$ (Tab. 4.1); while mutants $IS4_N$, $IIIS4_N$ and $IVS4_N$ did not result in expression of channels that conducted barium currents. This finding can either be explained by insufficient trafficking of the constructs to the membrane or by an impaired function of the channels. Applying a more negative holding potential (-140 mV) had no effect suggesting that these constructs are not in an inactivated state. Subsequent analysis of the subcellular distribution of GFP-tagged constructs revealed that $IS4_N$, $IIIS4_N$ and $IVS4_N$ are less efficiently targeted to the membrane (see supplemental Fig. 4.7).

Channel gating of $IIS4_N$ was quite similar to wild type (wt); no significant shift in the activation curve was observed ($\Delta V = 1.2 \pm 1.2$ mV, Fig. 4.1). The role of individual $IIS4$ charges in $Ca_V1.2$ gating is presented in Supplemental Materials (Fig. 4.6, Tab. 4.1). At first glance, these results suggest that one or more of the other segments ($IS4$, $IIIS4$ and $IVS4$) play a role in voltage-dependent gating, while $IIS4$ has only a minor impact. However, combining $IIS4_N$ with mutations in S6 segments revealed, that it had a significant impact on channel activation.

4.3.2 Charge Neutralization in Segment IIS4 Rescues Gating Disturbances in the GAGA Ring in Segments IS6-IVS6

First we combined $IIS4_N$ with perturbing pore mutations in a highly conserved structure motif ("GAGA ring", Depil et al. 2011) of small residues in homologous positions of all four domains (Gly-432 (IS6), Ala-780 (IIS6), Gly-1193 (IIIS6), Ala-1503 (IVS6)). All of these mutations have been shown to shift the activation curve to the left and to decelerate deactivation (see also Beyl et al., 2009; Raybaud et al., 2007; Hohaus et al., 2005; Kudrnac et al., 2009; Tadross et al., 2010). For example, mutant G432W activates and deactivates (Fig. 4.2 A, C and D) with the slowest activation/deactivation time constant of about 18 ms observed at -50 mV (Fig. 4.2 D). However, gating disturbances induced by G432W in IS6 were "rescued" by combination with $IIS4_N$. In $G432W/IIS4_N$, the shift of the activation curve compared to wild type ($\Delta V = V_{0.5,mut} - V_{0.5,wt}$) was eliminated ($\Delta V = -0.5 \pm 1.1$ mV

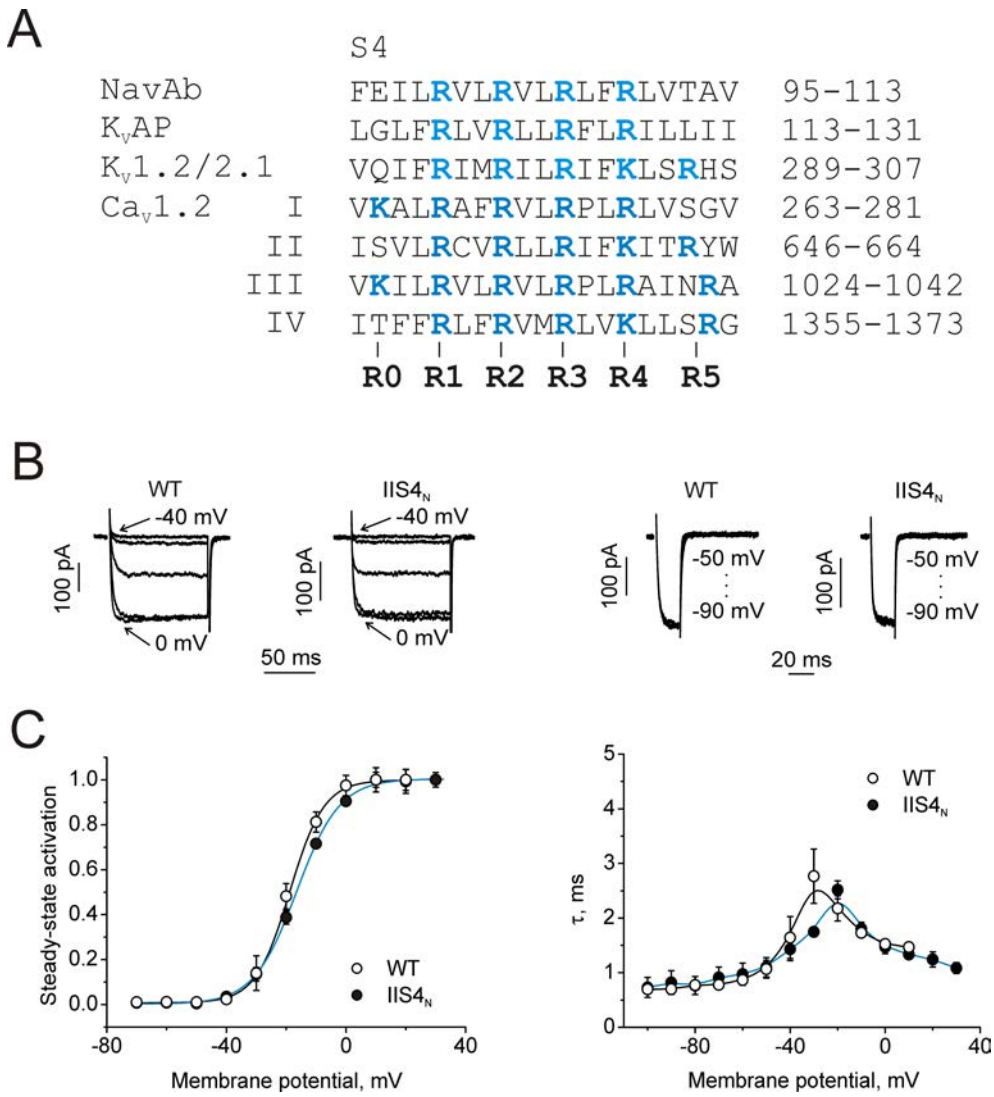

Figure 4.1: Charge neutralization in segment IIS4 of $Ca_V1.2$ has minor effects on activation gating.
A, alignment of S4 segments of NavAb (protein databank identifier: 3RVY), K_VAP (protein data bank identifier: 1ORS), $K_V1.2/2.1$ (protein data bank identifier: 2R9R) and $Ca_V1.2$ (accession number: P15381). Charged residues are blue.
B, *left panel* shows representative families of I_{Ba} through wild-type cannel and channel with the "charge-neutralized" IIS4 segment ($IIS4_N$) starting from threshold potential (-50 mV). Barium currents were evoked during depolarizing test pulses from a holding potential of -100 mV (increments, 10 mV). *Right panel* shows representative tail currents. Currents were activated during a -20 ms conditioning depolarization to 0 mV. Deactivation was recorded during subsequent repolarisations with 10 mV increments starting from -100 mV.
C, *left panel*: averaged activation curves of wild-type ($n = 9$) and $IIS4_N$ ($n = 11$) channels and *right panel* voltage dependent time constants of channel activation/deactivation.

(G432W/$IIS4_N$) vs. -14.9 ± 1.0 mV (G432W), Fig. 4.2) and current kinetics were correspondingly faster with a maximal activation/deactivation time constant of about 5 ms at -20 mV (Fig. 4.2 A, C, D). A similar result was obtained with G432N, shifting the activation curve to the left. Combining G432N with $IIS4_N$ reversed this shift ($\Delta V = -3.3 \pm 1.1$ mV (G432N/$IIS4_N$) vs. 17.9 ± 1.1 mV (G432N)) and also accelerated deactivation (supplemental Fig. 4.8). Comparable rescue effects on gating disturbances were observed for constructs G1193T/$IIS4_N$ and A1503G/$IIS4_N$. Substantial shifts in channel activation ($\Delta V = -31.0 \pm 1.3$ mV in G1193T and -22.6 ± 1.2 mV in A1503G) were reduced to -2.0 ± 1.1 mV and -1.0 ± 1.1 mV in G1193T/$IIS4_N$ and A1503G/$IIS4_N$ respectively (coloured bars in Fig. 4.3 B, Tab. 4.1). Current kinetics were also considerably faster; the maximal (slowest) time constants of current activation and deactivation for these constructs are given as coloured columns in Fig. 4.3 C.

Interestingly, combining $IIS4_N$ with the gating disturbing A780T in IIS6 (a pore mutation in its "own" domain II) shifted the activation curve only partially towards wild type ($\Delta V = -25.2 \pm 1.1$ mV (A780T) vs. $\Delta V = -13.2 \pm 1.1$ mV in A780T/$IIS4_N$), without inducing significant changes in current kinetics (see shifts of the voltage dependence inFig. 4.4 C, D).

4.3.3 Charge Neutralization in IIS4 does not Affect Gating Disturbances in Positions Neighbouring to GAGA

Mutations of residues upstream and downstream of the GAGA positions in segments IS6, IIIS6 and IVS6 (G432, G1193 and A1503, see alignment in Fig. 4.3 A) resulted in a wide spectrum of gating phenotypes. Gating disturbances induced either leftward or rightward shifts of the activation curve (ranging from -28.3 ± 1.2 mV (I781T) to $+26.9 \pm 1.2$ mV (L431P)). None of these mutants was, however, sensitive to combination with $IIS4_N$. This is evident from Fig. 4.3 illustrating the steady-state activation (Fig. 4.3 B) and the maximal time constants (Fig. 4.3 C). Neither the shifts of the activation curves nor the maximal time constants of the activation/deactivation were reversed towards wild type kinetics.

4.3.4 Charge Neutralization in Segment IIS4 Modulates Kinetics of IIS6 Pore Mutants

That $IIS4_N$ only partially rescued gating disturbances induced by A780T is not unexpected. If a hyperpolarisation-driven downward movement of $IIS4$ initiates pore closure by moving IIS6 towards its closed position, then replacement of the charged

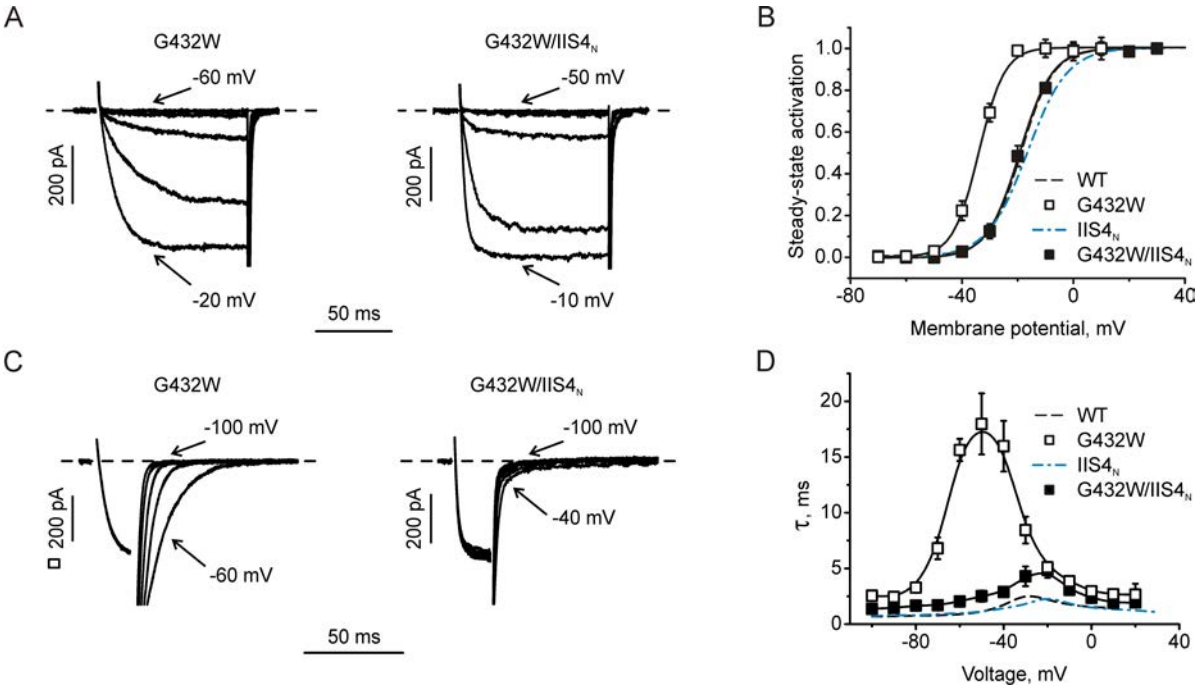

Figure 4.2: Charge neutralization in IIS4 rescues a gating disturbances induced by G432W in segment IS6.
A and C, representative activation (A) and tail currents (C) traces through G432W and $G432W/IIS4_N$ mutant channels.
B and D, averaged activation curves (B) and voltage dependence of the activation/deactivation time constants (D) of WT, G432W, $IIS4_N$ and $G432W/IIS4_N$.

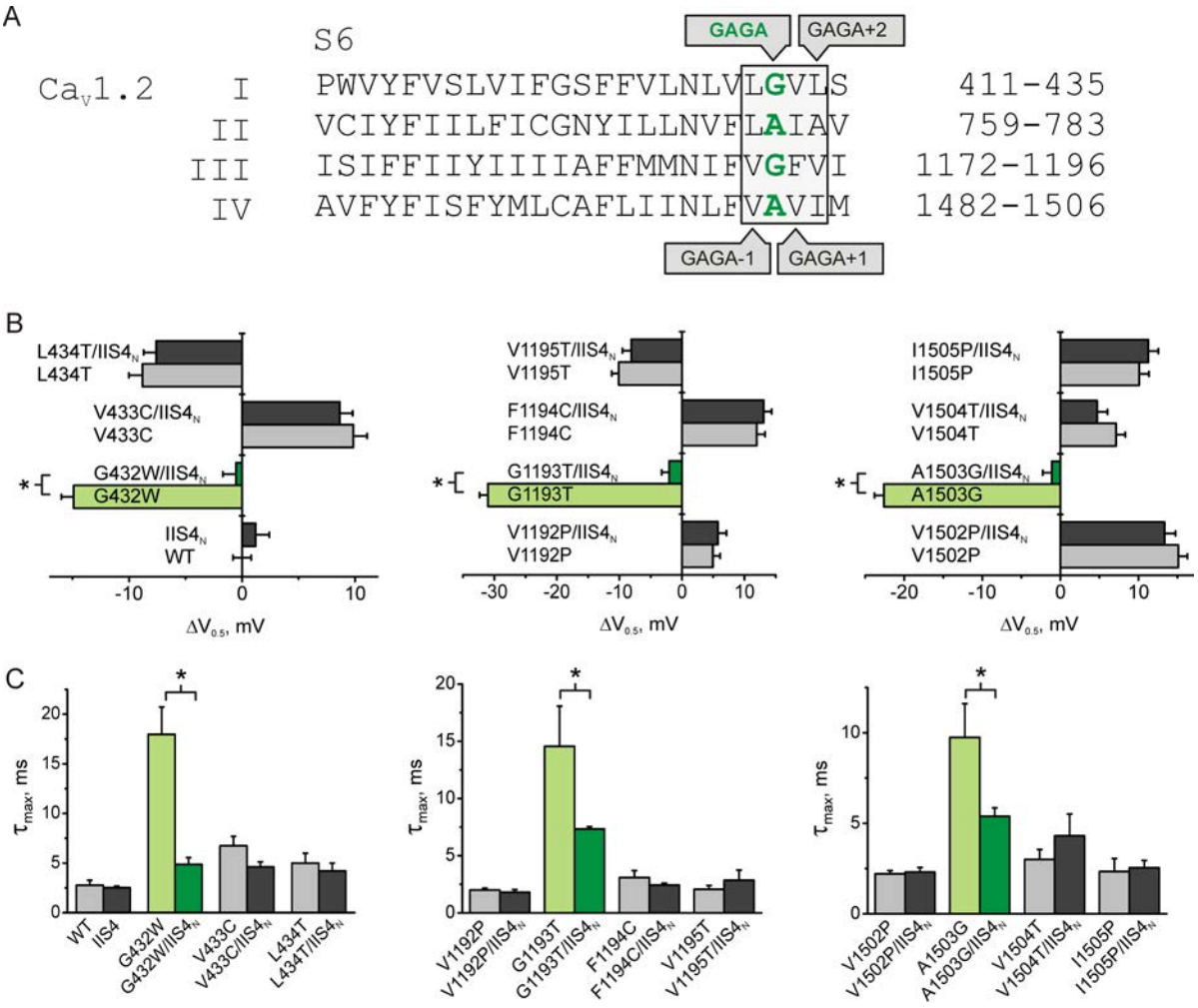

Figure 4.3: Charge neutralization in domain II (IIS4) rescues gating disturbances in GAGA positions of domains I, III and IV.
A, alignment of S6 segments of $Ca_V1.2$ (accession number: P15381). The "GAGA" ring of small conserved residues in IS6-IVS6 is highlighted in green. Mutated residues are boxed. B and C, shift of activation curve (B) and peak activation/deactivation time constants (C) of the studied pore mutations in segments IS6 (left), IIIS6 (middle) and IVS6 (right) either alone or in combination with $IIS4_N$. Statistically significantly different (t-test) values are marked with asterisks. Error bars indicate SEM.

arginines would inevitably decelerate the gate movement (channel closure) in domain II.

In line with such a scenario, constructs I781T/$IIS4_N$ and A782P/$IIS4_N$ displayed additional shifts of the activation curves compared to I781T and A782P. In I781T ΔV amounted -28.3 ± 1.2 mV while charge neutralization (I781T/$IIS4_N$) further increased ΔV to -36.0 ± 1.1 mV (Fig. 4.4 A, C middle column). Likewise, the shift of the activation curve in A782P/$IIS4_N$ ($\Delta V = -31.4 \pm 1.2$ mV) was also not rescued but increased compared to A782P (-24.2 ± 1.2 mV, Fig. 4.4 A, C right column).

Interestingly, charge neutralization in IIS4 decelerated deactivation of both constructs at negative voltages (from -60 mV to -100 mV), with little effect on kinetics of channel activation (from -40 mV to $+30$ mV). In L779P/$IIS4_N$, the leftward shift of the activation curve was less affected by charge neutralization compared to the L779P ($\Delta V = -13.3 \pm 1.7$ mV (L779P/$IIS4_N$) vs. -12.4 ± 1.2 mV (L779P), Tab. 4.1) suggesting that this residue does not interact with IIS4.

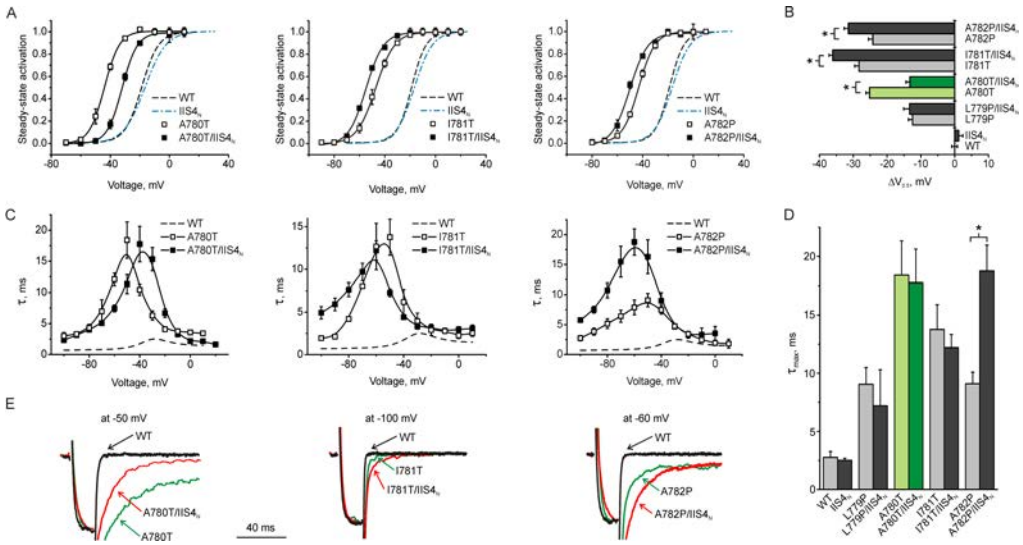

Figure 4.4: Interaction of IIS4 with IIS6.
A, averaged activation curves of WT ($n = 9$), $IIS4_N$ ($n = 11$) and mutations A780T (left), I781T (middle) and A782P (right) in domain II ($n = 5 - 10$).
B, shifts of the activation curves induced by IIS6 mutation (light bars) and in combination with $IIS4_N$ (dark bars). Statistically significant differences (unpaired t-test) are marked with asterisks.
C, voltage dependence of the activation/deactivation time constants for indicated constructs.
D, maximal activation/deactivation time constants of IIS6 mutations alone (light bars) and in combination with $IIS4_N$ (dark bars).
E, selected tail currents through WT, A780T and A780T/$IIS4_N$ mutant channels at the indicated voltages.

4.3.5 Mutant Cycle Analysis Reveals Energetic Coupling Between IIS4 and Residues of the GAGA Ring

The position-specific effects of S_4 neutralization in domain II on gating perturbations in distant S6 segments were investigated by means of mutant cycle analysis. This approach enables the estimation of interaction energies between the mutated pore residues in segments IS6-IVS6 and the voltage sensor in domain II (IIS_4) on the basis of the free energy changes (Yifrach & MacKinnon, 2002; Zandany et al., 2008; Ranganathan et al., 1996; Hidalgo & MacKinnon, 1995). The interaction energies were estimated by calculating the free energies as described in Kudrnac et al. (2009) according to

$$\Delta G_{mut} = RT \left(\frac{V_{0.5,mut}}{k_{mut}} - \frac{V_{0.5,wt}}{k_{wt}} \right) \tag{4.3}$$

$$\Delta G_{IIS4} = RT \left(\frac{V_{0.5,IIS4}}{k_{IIS4}} - \frac{V_{0.5,wt}}{k_{wt}} \right) \tag{4.4}$$

$$\Delta G_{mut/IIS4} = RT \left(\frac{V_{0.5,mut/IIS4}}{k_{mut/IIS4}} - \frac{V_{0.5,wt}}{k_{wt}} \right) \tag{4.5}$$

and thus follows

$$\Delta\Delta G = \Delta G_{mut/IIS4} - \Delta G_{mut} - \Delta G_{IIS4} \tag{4.6}$$

with $V_{0.5}$ representing the voltage of steady state (equilibrium) half-activation and k the slope factor (Tab. 4.1).

If the residues in segments IS6-IVS6 do not interact with the $IIS4_N$ segment, then the change in free energy ($\Delta G_{mut/IIS_4}$) of the combined construct should be equal to the sum of the changes in free energy (ΔG_{mut} and ΔG_{IIS_4}). If the residues are energetically coupled, then the change in free energy for the combination mutant would be significantly different from the sum of the two separate mutations.

Our data show that mutations in positions G432 (IS6), G1193 (IIIS6) and A1503 (VIS6) are energetically coupled with segment IIS4. This is evident from the non-additive shifts of the activation curves of the combined constructs (S6mut/$IIS4_N$), which strongly suggest interdependence of the gating perturbations in IIS4 and the S6 residues (e.g. $\Delta\Delta G = 3.68 \pm 0.90$ kcal/mol for G1193T/$IIS4_N$, see also Tab. 4.1). Analysis of the other combined constructs shows that mutations in IIS4 do not interact with a series of other mutations in IS6, IIIS6 or IVS6 (GAGA-1, GAGA+1 or GAGA+2), with $\Delta\Delta G \approx 0$ kcal/mol. We therefore conclude that the conformational changes in the voltage sensor IIS4 and the S6 residues outside the GAGA

ring are energetically independent. While $\Delta\Delta G$ of construct A780T/$IIS4_N$ was not significantly different from 0 ($\Delta\Delta G = 0.96 \pm 0.99$ kcal/mol), the next residue downstream I781T was found to be energetically coupled to $IIS4_N$ ($\Delta\Delta G$ of I781T/$IIS4_N$ $= -1.44 \pm 0.74$ kcal/mol, Tab. 4.1).

4.4 Discussion

If we translate the Hodgkin-Huxley model for potassium currents into current terminology, we can say that all four gating units ($S4$ segments) must be in an activated position before the channel can open (Hodgkin and Huxley, 1952). This hypothesis was supported by Horn et al. (2000) showing that immobilisation of only one $S4$ segment in its down position prevents Shaker activation. Interestingly, potassium channel closure (deactivation) seems to require only one $S4$ in its resting position (Gagnon and Bezanilla, 2009, see also Jensen et al. 2012). Here we demonstrate that a single voltage sensor ($IIS4$) in an asymmetric $Ca_V1.2$ interacts with a ring of conserved small residues (GAGA ring) in all four S6 segments.

Replacing charged residues in segments $IS4$-$IVS4$ with neutral glutamines resulted in only one functional construct ($IIS4_N$, Tab. 4.1). Mutants $IS4_N$, $IIIS4_N$ and $IVS4_N$ were expressed in the cytoplasm but either not sufficiently targeted to the membrane and/or not functional (supplementary Fig. 4.7). Fig. 4.1 illustrates that charge neutralization of $IIS4$ (replacing residues R1-R5 by glutamines, $IIS4_N$) has no detectable effects on channel kinetics. In order to resolve potential $IIS4_N$ effects on current kinetics we combined these mutations with S6 gating perturbations inducing pronounced shifts of the activation curve. In part we utilized previously studied Ca_V mutations (see Hohaus et al., 2005; Raybaud et al., 2007; Kudrnac et al., 2009; Tadross et al., 2010; Beyl et al., 2011; Depil et al., 2011) inducing $\Delta V > 10$ mV 10 mV regardless of the physico-chemical properties of the substituent (see marks and subscripts to Tab. 4.1). The resulting S6mut/$IIS4_N$ constructs emerged as tools to analyze voltage sensor/S6 interactions.

4.4.1 IIS4 Interactions with Segments IS6-IVS6

As shown in Fig. 4.2 – 4.4, combining $IIS4_N$ with mutations in the gating-sensitive regions of pore-forming S6 segments produced three kinetic phenotypes.

First, four of the S6 mutants (G432W (IS6), G1193T (IIIS6), A1503G (VIS6) and partially A780T (IIS6)) were rescued by $IIS4_N$ (colored bars on Fig. 4.3 and 4.4, see also Fig. 4.8). This is evident from the unexpected backwards shifts of the activation curves towards wild type (Fig. 4.3 B) and accompanying acceleration of channel kinetics (Fig. 4.3 C). Thermodynamic cycle analysis supports the hypothesis that $IIS4$ interacts with GAGA residues (e.g. $\Delta\Delta G(G432W/IIS4_N) = 1.84 \pm 0.72$ kcal/mol, $\Delta\Delta G(G432N/IIS4_N) = 1.43 \pm 0.65$ kcal/mol, $\Delta\Delta G(G1193T/IIS4_N) = 3.68$ ± 0.90 kcal/mol, $\Delta\Delta G(A1503G/IIS4_N) = 2.22 \pm 0.70$ kcal/mol, see Tab. 4.1). Interestingly, the rightward shift of the activation curve in A780T/$IIS4_N$ was less pronounced (Fig. 4.4 A, left column) and $\Delta\Delta G$ not significantly different from zero

(Tab. 4.1). We speculate that these peculiarities are caused by domain-specific interactions between IIS_4 and IIS6 (see detailed discussion below).

Second, pore mutants in segments IS6, IIIS6 and IVS6 upstream and downstream of the GAGA ring (see Fig. 4.3 A) were not significantly affected by charge neutralization in IIS_4 (Fig. 4.3 B, C; Fig. 4.8).

The effect of IIS_{4N} in these constructs was comparable to the one observed for wild type (IIS_{4N}, Fig. 4.1). Additional experiments were carried out to analyze a potential "mutation dependence" of the position-specific rescue effect. As illustrated in Fig. 4.8 (in Supplementary Material), only substitution G432N in segment IS6 was rescued (G432N/IIS_{4N}, green bars, Fig. 4.8) while alternative mutations of neighboring residues (L431V, V433L, L434V) were not sensitive to IIS_{4N} (compare with similar findings in Fig. 4.3 B, C).

Third, combining IIS_{4N} with I781T and I782P augmented the gating disturbances as evident from the additional shift of the activation curve to the left (Fig. 4.4 A) and deceleration of deactivation kinetics (Fig. 4.4 C). If we envisage the voltage sensor predominantly "pushing" the gating structures of $Ca_V1.2$ into the closed conformation (Beyl et al., 2009), then charge neutralization of IIS_4 would decelerate channel closure at negative voltages (i.e. slow deactivation). Such "expected gating changes" were observed only for constructs I781T/IIS_{4N} and A782P/IIS_{4N} (Fig. 4.4).

4.4.2 Dual Role of A780?

Interestingly, the activation curve of A780T/IIS_{4N} was shifted towards the wild type position, but only half way (Fig. 4.4 A, left column). This distinguishes A780T from the other GAGA mutants. We speculate that on the one hand IIS_{4N} would potentially shift the activation curve of A780T/IIS_{4N} to the right (Fig. 4.3 B). On the other hand A780 is part of the IIS6 gating structure where IIS_{4N} induces leftward shifts (compare with other IIS6 mutants I781T and A782P, Fig. 4.4). Such opposing effects could explain an incomplete backward shift of the activation curve of A780T/IIS_{4N} (Fig. 4.4 A).

4.5 Conclusions and Outlook

The principal finding of our study is that segment IIS_4 interacts with a ring of conserved small residues in segments IS6-IVS6 (GAGA-ring, Depil et al. 2011). In general the interaction of a single voltage sensor with all four S6 (and associated gate structures) suggests either interactions of IIS_4 with each of them (Scheme 1) or, alternatively, interactions with the gate structures in domain II that are cooperatively linked to other domains (Scheme 2).

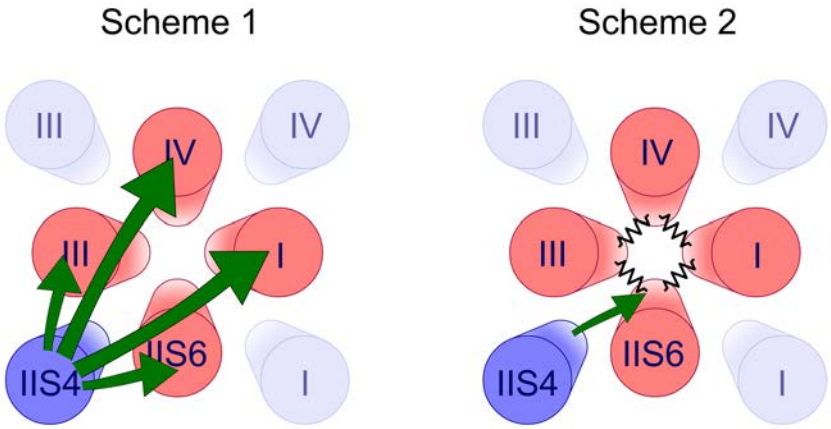

The distances between the GAGA residues (corresponding to AAAA in the crystal structure of a homologous bacterial sodium channel NavAb, Payandeh et al., 2011) and the voltage sensor segments are > 20 Å (Fig. 4.5 B) making a direct interaction of IIS_4 with G432, G1193 and A1503 unlikely. We favor Scheme 2: The interactions between S_4 and S_6 may occur via the S_4-S_5 linkers (Fig. 4.5 A). Channel closure is initiated by downward movement of an S_4 segment and subsequent translocation of the corresponding S6 towards the resting position. In its closing position a single S6 segment enables e.g. hydrophobic interactions with gate structures of neighboring domains (see Beyl et al. 2011). The effect that only conformational changes in the GAGA positions are reversed by charge neutralization in IIS_4 warrants further research.

We speculate that in $Ca_V1.2$ (in analogy to K_V) any single S_4 segment may initiate channel closure under hyperpolarizing voltage (Gagnon and Bezanilla, 2009). To enable channel opening, however, all four S_4 segments must be activated (Horn et al. 2000). Phillips and Swartz (2010) have shown that K_V opens while S_4 segments are still moving (i.e. they do not reach their fully activated position). We therefore further speculate that opening of $Ca_V1.2$ occurs when all four S_4 segment left resting state.

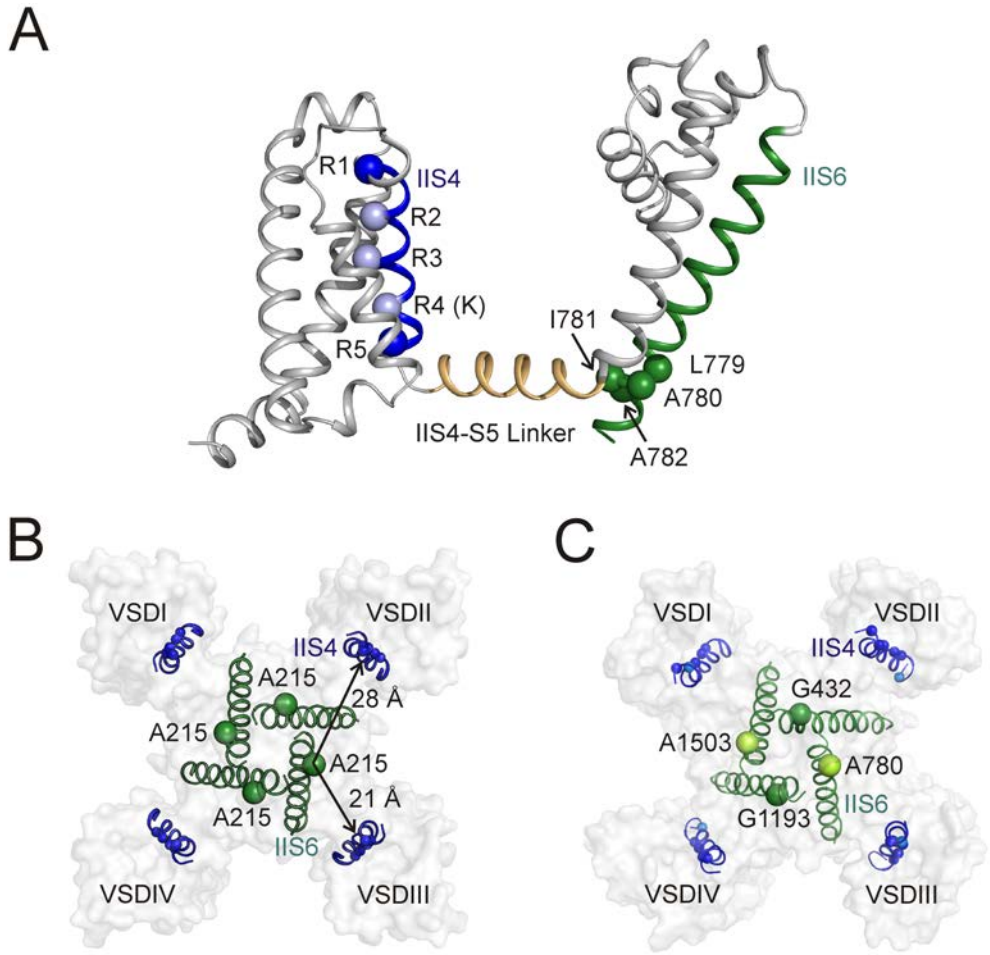

Figure 4.5: $Ca_V1.2$ homology model based on NavAb crystal structure illustrates the location of the G/A/G/A ring with respect to S4.
A, Blue spheres represent the arginine (R650, R653, R656, R662) and lysine (K659) positions in segment IIS4. A previously identified gating-sensitive motif (LAIA) (Hohaus et al., 2005) in IIS6 is shown as green spheres. The linker helix is colored orange. Figures generated with Pymol (The PyMOL Molecular Graphics System, Version 1.2r3pre, Schrödinger, LLC).
B, C Bottom view of the pore domain and S4 segments of NavAb crystal structure and $Ca_V1.2$ homology model colored as in panel A. The GAGA ring (Depil et al., 2011) (corresponding to AAAA ring in NavAb) is shown as green spheres. The distances between the AAAA ring in the NavAb crystal structure (corresponding to GAGA in $Ca_V1.2$) with respect to the voltage-sensing domains are indicated.

In wild type $Ca_V1.2$, S6 segments form a tight closed conformation, with the GAGA ring playing a key role. Hence, substitution of any of the GAGA residues by a bulky tryptophan (G432W), polar threonine (A780T) or a helix-bending proline (A780P) disturbs the finely tuned closure mechanism, as is evident from the slow deactivation. Such a slowing of S6 gating would affect the corresponding S4 transitions to the resting state and, correspondingly, translocation of all S4 segments in their resting position interferes with the pore closure of the mutants. In such a scenario, removal of a "disturbing IIS4 interaction" with the cooperative GAGA ring might relieve spatial constraints thereby providing more flexibility for pore-closing interactions (Beyl et al. 2011). Cooperative interactions are not restricted to interactions within the GAGA ring. Contributions of residues in segments IS6 and IIS6 to activation gating in $Ca_V1.2$ have previously been demonstrated for Ser-435 (IS6) and Ile-781 (IIS6) (Kudrnac et al. 2009), suggesting that paired interactions between additional S6 gating structures may stabilize the closed state.

4.6 Tables

Table 4.1: Midpoints and slope factors (k) of the activation curves and free energy changes during channel opening (ΔG and $\Delta\Delta G = \Delta G_{mut/IIS4_N} - \Delta G_{IIS4_N} - \Delta G_{mut}$). Numbers of experiments are indicated in parentheses.

Mutant	**$V_{0.5}$** [mV]	**k** [mV]	**ΔG** [kcal/mol]	**$\Delta\Delta G$** [kcal/mol]
WT	-18.8 ± 0.9 (9)	5.7 ± 0.9		
R650Q (R1)	-22.9 ± 0.8 (9)	6.3 ± 0.6	-0.16 ± 0.39	
R653Q (R2)	-18.5 ± 0.8 (9)	6.5 ± 0.7	0.26 ± 0.37	
R656Q (R3)	-21.1 ± 0.8 (6)	4.6 ± 0.7	-0.74 ± 0.54	
K659Q (R4)	-17.7 ± 0.8 (6)	7.3 ± 0.7	0.51 ± 0.35	
R662Q (R5)	-8.4 ± 1.3 (6)	4.8 ± 0.7	0.89 ± 0.38	
650RQ/653RQ (R1/R2)	-25.1 ± 0.9 (6)	5.7 ± 0.6	-0.63 ± 0.43	
R1/R2/R3	-18.2 ± 0.7 (6)	7.8 ± 0.6	0.56 ± 0.33	
R1/R2/R3/R4	-23.9 ± 1.0 (6)	6.3 ± 0.7	-0.28 ± 0.42	
R1/R2/R3/R4/R5 ($IIS4_N$)[1]	-17.5 ± 0.8 (11)	6.7 ± 0.7	0.39 ± 0.36	
GAGA mutations				
G432W[2]	-33.7 ± 0.6 (8)	4.7 ± 0.4	-2.25 ± 0.48	
G432N	-36.7 ± 0.6 (6)	6.1 ± 0.5	-1.58 ± 0.43	
A780T[2]	-44.0 ± 0.6 (5)	5.1 ± 0.6	-3.10 ± 0.67	
G1193T[3]	-49.8 ± 1.0 (7)	5.1 ± 0.6	-3.76 ± 0.74	
A1503G[2]	-41.4 ± 0.8 (5)	5.8 ± 0.5	-2.23 ± 0.48	
G432W / $IIS4_N$	-19.3 ± 0.7 (8)	5.8 ± 0.7	-0.01 ± 0.40	1.84 ± 0.72[4]
G432N / $IIS4_N$	-22.1 ± 0.7 (6)	7.7 ± 0.5	0.24 ± 0.33	1.43 ± 0.65[4]
A780T / $IIS4_N$	-32.0 ± 0.7 (10)	5.1 ± 0.7	-1.73 ± 0.64	0.96 ± 0.99
G1193T / $IIS4_N$	-20.8 ± 0.7 (5)	7.5 ± 0.6	0.32 ± 0.35	3.68 ± 0.90[4]
A1503G / $IIS4_N$	-19.8 ± 0.7 (6)	7.5 ± 0.7	0.38 ± 0.35	2.22 ± 0.70[4]
GAGA-1 mutations				
L431P	8.1 ± 0.7 (5)	7.4 ± 1.0	2.56 ± 0.33	
L431V	-8.4 ± 1.3 (4)	6.7 ± 0.8	1.19 ± 0.34	
L779P	-31.2 ± 0.8 (6)	6.1 ± 0.6	-1.02 ± 0.45	
V1192P	-13.8 ± 0.7 (5)	6.6 ± 1.0	0.70 ± 0.37	
V1502P	-3.6 ± 0.7 (6)	5.4 ± 0.6	1.52 ± 0.32	
L431P / $IIS4_N$	no measurable currents observed			
L431V / $IIS4_N$	-10.1 ± 0.9 (4)	7.7 ± 0.6	1.15 ± 0.33	-0.43 ± 0.60

L779P / $IIS4_N$	-32.1 ± 1.5 (5)	5.4 ± 1.6	-1.50 ± 1.06	-0.87 ± 1.21
V1192P / $IIS4_N$	-13.0 ± 1.0 (5)	5.5 ± 1.1	0.56 ± 0.42	-0.53 ± 0.67
V1502P / $IIS4_N$	-5.4 ± 1.0 (7)	6.6 ± 1.0	1.44 ± 0.33	-0.48 ± 0.59
GAGA+1 mutations				
V433C	-8.2 ± 0.8 (5)	5.0 ± 0.6	0.96 ± 0.35	
V433L	-30.1 ± 0.6 (5)	6.1 ± 0.5	-0.95 ± 0.39	
I781T	-47.1 ± 0.9 (5)	7.4 ± 0.7	-1.75 ± 0.48	
F1194C	-6.8 ± 0.9 (5)	4.4 ± 0.6	1.02 ± 0.36	
V1504T	-11.6 ± 0.7 (7)	4.9 ± 0.6	0.55 ± 0.36	
V433C / $IIS4_N$	-12.4 ± 0.7 (7)	5.7 ± 0.6	0.65 ± 0.35	-0.70 ± 0.62
V433L / $IIS4_N$	-31.1 ± 1.0 (4)	5.7 ± 0.6	-1.25 ± 0.47	-0.70 ± 0.71
I781T / $IIS4_N$	-54.8 ± 0.6 (9)	6.7 ± 0.4	-2.79 ± 0.42	-1.44 ± 0.74[4]
F1194C / $IIS4_N$	-5.7 ± 0.9 (5)	5.6 ± 0.6	1.33 ± 0.33	-0.09 ± 0.61
V1504T / $IIS4_N$	-14.0 ± 0.9 (5)	5.4 ± 0.6	0.41 ± 0.38	-0.54 ± 0.64
GAGA+2 mutations				
L434T	-27.6 ± 0.8 (6)	6.1 ± 0.7	-0.71 ± 0.44	
L434V	-30.2 ± 0.7 (6)	6.3 ± 0.6	-0.87 ± 0.41	
A782P	-43.0 ± 0.9 (6)	6.7 ± 0.8	-1.81 ± 0.55	
V1195T[3]	-28.9 ± 0.7 (7)	5.1 ± 0.7	-1.37 ± 0.55	
I1505P	-8.7 ± 0.8 (5)	5.5 ± 0.6	0.99 ± 0.34	
L434T / $IIS4_N$	-27.4 ± 0.8 (6)	6.4 ± 0.7	-0.57 ± 0.42	-0.25 ± 0.71
L434V / $IIS4_N$	-30.6 ± 0.8 (6)	6.8 ± 0.6	-0.69 ± 0.39	-0.22 ± 0.68
A782P / $IIS4_N$	-50.2 ± 0.8 (5)	7.4 ± 0.6	-2.00 ± 0.45	-0.58 ± 0.80
V1195T / $IIS4_N$	-25.3 ± 1.0 (6)	4.5 ± 0.8	-1.28 ± 0.66	-0.30 ± 0.94
I1505P / $IIS4_N$	-7.5 ± 0.9 (5)	5.1 ± 0.8	1.06 ± 0.36	-0.32 ± 0.61

1 No currents could be measured if the charges in segments $IS4$ ($IS4_N$), $IIIS4$ ($IIIS4_N$) and $IVS4$ ($IVS4_N$) were replaced by glutamines.

2 Data from Depil et al. (2011)

3 Data from Beyl et al. (2009)

4 statistically significantly different from zero ($p < 0.05$)

4.7 Supplemental Materials

4.7.1 Charge neutralization in IIS4 has small effect on channel gating

Neutralization of individual arginines (R650Q, R653Q, R656Q, R662Q) and lysine K659Q (Fig. 4.2, Tab. 4.1) shifted the activation curve in the hyperpolarizing (R650Q) or depolarizing (R662Q) directions. The leftward-shifted activation curve of R650Q can be understood in simple physical terms. Structure-activity studies on $Ca_V1.2$ have shown that the voltage dependence of the "pore-releasing" sensor movement is less pronounced than the voltage dependence of "pore-locking" sensor movement (Beyl et al., 2009). In other words, changes in membrane voltage are more efficient at closing than in opening the channel. In such a scenario a channel with reduced net gating charge would require stronger hyperpolarization for pore closure by the remaining charges (segments IS_4, $IIIS_4$ and IVS_4) of the gating machinery.

Rightward shifts of the activation curve cannot be interpreted in such simple terms. A rightward shift of the activation curve can be induced either by closed state stabilization or by a destabilization of the open state (Yifrach & MacKinnon, 2002). A rightward shift induced by mutation R662Q suggests a stabilization of the closed channel state as evident from the lack of acceleration of channel kinetics (Fig. 4.2 C, D, see also Fig. 4.1). This gating phenotype may reflect a direct interaction of R662 with the gating structures of the pore. The impact of other charges was minor (Tab. 4.1). Taken together, our study highlights a particular role of IIS_4 residues R650Q and R662Q in $Ca_V1.2$ gating. Specific roles of individual arginines have been discussed for voltage-gated K^+ and Na^+ channels (DeCaen et al., 2008; Cestèle et al., 2006; Zhang et al., 2005; Bao et al., 1999; Kontis et al., 1997) and may reflect specific interactions with adjacent amino acids in different segments.

4.7.2 Figure S1

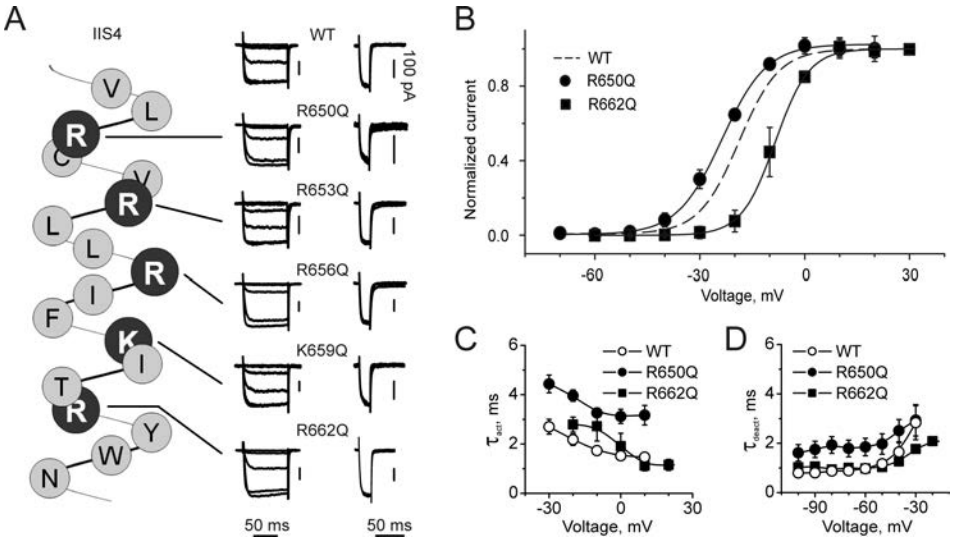

Figure 4.6: Effects of mutations in IIS4 on $Ca_V1.2$ gating.

A, *left panel* shows an α-helical representation of the amino acid sequence of segment IIS4 of the α_1-1.2 subunit. Substituted (positively charged) residues are shown in black. *Middle panel* shows representative families of I_{Ba} through wild-type and mutant channels starting from threshold potential (-50 mV). Barium currents were evoked during depolarizing test pulses from a holding potential of -100 mV (increments, 10 mV). *Right panel* shows representative tail currents of wild-type and mutant channels. Currents were activated during a 20 ms conditioning repolarization to 0 mV. Deactivation was recorded during subsequent repolarizations with 10 mV increments starting from -100 mV. Vertical scale bars represent 100 pA.

B, averaged activation curves of wild-type ($n = 9$) and mutants R650Q ($n = 9$) and R662Q ($n = 6$).

C-D, Mean time constants of channel activation I and deactivation (D) are plotted against test potential. Data were obtained by fitting the (de)activation phase of currents to a mono-exponential function. Solid lines represent fits by B-splines.

4.7.3 Fingerprints of the IIS4 – IIS6 interaction

A region of gating sensitive residues in IIS6 was previously identified (Hohaus et al., 2005, LAIA motif). Interestingly, these residues were recently suggested to closely interact with the S4-S5 linker region of $Ca_V2.3$ suggesting common elements in the transduction mechanism in different Ca_V (Wall-Lacelle et al., 2011). A782P (forming part of LAIA) stabilizes the open state compared to wild type and combination with $IIS4_N$ resulted in a further shift of the activation curve to the left and a further slowing-down of channel kinetics (Fig. 4.2 C). If we envisage the voltage sensor predominantly "pushing" the gating structures of $Ca_V1.2$ into the closed conformation (Beyl et al., 2009), then charge neutralization of IIS4 would be expected to decelerate channel closure at negative voltages (deactivation). These "expected" gating changes were, however, observed only for constructs I781T/$IIS4_N$ and A782P/$IIS4_N$. For the IIS6 mutation A780T, the activation curve was shifted towards wild type but did not completely rescue the gating perturbation (Fig. 4.2 E, colored bars). The half way shift was not accompanied by normalization of channel closure (Fig. 4.2 D and F). This distinguishes A780T from the other mutants of the G/A/G/A ring. We speculate that A780 may participate in two processes: i) stabilization of the open state, like other residues (Depil et al., 2011) and ii) executing pore closure under downward movement of IIS4. Thus, on the one hand charge neutralization of IIS4 diminishes stabilization of the open state as evident from the shifted the activation curve towards wt. This effect resembles the kinetics of constructs G432W/$IIS4_N$ G1193T/$IIS4_N$ and A1503G/$IIS4_N$. On the other hand lack of "IIS4 pushing force" on IIS6 destabilizes the closed state, thereby shifting the activation curve leftwards. Consequently, charge neutralization in construct A780T/$IIS4_N$ induces only "partial rescue" of the gating disturbances.

4.7.4 Figure S2

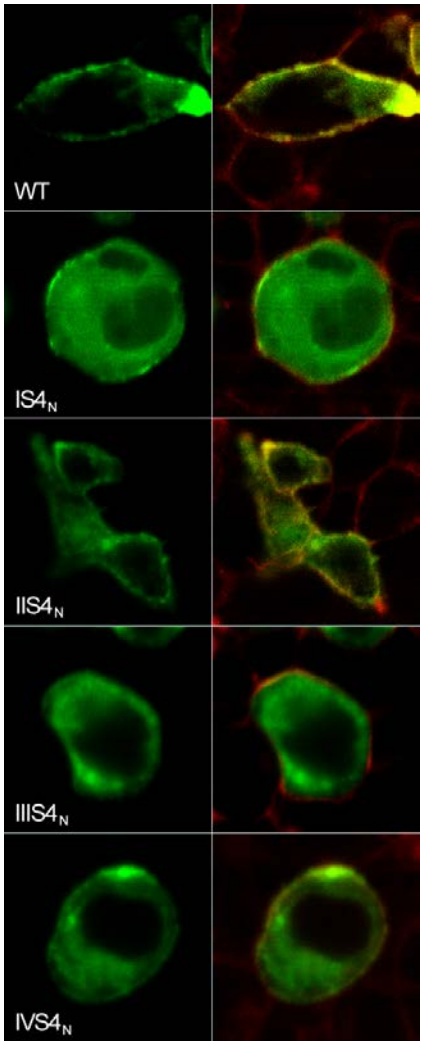

Figure 4.7: Localization of wild-type and mutant $Ca_V1.2$ α_1-subunits within tsA-201cells.
Transiently transfected tsA-201 cells expressing wild-type (WT) $Ca_V1.2$ channel and GFP-tagged (green) constructs $IS4_N$, $IIS4_N$, $IIIS4_N$ and $IVS4_N$ are shown (left column). All GFP-tagged $Ca_V1.2$ α_1-subunits were co-expressed with β_2 and α_2-δ-subunits, and the cells were stained with the plasma membrane marker FM4-64 (red). Colocalization of GFP proteins and the FM4-64 marker is visualized in yellow (right column). Membrane localization was more prominent for wild type and GFP-$IIS4_N$ channels while GFP-$IS4_N$, GFP-$IIIS4_N$ and GFP-$IVS4_N$ were mostly localized in the cytosole. These data suggest less efficiently transport of GFP-$IS4_N$, GFP-$IIIS4_N$ and GFP-$IVS4_N$ to the membrane. It can, however, not be excluded that GFP-$IS4_N$, GFP-$IIIS4_N$ and GFP-$IVS4_N$ do not form functional channel proteins.

4.7.5 Figure S3

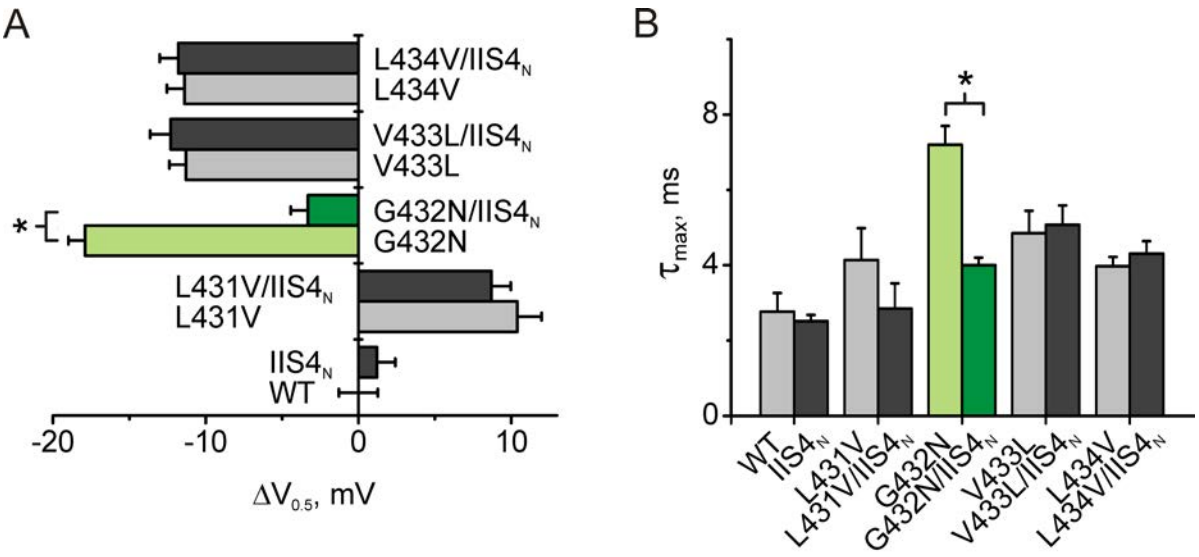

Figure 4.8: Charge neutralization in domain II (IIS4) rescues gating disturbances in position G432 of domains I.
Shift of activation curve (A) and peak activation/deactivation time constants (B) of the studied pore mutations in segments IS6 either alone or in combination with $IIS4_N$. Statistically significantly different (t-test) values are marked with asterisks. Error bars indicate SEM.

4.8 References

Armstrong, C.M., and F. Bezanilla. 1973. Currents related to movement of the gating particles of the sodium channels. Nature. 242:459-461.

Bao H., A. Hakeem, M. Henteleff, JG. Starkus and MD Rayner. 1999. Voltage-insensitive gating after charge-neutralizing mutations in the S4 segment of Shaker channels. J. Gen. Physiol. 113:139–151.

Beyl, S., K. Depil, A. Hohaus, A. Stary-Weinzinger, E. Timin, W. Shabbir, M. Kudrnac, and S. Hering. 2011. Physicochemical properties of pore residues predict activation gating of $Ca_V1.2$: a correlation mutation analysis. Pflugers Arch. 461:53-63.

Beyl, S., P. Kügler, M. Kudrnac, A. Hohaus, S. Hering, and E. Timin. 2009. Different pathways for activation and deactivation in $Ca_V1.2$: a minimal gating model. J. Gen. Physiol. 134:231-241; S1-2.

Bezanilla, F., E. Perozo, and E. Stefani. 1994. Gating of Shaker K^+ channels: II. The components of gating currents and a model of channel activation. Biophys. J. 66:1011–1021.

Bezanilla, F. 2000. The voltage sensor in voltage-dependent ion channels. Physiol. Rev. 80:555-592.

Catterall, W.A. 2010. Ion channel voltage sensors: structure, function, and pathophysiology. Neuron. 67:915-928.

Cestèle S., V. Yarov-Yarovoy, Y. Qu, F. Sampieri, T. Scheuer and W.A. Catterall. 2006. Structure and function of the voltage sensor of sodium channels probed by a beta-scorpion toxin. J. Biol. Chem. 281:21332–21344.

DeCaen PG., V. Yarov-Yarovoy, Y. Zhao, T. Scheuer and W.A. Catterall. 2008. Disulfide locking a sodium channel voltage sensor reveals ion pair formation during activation. Proc. Natl. Acad. Sci. U.S.A. 105:15142–15147.

Del Camino, D., M. Kanevsky, and G. Yellen. 2005. Status of the Intracellular Gate in the Activated-Not-Open State of Shaker K^+ Channels. J Gen Physiol. 126:419–428.

Depil, K., S. Beyl, A. Stary-Weinzinger, A. Hohaus, E. Timin, and S. Hering. 2011. Timothy mutation disrupts the link between activation and inactivation in $Ca_V1.2$ protein. J. Biol. Chem. 286:31557-31564.

Ellis, S.B., M.E. Williams, N.R. Ways, R. Brenner, A.H. Sharp, A.T. Leung, K.P. Campbell, E. McKenna, W.J. Koch, and A. Hui. 1988. Sequence and expression of mRNAs encoding the alpha 1 and alpha 2 subunits of a DHP-sensitive calcium channel. Science. 241:1661-1664.

Eswar, N., B. Webb, M.A. Marti-Renom, M.S. Madhusudhan, D. Eramian, M.-Y. Shen, U. Pieper, and A. Sali. 2006. Comparative protein structure modeling using Modeller. Curr Protoc Bioinformatics. Chapter 5:Unit 5.6.

Gagnon, D.G., and F. Bezanilla. 2009. A single charged voltage sensor is capable of gating the Shaker K^+ channel. J. Gen. Physiol. 133:467–483.

Hackos, D.H., T.-H. Chang, and K.J. Swartz. 2002. Scanning the intracellular S6 activation gate in the shaker K^+ channel. J. Gen. Physiol. 119:521-532.

Hamill, O.P., A. Marty, E. Neher, B. Sakmann, and F.J. Sigworth. 1981. Improved patch-clamp techniques for high-resolution current recording from cells and cell-free membrane patches. Pflugers Arch. 391:85-100.

Hemara-Wahanui, A., S. Berjukow, C.I. Hope, P.K. Dearden, S.-B. Wu, J. Wilson-Wheeler, D.M. Sharp, P. Lundon-Treweek, G.M. Clover, J.-C. Hoda, J. Striessnig, R. Marksteiner, S. Hering, and M.A. Maw. 2005. A CACNA1F mutation identified in an X-linked retinal disorder shifts the voltage dependence of $Ca_V1.4$ channel activation. Proc. Natl. Acad. Sci. U.S.A. 102:7553-7558.

Hidalgo, P., and R. MacKinnon. 1995. Revealing the architecture of a K^+ channel pore through mutant cycles with a peptide inhibitor. Science. 268:307-310.

Hodgkin, A.L., and A.F. Huxley. 1952. A quantitative description of membrane current and its application to conduction and excitation in nerve. J. Physiol. (Lond.). 117:500-544.

Hohaus, A., S. Beyl, M. Kudrnac, S. Berjukow, E.N. Timin, R. Marksteiner, M.A. Maw, and S. Hering. 2005. Structural determinants of L-type channel activation in segment IIS6 revealed by a retinal disorder. J. Biol. Chem. 280:38471-38477.

Horn, R., S. Ding, and H.J. Gruber. 2000. Immobilizing the moving parts of voltage-gated ion channels. J. Gen. Physiol. 116:461-476.

Hoshi, T., W.N. Zagotta, and R.W. Aldrich. 1994. Shaker Potassium Channel Gating. I: Transitions Near the Open State. J. Gen. Physiol. 103:249–278.

Jensen, M.Ø., V. Jogini, D.W. Borhani, A.E. Leffler, R.O. Dror, and D.E. Shaw. 2012. Mechanism of Voltage Gating in Potassium Channels. Science. 336:229–233.

Kontis, KJ., A. Rounaghi and AL. Goldin. 1997. Sodium channel activation gating is affected by substitutions of voltage sensor positive charges in all four domains. J. Gen. Physiol. 110:391–401.

Kudrnac, M., S. Beyl, A. Hohaus, A. Stary, T. Peterbauer, E. Timin, and S. Hering. 2009. Coupled and independent contributions of residues in IS6 and IIS6 to activation gating of $Ca_V1.2$. J. Biol. Chem. 284:12276-12284.

Ledwell, J.L., and R.W. Aldrich. 1999. Mutations in the S4 region isolate the final voltage-dependent cooperative step in potassium channel activation. J. Gen. Physiol. 113:389-414.

Long, S.B., E.B. Campbell, and R. Mackinnon. 2005. Crystal structure of a mammalian voltage-dependent Shaker family K^+ channel. Science. 309:897-903.

Murata, Y., H. Iwasaki, M. Sasaki, K. Inaba, and Y. Okamura. 2005. Phosphoinositide phosphatase activity coupled to an intrinsic voltage sensor. Nature. 435:1239-1243.

Pathak, M., L. Kurtz, F. Tombola, and E. Isacoff. 2005. The cooperative voltage sensor motion that gates a potassium channel. Journal of General Physiology. 125:57–69.

Payandeh, J., T. Scheuer, N. Zheng, and W.A. Catterall. 2011. The crystal structure of a voltage-gated sodium channel. Nature. 475:353-358.

Perez-Reyes, E., A. Castellano, H.S. Kim, P. Bertrand, E. Baggstrom, A.E. Lacerda, X.Y. Wei, and L. Birnbaumer. 1992. Cloning and expression of a cardiac/brain beta subunit of the L-type calcium channel. J. Biol. Chem. 267:1792-1797.

Phillips, L.R., and K.J. Swartz. 2010. Position and motions of the S4 helix during opening of the Shaker potassium channel. J. Gen. Physiol. 136:629–644.

Ramsey, I.S., M.M. Moran, J.A. Chong, and D.E. Clapham. 2006. A voltage-gated proton-selective channel lacking the pore domain. Nature. 440:1213-1216.

Ranganathan, R., J.H. Lewis, and R. MacKinnon. 1996. Spatial localization of the K^+ channel selectivity filter by mutant cycle-based structure analysis. Neuron. 16:131-139.

Raybaud, A., E.-E. Baspinar, F. Dionne, Y. Dodier, R. Sauvé, and L. Parent. 2007. The role of distal S6 hydrophobic residues in the voltage-dependent gating of $Ca_V2.3$ channels. J. Biol. Chem. 282:27944-27952.

Raybaud, A., Y. Dodier, P. Bissonnette, M. Simoes, D.G. Bichet, R. Sauvé, and L. Parent. 2006. The role of the GX9GX3G motif in the gating of high voltage-activated Ca^{2+} channels. J. Biol. Chem. 281:39424-39436.

Sasaki, M., M. Takagi, and Y. Okamura. 2006. A voltage sensor-domain protein is a voltage-gated proton channel. Science. 312:589-592.

Schoppa, N.E., and F.J. Sigworth. 1998a. Activation of Shaker Potassium Channels I. Characterization of Voltage-Dependent Transitions. J. Gen. Physiol. 111:271–294.

Schoppa, N.E., and F.J. Sigworth. 1998b. Activation of Shaker Potassium Channels II. Kinetics of the V2 Mutant Channel. J. Gen. Physiol. 111:295–311.

Schoppa, N.E., and F.J. Sigworth. 1998c. Activation of Shaker potassium channels. III. An activation gating model for wild-type and V2 mutant channels. J. Gen. Physiol. 111:313-342.

Splawski, I., K.W. Timothy, N. Decher, P. Kumar, F.B. Sachse, A.H. Beggs, M.C. Sanguinetti, and M.T. Keating. 2005. Severe arrhythmia disorder caused by cardiac L-type calcium channel mutations. Proc. Natl. Acad. Sci. U.S.A. 102:8089-8096; discussion 8086-8088.

Splawski, I., K.W. Timothy, L.M. Sharpe, N. Decher, P. Kumar, R. Bloise, C. Napolitano, P.J. Schwartz, R.M. Joseph, K. Condouris, H. Tager-Flusberg, S.G. Priori, M.C. Sanguinetti, and M.T. Keating. 2004. $Ca_V1.2$ calcium channel dysfunction causes a multisystem disorder including arrhythmia and autism. Cell. 119:19-31.

Smith-Maxwell, C.J., J.L. Ledwell, and R.W. Aldrich. 1998a. Role of the S4 in Cooperativity of Voltage-Dependent Potassium Channel Activation. J. Gen. Physiol. 111:399–420.

Smith-Maxwell, C.J., J.L. Ledwell, and R.W. Aldrich. 1998b. Uncharged S4 Residues and Cooperativity in Voltage-Dependent Potassium Channel Activation. J. Gen. Physiol. 111:421–439.

Stary, A., Y. Shafrir, S. Hering, P. Wolschann, and H.R. Guy. 2008. Structural model of the $Ca_V1.2$ pore. Channels (Austin). 2:210-215.

Stefani, E., L. Toro, E. Perozo, and F. Bezanilla. 1994. Gating of Shaker K^+ channels: I. Ionic and gating currents. Biophys. J. 66:996–1010.

Sukhareva, M., D.H. Hackos, and K.J. Swartz. 2003. Constitutive Activation of the Shaker KV Channel. J. Gen. Physiol. 122:541–556.

Tadross, M.R., M. Ben Johny, and D.T. Yue. 2010. Molecular endpoints of Ca^{2+}/calmodulin- and voltage-dependent inactivation of $Ca_V1.3$ channels. J. Gen. Physiol. 135:197-215.

Wall-Lacelle, S., M.I. Hossain, R. Sauvé, R. Blunck, and L. Parent. 2011. Double mutant cycle analysis identified a critical leucine residue in the IIS_4S_5 linker for the activation of the $Ca_V2.3$ calcium channel. J. Biol. Chem. 286:27197-27205.

Yifrach, O., and R. MacKinnon. 2002. Energetics of pore opening in a voltage-gated K^+ channel. Cell. 111:231-239.

Zagotta, W.N., T. Hoshi, and R.W. Aldrich. 1994a. Shaker Potassium Channel Gating. III: Evaluation of Kinetic Models for Activation. J. Gen. Physiol. 103:321–362.

Zagotta, W.N., T. Hoshi, J. Dittman, and R.W. Aldrich. 1994b. Shaker Potassium Channel Gating. II: Transitions in the Activation Pathway. J. Gen. Physiol. 103:279–319.

Zandany, N., M. Ovadia, I. Orr, and O. Yifrach. 2008. Direct analysis of cooperativity in multisubunit allosteric proteins. Proc. Natl. Acad. Sci. U.S.A. 105:11697-11702.

Zhang, M., J. Liu, M. Jiang, D-M. Wu, K. Sonawane, H.R. Guy and G-N Tseng. 2005. Interactions between charged residues in the transmembrane segments of the voltage-sensing domain in the hERG channel. J. Membr. Biol. 207:169–181.

Zhao, Y., T. Scheuer, and W.A. Catterall. 2004a. Reversed voltage-dependent gating of a bacterial sodium channel with proline substitutions in the S6 transmembrane segment. Proc. Natl. Acad. Sci. U.S.A. 101:17873-17878.

Zhao, Y., V. Yarov-Yarovoy, T. Scheuer, and W.A. Catterall. 2004b. A gating hinge in Na^+ channels; a molecular switch for electrical signaling. Neuron. 41:859-865.

Zhen, X.-G., C. Xie, A. Fitzmaurice, C.E. Schoonover, E.T. Orenstein, and J. Yang. 2005. Functional architecture of the inner pore of a voltage-gated Ca^{2+} channel. J. Gen. Physiol. 126:193-204.

Appendix

Curriculum Vitæ

Personal Data

Name	Katrin Depil
Academic degree	Mag. pharm.
eMail	katrin.depil@univie.ac.at
Date of birth	September 13th, 1983
Citizenship	Austria

Scientific Career

2009 – 2012	October – September 6 Semesters PhD Studies "Structure-Activity Studies on the Opening- and Closure-Mechanism of L-Type Calcium-Channels" Department of Pharmacology and Toxicology University of Vienna University Assistant Pre-Doc Position Supervisor Univ. Prof. Dr. Steffen Hering Associate PhD-Student of the Governmental Funded Doctoral Program FWF "Molecular Drug Targets" Supervisor Dr. Eugen Timin
2002 – 2007	October – February 9 Semesters Pharmacy Studies University of Vienna Diploma Examination with Honors "Reaction Behaviours of Strong Acids with Thiophene-Derivatives"

Professional Experience

2007 – 2012	April – ongoing Full-time and part-time Employment as a local Pharmacist in Vienna Pharmacy "Apotheke Alt-Erlaa" 1230 Vienna, Pharmacy "Zur Mariahilf" 1230 Vienna, Pharmacy "Zum hl. Josef" 1190 Vienna
2002	August Department of Quality Assurance Boehriger Ingelheim Austria, 1120 Vienna

Teaching Experience

2009 – 2012	Instructor of compulsory lectures (c.l.) and elective courses (e.c.) SE Klinische Pharmakokinetik Rechenübungen (c.l.) VO Arzneimittelwechselwirkungen (e.c.) PR Pharmakologie, Pharmakotherapie und Toxikologie I (c.l.) PR Pharmakologie, Pharmakotherapie und Toxikologie II (c.l)
2006	October – December Tutor PR Arzneistoffanalytik (c.l.)

Education

1998 – 2002	September – June High School BORG Wr. Neustadt Graduation with Honors
1994 – 1998	September – June "Privatgymnasium der Redemptoristen" in Katzelsdorf a.d. Leitha

Scientific Methods

Electrophysiology	Patch Clamp Technique
Molecular Biology	Cell Culture, Transfection, Transformation, Mutagenesis, DNA-Preparation and DNA-Extraction
Analytics	HPLC, LC, GC-MS, NMR, Electrophoresis

Publications & Posters

Refereed Journal Publications	Depil K[1], Beyl S[1], Stary-Weinzinger A[1], Hohaus A, Timin E, Hering S : "Timothy mutation disrupts the link between activation and inactivation in $Ca_V1.2$ protein" J Biol Chem. 2011 Sep 9;286(36):31557-64. Epub 2011 Jun 17.
	Beyl S[1], Depil K[1], Hohaus A, Stary-Weinzinger A, Timin E, Shabbir W, Kudrnac M, Hering S : "Physicochemical properties of pore residues predict activation gating of $Ca_V1.2$: A correlation mutation analysis" Pflugers Arch. 2011 Jan;461(1):53-63. Epub 2010 Oct 7.
Submitted Journal Publications	Beyl S, Depil K, Hohaus A, Stary-Weinzinger A, Linder T, Timin E, Hering S : "Neutralization of a single voltage sensor (IIS4) affects gating determinants in all four pore forming S6 segments of $Ca_V1.2$" Submitted in the Journal of General Physiology
Journal Publications in Preparation	Stary-Weinzinger A[1], Shabbir W[1], Depil K, Linder T, Beyl S, Timin E, Hering S : "T1143 is essential for $Ca_V1.2$ inhibition by Diltiazem: Refined drug binding model"
	Depil K, Hering S, Stary-Weinzinger A : "Asparagine Mutations alter Voltage-dependend Inactivation of S6 Segments in $Ca_V1.2$"
Conference Posters	Depil K, Beyl S, Hohaus A, Stary-Weinzinger A, Timin E, Shabbir W., Kudrnac M., Hering S.: "Physicochemical properties of pore residues predict activation gating of $Ca_V1.2$: A correlation mutation analysis" 55th Biophysical Society Annual Meeting, Baltimore, Maryland, USA; 05.03.2011 – 09.03.2011
	Depil K, Beyl S, Stary-Weinzinger A, Hohaus A, Timin E, Hering S.: "Timothy mutation affects tightly sealing point of $Ca_V1.2$ activation gate" 17th Scientific Symposium of the APHAR Society, Innsbruck, Austria; 29.09.2011 – 30.09.2011

[1] authors contributed equally to this work

Conference Posters – continued

Stary-Weinzinger A, Depil K, Beyl S, Timin E, Hering S.:
"Mutational analysis in the bundle crossing region guides the design of $Ca_V1.2$ homology models"
55th Biophysical Society Annual Meeting, Baltimore, Maryland, USA; 05.03.2011 – 09.03.2011

Beyl S, Depil K, Hohaus A, Stary-Weinzinger A, Timin E, Hering S.:
"Neutralizing the charges in a voltage sensor repairs gating perturbations in the pore of $Ca_V1.2$"
56th Biophysical Society Annual Meeting, San Diego, California, USA; 25.02. 2012 – 29.02.2012

Beyl S, Depil K, Hohaus A, Stary-Weinzinger A, Timin E, Hering S.:
"Neutralizing the charges in a voltage sensor repairs gating perturbations in the pore of $Ca_V1.2$"
1st European Calcium Channel Conference, Alpbach, Austria; 16.05.2012 – 20.05.2012